

國立臺灣大學工學院環境工程學研究所

碩士論文

Graduate Institute of Environmental Engineering

College of Engineering

National Taiwan University

Master Thesis



利用廢油砂焦炭透過微波化學活化法及傳統化學活化法合成

活性碳應用於去除水溶液中的二價汞

Preparation of Activated Carbon from Waste Oil Sands Coke by
Microwave and Conventional Chemical Activation for Removal of
Mercury (II) from Aqueous Solution

施東甫

Tung-Fu Shih

指導教授：席行正 博士

Advisor: Hsing-Cheng Hsi, Ph.D.

中華民國 106 年 8 月

August 2017

國立臺灣大學碩士學位論文
口試委員會審定書

利用廢油砂焦炭透過微波化學活化法及傳統化學活化法合成活性
碳應用於去除水溶液中的二價汞

Preparation of Activated Carbon from Waste Oil Sands Coke by
Microwave and Conventional Chemical Activation for Removal of
Mercury (II) from Aqueous Solution

本論文係 施東甫 君(學號 R04541127)在國立臺灣大學環境
工程學研究所完成之碩士學位論文，於民國 106 年 7 月 28 日承下
列考試委員審查通過及口試及格，特此證明

論文審查委員：

林 錕 松
黃 盈 賓
席 行 正
侯 嘉 洪

林錕松 博士
元智大學化學工程與材料科學學系教授

黃盈賓 博士
工業技術研究院產業服務中心研究員

席行正 博士
國立臺灣大學環境工程學研究所教授

侯嘉洪 博士
國立臺灣大學環境工程學研究所副教授

指導教授：

席行正

所

長：

林正芳

致謝



在這短短兩年內，終於，完成了這個階段性任務。對我而言，要感謝的人真的太多了，一路走來沒有你們的幫助，就沒有辦法順利完成學業。

首先，要感謝席行正老師，也是我的指導教授。在專業上的建議，儘管我的進度落後，老師總是很有耐心。而平常老師給我們一種亦師亦友親切感，不論是甚麼問題，老師總可以朋友的角度給我們建議。

而我的父母，從小就提供給我最好的教育資源。從國中一路到研究所，都讓我不必為生活而擔憂。如今我所擁有的一切及小小的成就，都要歸功於我的父母。當你們的兒子，很幸運。感謝宛蓉，常常陪我熬夜趕論文、趕數據，不管在精神上的鼓勵或是心理上的支持，都對我有很大的幫助。最後在交大打 BET 時候，宛蓉也不厭其煩的陪我等待。

實驗室的大學長及大學姐，哲榮與映琳。總是在我實驗遇到困難時無條件地給我建議，特別是映琳學姊協助我在北醫做總汞分析，讓我能夠順利完成大量數據，且在分析數據上提供我非常多的幫助。子琇、明茵、孟竺在最後關頭也在口試一直提醒我細節，讓我口試順利通過。明茵在 XPS 的分峰上也幫了我很大的忙。昱廷、秉圻一起打球的好隊友，可以讓我在忙碌的實驗過程中有個紓壓的管道，。丁昱、韻心也常常在汞吸附實驗中互相打氣，遇到問題也常常一起討論。昇憲則總是可以活絡實驗室的氣氛，騙學姊之類的。感謝好朋友哲嘉，聽我試報，給我建議，讓我在簡報的流暢度有所提升。

特別感激侯老師的、劉老師、白老師及官老師的 BET 分析儀與簡老師的 CVAAS，沒有你們的幫忙，實驗的數據不可能如期完成，十分感謝。

中文摘要



汞為一重金屬，其毒性及生物累積性容易造成人類與其他哺乳類的健康危害。若汞經由人類活動排放至水體中若未經過控制，則會造成地區性的嚴重危害。活性炭吸附為目前控制水溶液中之汞的主要方法之一。同時，經過硫改質的活性炭含有硫官能基於其表面，在水溶液中吸附汞顯示了高效及高選擇性。

廢油砂焦碳(Waste oil sands coke)為從油砂提煉石油的過程中產生的副產物。2012 年末之前已有 7700 萬噸的廢油砂焦碳因無法有效處置被儲存，已佔了大量土地。同時，由於其含有約 90%的碳，可以不必經由碳化步驟，適合作為活性炭的前驅物。並且油砂焦碳含有約 5-6%之硫，可以預測其製備之活性炭對汞的吸附效果佳。

本研究透過反應曲面法(Response surface methodology)結合中央合成設計實驗(Central composite design)作為觀察活性炭性質隨不同條件變化之工具。就產率、硫含量、及比表面積而言。發現微波化學活化的可預測性較差，而傳統化學活化法則相對穩定。

在吸附動力學方面，在初始濃度為 $100 \text{ mg-Hg}^{2+}/\text{L}$ 測試條件下，不論透過微波化學活化法或傳統化學活化法，均以擬二階動力學模式適合模擬實驗結果。在等溫吸附的實驗中則以 Freundlich equation 較符合等溫吸附實驗結果。而在飽和吸附容量的實驗中，在初始濃度為 $100 \text{ mg-Hg}^{2+}/\text{L}$ 測試條件下，油砂焦碳飽和吸附容量為 $12.58 \text{ mg-Hg}^{2+}/\text{g-AC}$ ，去除率為 14.44%；透過微波化學活化產生之活性炭飽和吸附容量達 $82.26 \text{ mg-Hg}^{2+}/\text{g-AC}$ ，去除率可高達 94.83%；而透過傳統化學活化產生之活性炭飽和吸附容量 $92.89 \text{ mg-Hg}^{2+}/\text{g-AC}$ ，去除率可高達 97.81%。研究結果顯示，

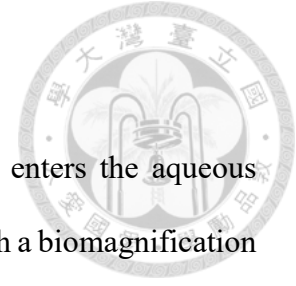
不論透過微波化學活化或是傳統化學活化，均可有效將廢油砂焦炭轉化成有效的活性碳吸附劑應用於水相汞污染去除。透過 X 射線光電子能譜儀之分析可將去除效率之提升歸因於活化過程中 COO 及 C-O-官能基的形成。



透過反應曲面法結合中央合成設計實驗優化微波活化的操作參數可以獲得，若欲達到 94% 以上之去除效率，則活化功率為 750-1000 瓦，活化時間為 4-5 分鐘。而傳統活化則是活化溫度為 700-800°C，活化時間為 45-80 分鐘。

關鍵字：汞、活性碳、吸附、油砂焦炭、微波、中央合成設計實驗、反應曲面法

Abstract

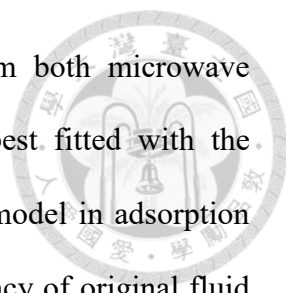


Mercury is a toxic element existing in nature. After mercury enters the aqueous system, it will be transformed into methylmercury and then go through a biomagnification process. If the release of mercury by human activities was not well controlled, it may result in the regional disaster. Activated carbon is the common sorbent used in removal of different kinds of substances in various phases. It has also been proven that activated carbon impregnated with different forms of sulfur is capable of improving the efficiency on adsorption of mercury in aqueous system.

Oil sands coke is a byproduct in the process of upgrading the crude oil from oil sands. Moreover, it has high carbon content and sulfur content (approximately 5-6 wt%), which results into that oil sands coke is a good precursor of activated carbon used in removal of mercury from aqueous solution.

In this study, activated carbons from oil sands coke were successfully prepared by microwave and conventional chemical activation under a series of activation conditions designed by response surface methodology in combination with central composite design (CCD-RSM). By doing so, the change of physical and chemical characteristics was able to be observed by the CCD-RSM analysis.

Compared with conventional chemical activation, microwave chemical activation can develop the surface area and pore volume of activated carbon in the shorter time at similar S_{BET} . Moreover, activated carbon from microwave chemical activation also has higher production yield at similar S_{BET} . The physical and chemical properties of activated carbon from conventional chemical activation is more predictable than activated carbon from microwave chemical activation, in terms of their variation on the activation parameters.



The mercury (II) adsorption data for activated carbons from both microwave chemical activation and conventional chemical activation were best fitted with the pseudo-second order model in adsorption kinetics and Freundlich model in adsorption isotherm. The mercury (II) adsorption capacity and removal efficiency of original fluid coke were 12.58 mg-Hg²⁺/g-AC and 14.44% respectively. The mercury (II) adsorption capacity and removal efficiency of activated carbon from microwave activation were 82.26 mg-Hg²⁺/g-AC and 94.83% respectively. The mercury (II) adsorption capacity and removal efficiency of activated carbon from conventional activation were 92.89 mg-Hg²⁺/g-AC and 97.81% respectively. These results suggest that both conventional activation and microwave activation are able to transform the fluid coke into a suitable sorbent for mercury removal from aqueous phase. Pearson correlation analysis shows that the oxygen content and hydrogen content may be the main factors in determining mercury adsorption capacity of the resulting activated carbon. Based on the XPS analysis, the improvement of mercury (II) adsorption capacities can be attributed to the formation of various oxygenated functional groups, such as phenolic, alcoholic, etheric groups (C-O-) and carboxyl or ester functional groups (COO).

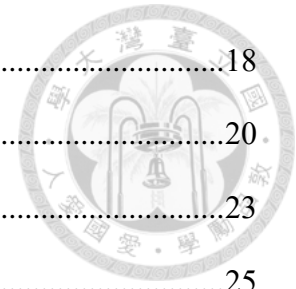
The optimized operating condition of microwave chemical activation can be observed at the power level of 750-1000 W and the time of 4-5 min and the removal efficiency would achieve 94%. The optimized operating condition of conventional chemical activation can be observed at the temperature of 700-800°C and the time of 45-85 min and the removal efficiency would achieve 94%.

Keywords: mercury; activated carbon; adsorption; oil sands coke; microwave; central composite design; response surface methodology

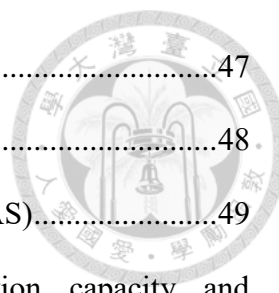
Contents



口試委員會審定書	i
致謝	ii
中文摘要	iii
Abstract.....	v
Contents	vii
List of Figures.....	x
List of Tables	xiii
Chapter 1 Introduction.....	1
1.1 Motivation.....	1
1.2 Research Objectives.....	2
Chapter 2 Literature Review	3
2.1 Mercury.....	4
2.1.1 Global mercury cycle	4
2.1.2 Inorganic mercury	7
2.1.3 Organic mercury.....	8
2.1.4 Mercury removal from water	9
2.2 Activated Carbon	11
2.2.1 Introduction	11
2.2.2 Preparation of activated carbon.....	11
2.2.3 Types of activated carbon.....	13
2.2.4 Physical and chemical characterization of activated carbon.....	14
2.3 Mercury (II) Adsorption by Activated Carbon	16
2.3.1 Adsorption condition.....	16



2.3.2	Characteristics of activated carbon	18
2.3.3	Adsorption kinetic model	20
2.3.4	Adsorption isotherm model	23
2.4	Waste Oil sands coke	25
2.4.1	Oil sands	25
2.4.2	Oil sands coke	25
2.5	Response Surface Methodology	29
Chapter 3	Materials and Methods	32
3.1	Research Framework	32
3.2	Design of Experiment	34
3.2.1	Preparation of activated carbon	34
3.3	Preparation of Activated Carbon	36
3.3.1	Materials and instruments	36
3.3.2	Impregnation	37
3.3.3	Microwave chemical activation	37
3.3.4	Conventional chemical activation	40
3.3.5	After activation	41
3.4	Physical and Chemical Characterization of Activated Carbon	42
3.4.1	Surface area, pore volume and pore size distribution	42
3.4.2	Scanning electron microscope (SEM)	43
3.4.3	Elemental analysis (EA)	43
3.4.4	X-ray photoelectron spectroscopy (XPS)	44
3.5	Mercury (II) Adsorption Experiment	45
3.5.1	Materials and instruments	45
3.5.2	Adsorption kinetic experiment	47



3.5.3	Adsorption isotherm experiment.....	47
3.5.4	Adsorption capacity experiment	48
3.5.5	Cold vapor atomic absorption spectroscopy (CVAAS).....	49
3.5.6	Correlation analysis of mercury (II) adsorption capacity and characteristics of activated carbon	52
Chapter 4 Results and Discussion.....		53
4.1	Physical and Chemical Characterization of Activated Carbon.....	53
4.1.1	Morphology of activated carbon	54
4.1.2	Production yield	57
4.1.3	Surface area and pore volume	62
4.1.4	Pore size distribution (PSD).....	67
4.1.5	Elemental analysis (EA).....	71
4.1.6	X-ray photoelectron spectroscopy (XPS).....	74
4.1.7	Comparison of different impregnation ratios (IR)	77
4.1.8	Comparison of activation methods.....	80
4.2	Mercury (II) Adsorption Experiment.....	83
4.2.1	Adsorption kinetic experiment	83
4.2.2	Adsorption isotherm experiment.....	89
4.2.3	Adsorption capacity experiment	92
4.2.4	Correlation analysis of mercury (II) adsorption capacity and characteristics of activated carbon	100
Chapter 5 Conclusions and Recommendations.....		102
5.1	Conclusions	102
5.2	Recommendations.....	105
Reference.....		106

List of Figures



Figure 2-1 Global mercury cycle (UNEP, 2013)	4
Figure 2-2 Estimated emissions to air from anthropogenic sources in 2010.....	6
Figure 2-3 Effect of S_{BET} on mercury (II) adsorption capacity (Cai and Jia, 2010).....	18
Figure 2-4 SEM images of (a) Fluid coke and (b) Delayed coke (Hill <i>et al.</i> , 2014).....	26
Figure 2-5 Figure of RSM (Anderson and Whitcomb, 2007)	29
Figure 2-6 CCD for (a) two variables and (b) three variables (Bezerra <i>et al.</i> , 2008).....	30
Figure 3-1 Research framework	33
Figure 3-2 Dried mixture in the 50 mL Ceramic Crucible	39
Figure 3-3 Microwave muffle furnace.....	39
Figure 3-4 Calibration curve of microwave muffle furnace.....	39
Figure 3-5 Combustion boat	40
Figure 3-6 Cylindrical quartz tube in the tubular furnace	40
Figure 3-7 Calibration curve of CVAAS	51
Figure 4-1 SEM images of RAW: (a) 400x, (b) 2500x and (c) 10000x	55
Figure 4-2 SEM images of R1-M-P941-t14.25: (a) 400x, (b) 2500x and (c) 10000x.....	55
Figure 4-3 SEM images of R4-M-P941-t14.25: (a) 400x, (b) 2500x and (c) 10000x.....	56
Figure 4-4 SEM images of R1-C-T741-t132: (a) 400x, (b) 2500x and (c) 10000x	56
Figure 4-5 CCD-RSM analysis for the production yield versus power level and time of microwave chemical activation	61
Figure 4-6 CCD-RSM analysis for the production yield versus temperature and time of conventional chemical activation	61
Figure 4-7 PSD of activated carbons with IR=1 from microwave chemical activation fitted by BJH (a)	68

Figure 4-8 PSD of activated carbons with IR=1 from microwave chemical activation fitted by BJH (b)	68
Figure 4-9 PSD of activated carbons with IR=1 from conventional chemical activation fitted by BJH.....	68
Figure 4-10 PSD of activated carbons with IR=1 from microwave chemical activation fitted by NLDFT (a).....	70
Figure 4-11 PSD of activated carbons with IR=1 from microwave chemical activation fitted by NLDFT (b)	70
Figure 4-12 PSD of activated carbons with IR=1 from conventional chemical activation fitted by NLDFT	70
Figure 4-13 CCD-RSM analysis for the sulfur content versus power level and time of microwave chemical activation	73
Figure 4-14 CCD-RSM analysis for the sulfur content versus temperature and time of conventional chemical activation	73
Figure 4-15 Survey scan for activated carbons from microwave activation	75
Figure 4-16 Survey scan for activated carbons from conventional activation	75
Figure 4-17 PSD of R1-M-P659-t14.25, R2-M-P659-t14.25 and R4-M- P659-t14.25 from microwave chemical activation fitted by NLDFT	79
Figure 4-18 PSD of R1-M-P941-t14.25, R2-M-P941-t14.25 and R4-M- P941-t14.25 from microwave chemical activation fitted by NLDFT	79
Figure 4-19 PSD of R1-M-P800-t16, R2-M-P800-t16 and R4-M-P800-t16 from microwave chemical activation fitted by NLDFT	79
Figure 4-20 Comparison of different activation methods: PSD of BJH model.....	82
Figure 4-21 Comparison of different activation methods: PSD of NLDFT model.....	82
Figure 4-22 Pseudo-first kinetic model	84

Figure 4-23 Pseudo-second kinetic model fitting for samples from microwave and conventional chemical activation	85
Figure 4-24 Elovich kinetic model	87
Figure 4-25 Langmuir adsorption isotherm model for samples from microwave and conventional chemical activation	89
Figure 4-26 Freundlich adsorption isotherm model for samples from microwave and conventional chemical activation	90
Figure 4-27 Temkin adsorption isotherm model for samples from microwave and conventional chemical activation	91
Figure 4-28 Effect of S_{BET} on Hg^{2+} adsorption capacity	96
Figure 4-29 Effect of S_{BET} on Hg^{2+} removal efficiency	96
Figure 4-30 CCD-RSM analysis for the removal efficiency versus power level and time of microwave chemical activation	98
Figure 4-31 CCD-RSM analysis for the removal efficiency versus temperature and time of conventional chemical activation	98
Figure 4-32 Effect of hydrogen content on removal efficiency	101

List of Tables

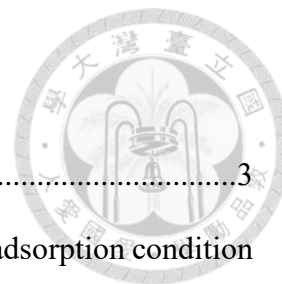
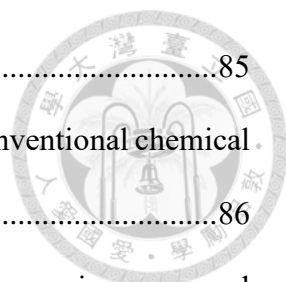


Table 2-1 Terms in literature review	3
Table 2-2 Review of mercury (II) adsorption capacity from different adsorption condition	17
Table 2-3 Pseudo-first-order model	20
Table 2-4 Pseudo-second-order model	21
Table 2-5 Elovich kinetic model.....	22
Table 2-6 Langmuir adsorption isotherm model	23
Table 2-7 Freundlich adsorption isotherm model.....	24
Table 2-8 Temkin adsorption isotherm model.....	24
Table 2-9 Elemental analysis of cokes	26
Table 2-10 Review of activated carbon from oil sands coke.....	28
Table 2-11 Review of CCD-RSM used in preparation of activated carbon	31
Table 3-1 CCD-RSM used in microwave chemical activation.....	34
Table 3-2 CCD-RSM used in conventional chemical activation.....	35
Table 3-3 Experiment equipment	36
Table 3-4 Instruments	36
Table 3-5 Chemicals	36
Table 3-6 Impregnation ratio corresponding drying days	37
Table 3-7 Comparison of setting and real power level	38
Table 3-8 Instruments of physical and chemical characterization.....	42
Table 3-9 The assignment of the XPS peaks (Terzyk, 2001)	44
Table 3-10 Experiment equipment	45
Table 3-11 Instruments	45

Table 3-12 Chemicals	45
Table 3-13 Adsorption condition of mercury (II) adsorption kinetic	47
Table 3-14 Adsorption condition of mercury (II) adsorption isotherm	48
Table 3-15 Adsorption condition of mercury (II) adsorption capacity	49
Table 3-16 Calibration curve concentration	51
Table 4-1 Yield of activated carbon from microwave chemical activation	59
Table 4-2 Yield of activated carbon from conventional chemical activation	60
Table 4-3 The physical properties of activated carbon from microwave chemical activation.....	63
Table 4-4 The physical properties of activated carbon from microwave chemical activation.....	64
Table 4-5 The physical properties of activated carbon from conventional chemical activation.....	65
Table 4-6 CCD-RSM for physical properties	66
Table 4-7 Elemental analysis: microwave chemical activation.....	71
Table 4-8 Elemental analysis: conventional chemical activation	72
Table 4-9 The relative content of carbon functional group on the surface of activated carbons from microwave activation.....	76
Table 4-10 The relative content of carbon functional group on the surface of activated carbons from conventional activation.....	76
Table 4-11 Comparison of different impregnation ratios (IR).....	78
Table 4-12 Comparison of different activation methods	81
Table 4-13 Pseudo-first kinetic model parameters for samples from microwave and conventional chemical activation	84
Table 4-14 Pseudo-second kinetic model for samples from microwave and conventional	



chemical activation	85
Table 4-15 Elovich kinetic model for samples from microwave and conventional chemical activation.....	86
Table 4-16 Adjusted Elovich kinetic model parameters for samples from microwave and conventional chemical activation	86
Table 4-17 Calculated equilibrium time for samples from microwave and conventional chemical activation	88
Table 4-18 Langmuir adsorption isotherm model parameters for samples from microwave and conventional chemical activation.....	89
Table 4-19 Freundlich adsorption isotherm model parameters for samples from microwave and conventional chemical activation	90
Table 4-20 Temkin adsorption isotherm model parameters for samples from microwave and conventional chemical activation.....	91
Table 4-21 Mercury adsorption performance for raw coke and the samples from microwave chemical activation	93
Table 4-22 Mercury adsorption performance for raw coke and the samples from: conventional chemical activation	94
Table 4-23 The differences between a previous work and this study.....	95
Table 4-24 CCD-RSM for mercury (II) adsorption capacity and removal efficiency.....	99
Table 4-25 Pearson's correlation coefficient applied in microwave chemical activation.....	101



Chapter 1 Introduction



1.1 Motivation

Mercury is a toxic element. Exposure to different chemical forms of mercury results in different kinds of human diseases. Moreover, once mercury enters into the environment, it would be transformed into methylmercury and then go through a biomagnification process. Although mercury entering to waterbody from anthropogenic sources comprises little amount of total mercury entering to waterbody at the global scale, regional mercury pollution is still able to cause deadly effect on human and other animals.

Activated carbon is a widely used sorbent for removal of various of toxic substances, including mercury from water. Moreover, it has been proven that activated carbon with sulfur can improve the mercury (II) adsorption capacity. Compared with other common precursors or starting materials, waste oil sands coke containing high proportion of carbon and sulfur may be an excellent precursor. Simultaneously, oil sands coke is a waste from the process of upgrading the crude oil.

In activated carbon production process, compared with conventional chemical activation, microwave chemical activation has some advantages including heating without contact, rapid start and stop, heating from inside of the objects, as well as reducing the energy consumption. Thus, it is important to know the resulting properties of activated carbon from microwave chemical activation and compare these properties to those from convention chemical activation discussed how the power level and activation time of microwave activation influence the properties of resulting activated carbons.

Response surface methodology in combination with central composite design (CCD-RSM) is usually utilized to observe the changing process between different activation conditions. It is a useful technology to systematically understand the dependence of

activated carbon properties on the operating parameter of microwave and conventional chemical activation.

To sum up, activated carbon prepared from waste oil sands coke by microwave chemical activation might have high mercuric mercury (mercury (II)) adsorption capacity and is worth to better understand on how to optimize their production procedure.

1.2 Research Objectives

The research objectives of this study are shown as follows:

1. preparing activated carbons by microwave and conventional chemical activation and observe the change from different activation conditions;
2. discovering the differences between activated carbons from microwave chemical activation at similar S_{BET} ;
3. examining the mercury (II) adsorption performances of the prepared activated carbons, including understanding the adsorption kinetic, isotherm and adsorption capacity;
4. analyzing the influencing factors determining the mercury adsorption capacity.

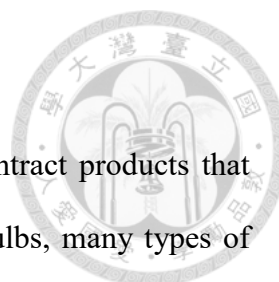
Chapter 2 Literature Review



According to the abovementioned description in Chapter 1, there are multiple terms should be introduced which is listed in Table 2-1.

Table 2-1 Terms in literature review

Title	Content
Mercury	<ul style="list-style-type: none">● Global mercury cycle● Introduction and toxicology of mercury in different chemical forms● Mercury removal technologies in aqueous solution
Activated carbon	<ul style="list-style-type: none">● Introduction and preparation of activated carbon
Mercury (II) Adsorption by Activated Carbon	<ul style="list-style-type: none">● Factors influencing the activated carbon adsorption capacity● Review of mercury (II) adsorption capacity from different adsorption condition
Waste Oil sands coke	<ul style="list-style-type: none">● Source, situation and characterization of oil sands coke● Review of activated carbon from oil sands coke
Response Surface Methodology	<ul style="list-style-type: none">● Introduction of response surface methodology and central composite design● Review of CCD-RSM applied to preparation of activated carbon



2.1 Mercury

Mercury (Hg) is a toxic element. It is usual for human to contract products that traditionally contain mercury, such as batteries, fluorescent light bulbs, many types of thermometers, thermostats, amalgam in dental fillings, thimerosal in vaccines and automotive switches (USEPA, 2016). In the US Clean Air Act Amendments (CAAA) of 1990, mercury is defined as the hazardous air pollutant (HAP) owing to its negative effects on both human health and environment (Sowlat *et al.*, 2014). Thus, preventing mercury and its compound from entering into the environment is important.

2.1.1 Global mercury cycle

Emissions of mercury may be classified into natural sources, anthropogenic sources as well as re-emission and re-mobilization of mercury (Figure 2-1).

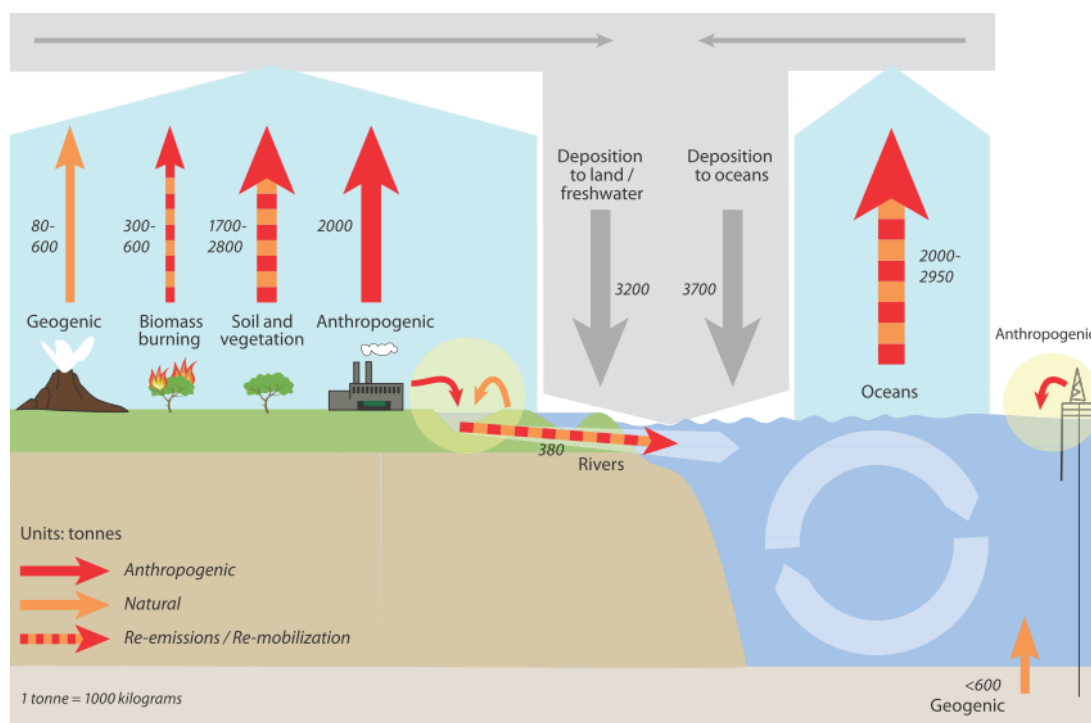
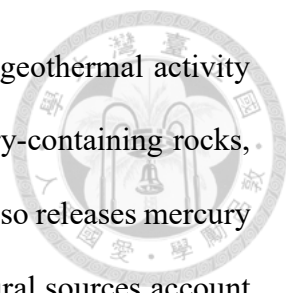


Figure 2-1 Global mercury cycle (UNEP, 2013)



There are two parts in natural sources: natural weathering and geothermal activity (UNEP, 2013). Natural weathering means the erosion of the mercury-containing rocks, which release mercury to air, lake or rivers. The geothermal activity also releases mercury from the crust to air and ocean, for instance, volcanic eruption. Natural sources account for 10% of all amount of mercury which enters the atmosphere (UNEP, 2013).

Anthropogenic sources account for 30% of all amount of mercury which enters the atmosphere. Four major anthropogenic sources (Figure 2-2) are artisanal and small-scale gold mining (24%), coal burning (24%), cement production (10%), and primary non-ferrous metal (Al, Cu, Pb, and Zn) production (8.5%) (UNEP, 2013). It is hard to control mercury emission from artisanal and small-scale gold mining, because emission sites are scattering, irregular and even unlawful (USEPA, 2016; UNEP, 2013). Coal and other fossil fuel combustion comprise about 25% anthropogenic sources of mercury. Coal-fired power plants comprise about 16% anthropogenic sources of mercury (Landis *et al.*, 2014; UNEP, 2013).

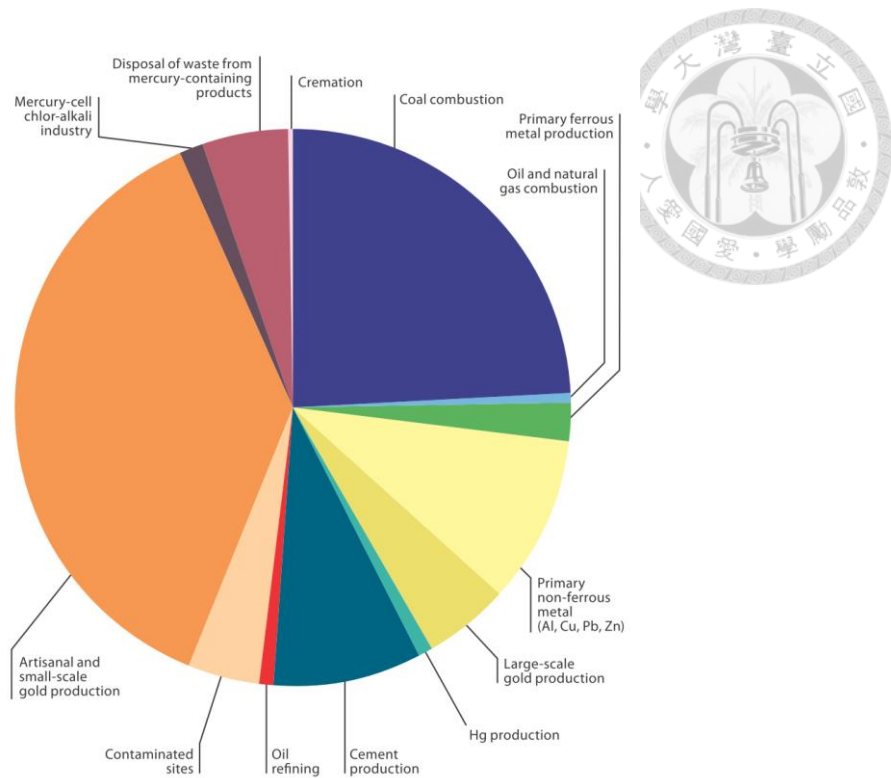
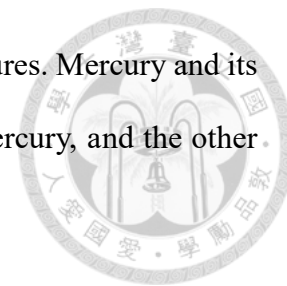


Figure 2-2 Estimated emissions to air from anthropogenic sources in 2010 (UNEP, 2013)

Re-emission and re-mobilization of mercury account for 60% of all amount of mercury which enters the atmosphere. Re-emission of mercury means that after mercury deposited on soils, surface waters and vegetation, mercury returns to the air. For example, burning of biomass would release mercury to the air. Re-mobilization means that after mercury deposited on soils or sediments, it enters or re-enters to the aquatic system. For instance, rain washes mercury from soil and enters to the river. Re-emission and re-mobilization of mercury can not be regarded as natural sources or anthropogenic sources, because it is hard to identify their sources. Nevertheless, human activities such as land use and the increase of global temperature also raise the emission of mercury (UNEP, 2013).

After mercury enters into the environment, the physical and chemical reaction would

happen, which might change toxicity and pathways of human exposures. Mercury and its compounds can be divided into two categories. One is inorganic mercury, and the other is organic mercury.



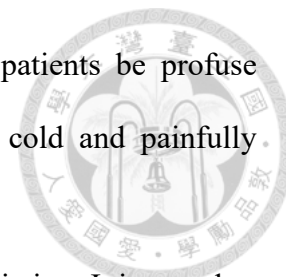
2.1.2 Inorganic mercury

The inorganic forms of mercury contain liquid metallic mercury and mercury vapor, mercurous mercury and mercuric mercury and dental amalgam. Directly ingesting liquid metallic mercury is not obviously toxic, because mercury is hard to be absorbed from the gastrointestinal tract (Clarkson and Magos 2006; Cantor, 1951). However, mercury vapor from metallic mercury may cause health hazards.

Mercury vapor (Hg^0) is stable and able to remain in the atmosphere for a long time because of its chemical stability. After mercury vapor is inhaled by lung, all tissues in the body will be well distributed, because uncharged monatomic gas is high diffusible and lipid soluble. Then, there are two processes in the body. First, dissolved mercury vapor in the bloodstream would cross the blood-brain and placental barriers, which would affect brain function. Second, dissolved mercury would be oxidized to mercuric mercury. For acute toxicity, mercury vapor exposure cause dyspnea, and then paroxysmal cough, chest pain, pulmonary infiltration, chills, nausea, and vomiting (Clarkson and Magos 2006). For chronic toxicity, if mercury concentration of urine is in the range of 50 to 100 $\mu\text{g/L}$, kidney and nervous system would hurt, causing insomnia, memory disturbances, irritability, and fatigue (WHO, 1991).

Mercurous mercury (Hg_2^{2+}) is a category of compounds containing Hg-Hg^{2+} . For instance, mercurous chloride (calomel) used as a laxative and teething powders. Once mercurous chloride enters the body, the mercuric ion will be released. Then mercuric ion is separated into uncharged mercury Hg^0 and mercuric ion (Hg^{2+}). It is mercuric ion that has been regarded as a major substance causing laxative, and antiseptic action. Pink

disease (acrodynia) was described in 1920. Pink disease makes patients be profuse sweating, and marked reddening of the extremities, which were cold and painfully sensitive to touch.

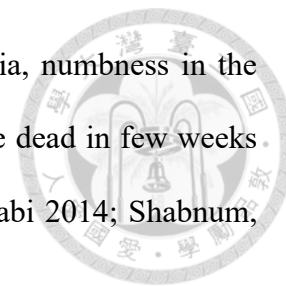


Water-soluble mercuric mercury (Hg^{2+} or mercury (II)) is a toxic ion. It is mortal to ingest only 1 gram of mercuric mercury. Taking in 1 gram of mercuric mercury would make the kidney function completely lost. On the other side mercuric mercury is also able to cause stomatitis and gastroenteritis. As for occupational exposure utilization of mercuric mercury in diaper washes, it attributes acrodynia (Clarkson and Magos 2006; Warkany and Hubbard, 1953).

2.1.3 Organic mercury

There are three parts in organic mercury: methylmercury, ethylmercury and other organomercurials. Methylmercury in this thesis refers to monomethylmercury compounds. Humans are often exposed from consumption of fish and marine mammals. In global mercury cycle, after inorganic mercury dissolved in rain drops enters into fresh and ocean water, it will subside into aquatic sediments. Then owing to the methylation of inorganic mercury by microorganisms in sediments, methylmercury exists in sediments and enters into food chain so that methylmercury exists in most of the aquatic species (Kim *et al*, 2016; Burger and Gochfeld, 2011). As soon as methylmercury enters into aquatic species, it goes through a biomagnification process, which means that methylmercury concentration in aquatic species increases, as its level of a food chain increases. Through total mercury in blood or hair, we could understand the mercury levels in the brain (Kim *et al*, 2016; Clarkson and Magos 2006). One of the most widely known cases is Minamata disease in Japan. Because of the release of mercury from Chisso Corporation's chemical factory for the production of acetaldehyde, local populace ate shellfish and fish containing methylmercury in Minamata Bay and the Shiranui Sea. One

who suffers from Minamata disease has syndromes including ataxia, numbness in the hands and feet, muscle weakness and so on. Extremely, they will be dead in few weeks after syndromes happen (Eto, 1997; Almeida and Stearns, 1998; Nabi 2014; Shabnum, 2014).



Diethylmercury was used for the treatment of syphilis, but then it was found that it would hurt the central nervous system, for example, Patient are incoordination of movement. There is also a case in rural Iraq in the 1950s. They used ethylmercury p-toluene sulfanilamide as a fungicide in wheat seeds, which were utilized in bread preparation. The symptoms are similar to symptoms of exposure to methylmercury. Moreover, kidney damage like albuminuria and syndrome are also proven in clinical experiments (Clarkson and Magos 2006).

Other organomercurials are also used as preservatives and antifungal agents but usage amount of organomercurials has decreased because of the stricter regulations of mercury compounds (Clarkson and Magos 2006).

2.1.4 Mercury removal from water

Mercury removal technologies include phytoremediation, constructed wetlands, bioremediation, activated carbon adsorption, adsorbents from agricultural and forest wastes, manganese sand, ion-exchange resins, polythiol-functionalized alumina membranes, nanoporous adsorbent materials, crown thioethers, polymeric chelating fibers and extraction from aqueous solutions (Atwood and Zaman, 2006). Among these technologies, activated carbon has been commonly used for removal of metal ions including mercury from aqueous solution because it is effective (Attari *et al.*, 2016; Rao *et al.*, 2009; Zhang *et al.*, 2005; Yardim *et al.*, 2003; Mohan *et al.*, 2001; Gomez-Serrano *et al.*, 1998). However, application of activated carbon also has some disadvantages, such as the high cost for large scale and difficulty in preparation and regeneration processes

(Attari *et al.*, 2016; Zhang *et al.*, 2005).





2.2 Activated Carbon

2.2.1 Introduction

Activated carbons with the high surface area have been commonly applied in different fields including removal of toxic substances from water and air, separating/purifying liquids and gases and being catalyst and catalyst support (Torres-Pérez *et al*, 2015; Yang *et al*, 2010).

2.2.2 Preparation of activated carbon

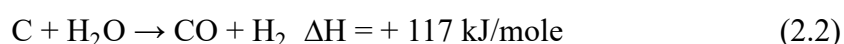
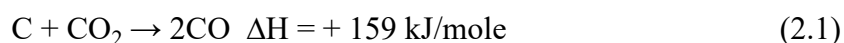
Activated carbons are prepared from carbon-containing precursors such as cokes, coal and agricultural residues. After precursors are carbonized and activated, activated carbons will be produced. These two processes are called carbonization (or pyrolysis) and activation (or oxidation). Moreover, if precursors are simultaneously carbonized and activated, this process would be called “One step carbonization/activation process” (Ioannidou and Zabaniotou, 2007; Marsh and Reinoso, 2006).

Carbonization means heating the raw material with the high level of carbon content at temperatures below 1000°C commonly in the range of 600-900°C in the condition with inert gases without oxygen. Through carbonization, the raw material changes into tars, oils, gases and a carbonized material, which is called char. Compared to raw material, char contains less oxygen, hydrogen, nitrogen, and sulfur, because they are mostly removed as volatile gaseous products. Carbon atoms in char exist as flat aromatic sheets that are cross-linked randomly. The porosity of activated carbon is developed due to randomly cross-linked flat aromatic sheets during activation process (Cecen, 2014; Marsh and Reinoso, 2006).

The pore structure needs to be further developed by oxidation. This oxidation process is called activation or oxidation. Although it is an oxidation process, char can't

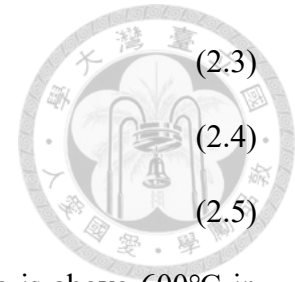
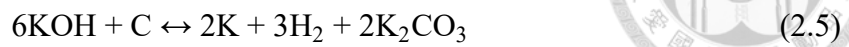
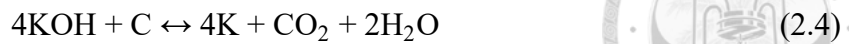
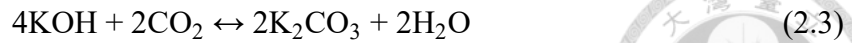
be heated with molecular oxygen, because it is hard to control carbon reacting with molecular oxygen, which causes burning, even flames and then is not capable of penetrating into the interior of the carbon. During activation/oxidation process, char is able to develop a great number of micropores, highly porous structure and high surface area. These three properties contribute that activated carbon is an excellent adsorbent. There are two types of on activation procedures: thermal/physical activation or chemical activation (Cecen, 2014; Marsh and Reinoso, 2006).

Thermal/Physical activation is defined as heating char with either carbon dioxide or steams or both of them at 800-1000°C. This process leads two major reactions shown in equation (2.1) and (2.2) (Marsh and Reinoso, 2006).



Chemical activation is defined as that after char was impregnated with chemical agent, the mixture is heated to temperatures of 400-800°C. Finally, activated carbon is prepared after the heated mixture was washed repeatedly (Cecen, 2014). Compared to physical activation, chemical activation has some advantages: lower temperature for pyrolysis, activated carbon preparation in only one step, higher yield and higher surface area (Lillo-Ródenas *et al.*, 2003).

Activation with KOH is a common method to prepare highly developed porosity (Lu *et al.*, 2010). The activation mode of KOH is summarized below. First, activation would happen at temperatures above 700°C. Second, when the impregnation ratio (IR) increases, the development of porosity increases. Third, after narrow microporosity was developed, the wider microporosity is developed by widening the narrow micropore (Marsh and Reinoso, 2006). The reactions of KOH activation are described in equation (2.3), (2.4) and (2.5).



Lu *et al.* (2010) revealed that when the activation temperature is above 600°C in heating process, all KOH has been transformed into K₂CO₃. Then, K₂CO₃ is transformed in to K₂O and K, which results in the S_{BET} increases sharply at 600-730°C.

There are two heating ways: conventional heating and microwave heating. The conventional heating applied in the preparation of activated carbon uses the tubular furnace and heats objects by convection, conduction and radiation mechanisms. Conventional heating means that the heating the material from the outside, which causes temperature gradient from the surface to interior. Thus, in order to reduce the temperature gradient effect, tubular furnace should be operated at the slow heating rate so that it would take more energy in the heating process (Hesas *et al.*, 2013).

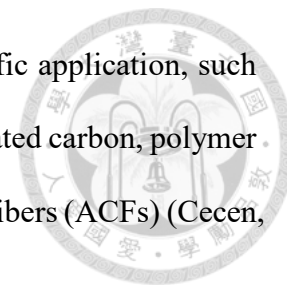
Microwave is defined as an electromagnetic wave of high frequency at 300 MHz to 300 GHz. Microwave has wave lengths from 10⁻³ m~1 m and general microwave ovens operate at a frequency 2.45 GHz corresponding to a wavelength of 12.2 cm (Jones *et al.*, 2002; Hesas *et al.*, 2013).

In the comparison of conventional heating, microwave heating has some advantages: heating without contact, rapid start and stop, heating from inside of the objects, reducing the energy consumption (Menéndez, *et al.* 2010; Saucier, *et al.* 2015).

2.2.3 Types of activated carbon

Based on the particle size, activated carbon can be classified to powder activated carbon (PAC) and granular activated carbon (GAC). The particle size of PAC is less than 100 μm, and the common particle size of PAC is in the range of 15-25 μm. The mean particle size of GAC is in the range of 1-5 mm.

There are also the specific forms of activated carbon for specific application, such as extruded activated carbon (EAC), bead activated carbon, impregnated carbon, polymer coated carbon, activated carbon cloths (ACCs) and activated carbon fibers (ACFs) (Cecen, 2014).



2.2.4 Physical and chemical characterization of activated carbon

As far as adsorption of metal cations is concerned, there are several characteristics influencing the adsorption capacity, including surface area, pore size distribution (PSD), electrokinetic properties, and the surface functional groups and the nature of the metal ions in the solution (Bansal and Goyal, 2005).

Surface area: International Union of Pure and Applied Chemistry (IUPAC) defined micropores as pores with the width lower than 2 nm, mesopores as pores with the width between 2-50 nm, and macropores as pores with the width larger than 50 nm. According to different carbonization and activation conditions, the surface area and pore volumes of activated carbon are various. The internal surface of activated carbon is one of the factors influencing adsorption abilities. The most used measurement method of internal surface is called the Brunauer-Emmett-Teller (BET) area, and the BET area per unit weight is defined as the specific surface area (S_{BET}). The BET area is measured by the amount of nitrogen (N_2) adsorbed at given pressure and at 77K (Cecen, 2014).

Total pore volume and pore size distribution (PSD): Total pore volume and PSD should be considered for seeking the causes of adsorption capacity. PSD is defined as the distribution of the pore volume with respect to pore radius (Cecen, 2014).

Surface functional groups: Surface functional groups also plays an important role of adsorption. The edges of the aromatic sheets in an activated carbon contain unpaired electrons and residual valencies, which are active sites. These sites are able to interact with different species such as hydrogen, nitrogen, and sulfur to produce different types of

surface groups (Cecen, 2014).



2.3 Mercury (II) Adsorption by Activated Carbon

Mercury (II) adsorption by activated carbon from aqueous solution depends on two major categories of factors. One is adsorption condition, and the other consists of many characteristics of activated carbon.

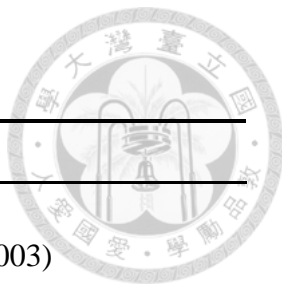
2.3.1 Adsorption condition

Adsorption condition contains initial concentration of Hg^{2+} , pH, activated carbon dosage, solution temperature (Abdelouahab-Reddam *et al.*, 2014; Wajima and Sugawara, 2011; Cai and Jia, 2010; Rao *et al.*, 2009; Zabihi *et al.*, 2009; Budinova *et al.*, 2008, Yardim *et al.*, 2003).

Adsorption capacity in this thesis means that when the mercury (II) concentration of the solution does not change, the amount of adsorbed mercury (II) per unit weight of activated carbon. The unit of adsorption capacity is $\text{mg-Hg}^{2+}/\text{g-AC}$.

Activated carbon dosage in this thesis means activated carbon weight added in per unit volume of solution. The unit of activated carbon dosage is g/L . Rao *et al.* (2009) shown that when the activated carbon dosage increases, the adsorption capacity decreased. Table 2-2 shows the studies that applied carbon materials on the removal of mercury (II). Table 2-2 can help this research to determine the adsorption condition and check whether the result of adsorption experiment is reasonable.

Table 2-2 Review of mercury (II) adsorption capacity from different adsorption condition



Type of activated carbon	Adsorption conditions	Adsorption capacity (mg-Hg ²⁺ /g-AC)	reference
Furfural activated by H ₂ SO ₄	Initial conc.: 10-40 mg-Hg ²⁺ /L AC dosage: 0.2 g/L pH: 5.5	42-174	(Yardim <i>et al.</i> , 2003)
Waste antibiotic material activated by K ₂ CO ₃	Initial conc.: 10-40 mg-Hg ²⁺ /L AC dosage: 0.2 g/L pH: 5.5	45-105	(Budinova <i>et al.</i> , 2008)
Walnut shell activated by ZnCl ₂	Initial conc.: 9.7-107 mg-Hg ²⁺ /L AC dosage: 1 g/L pH: 5.0	10-100	(Zabihi <i>et al.</i> , 2009)
Agricultural by-product/waste activated by steam	Initial conc.: 40 mg-Hg ²⁺ /L AC dosage: 4-6 g/L pH: 7	22.88-25.88	(Rao <i>et al.</i> , 2009)
Oil-sands fluid coke activated by KOH-SO ₂	Initial conc.: 100 mg-Hg ²⁺ /L AC dosage: 1 g/L pH: 4.8-5.0	43-72	(Cai and Jia, 2010)
Coal impregnated with K ₂ S	Initial conc.: 4814.2 mg-Hg ²⁺ /L Carbon dosage: 10 g/L pH: not reported	112.5-171.7	(Wajima and Sugawara, 2011)
Activated carbons impregnated with Na ₂ S or H ₂ SO ₄	Initial conc.: 20 mg-Hg ²⁺ /L AC dosage: 5 g/L pH: 2	3.57-4.01	(Abdelouahab-Reddam <i>et al.</i> , 2014)



2.3.2 Characteristics of activated carbon

Characteristics of activated carbon contain three parts: particle size, physical properties, and surface chemistry.

Several studies supposed that the larger the particle size has, the less ion the activated carbon adsorbs (Sekar *et al.*, 2004; Krishnan and Anirudhan, 2002; Mohan *et al.*, 2001).

Physical properties contain S_{BET} , specific pore volume and PSD.

Cai and Jia (2010) and Ekinici *et al.* (2002) indicated that adsorption capacity increases as S_{BET} increases. However, Lu *et al.* (2014) hold a contrary opinion. They thought S_{BET} isn't a key factor for mercury adsorption from their results. In my opinion, the S_{BET} ranges of Cai and Jia (2010) and Ekinici *et al.* (2002) are 13-2505 m^2/g and 460-1100 m^2/g , which are larger than the S_{BET} range of Lu *et al.* (2014): 797-870 m^2/g . In addition, in the narrow scale S_{BET} , Cai and Jia (2010) is not able to predict that S_{BET} has a positive correlation with adsorption capacity (Figure 2-3). Thus, whether S_{BET} is a key factor depends on the scale of the S_{BET} range. Furthermore, Zhang *et al.* (2005) regard the higher adsorption capacity can be attributed to the higher S_{BET} and larger micropore volume.

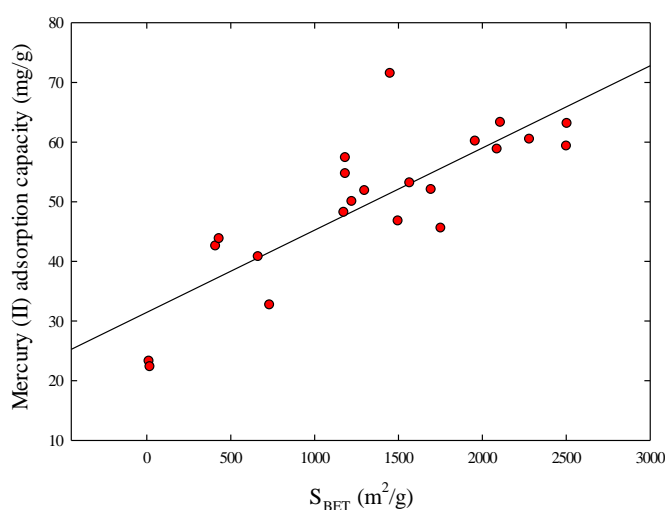
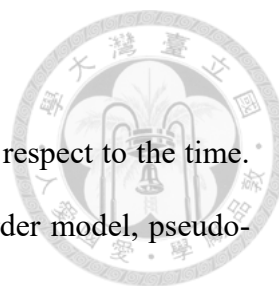


Figure 2-3 Effect of S_{BET} on mercury (II) adsorption capacity (Cai and Jia, 2010)

Surface chemistry of activated carbon plays an important role on mercury (II) adsorption. Lu *et al.* (2014) indicated that the ratio of micropores and acidic surface functional groups influenced the adsorption capacity. Abdelouahab-Reddam *et al.* (2014) indicated that compared with raw activated carbon, activated carbon impregnated with Na₂S and H₂SO₄ can raise the mercury (II) adsorption capacity. Cai and Jia (2010) shows that activated carbon which is derived from fluid coke by KOH-SO₂ activation also increases the mercury (II) adsorption capacity, as the amount of sulfur content per unit S_{BET} increases.



2.3.3 Adsorption kinetic model

In order to realize the adsorption amount of the adsorbent with respect to the time. Three kinetic models are usually used to describe it: pseudo-first-order model, pseudo-second-order model, and the Elovich kinetic model.

The pseudo-first-order model. The pseudo-first-order model equation is given as equation (2.6). The linear form of pseudo-first-order model equation is given as equation (2.7). Terms in the pseudo-first-order model equation are described in Table 2-3. There is a boundary condition in the derivation process from equation (2.6) to equation (2.7): when t equals to zero, q_t equals to zero (Azizian, 2004).

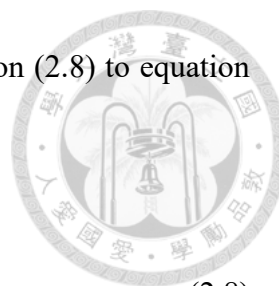
$$dq_t / dt = k_1(q_{e1} - q_t) \quad (2.6)$$

$$\ln(q_e) - \ln(q_{e1} - q_t) = k_1 t \quad (2.7)$$

Table 2-3 Pseudo-first-order model

	Unit	Definition
t	min	Agitation time
q_{e1}	mg-Hg ²⁺ /g-AC	Amount of mercury (II) adsorbed per unit mass of added activated carbon at equilibrium (from experiment)
q_t	mg-Hg ²⁺ /g-AC	Amount of mercury (II) adsorbed per unit mass of added activated carbon at time t
k_1	1/min	Model constant

The pseudo-second-order model. The pseudo-second-order model equation is given as equation (2.8). The linear form of pseudo-second-order model equation is given as equation (2.9). Terms in the pseudo-first-order model equation are described in Table 2-4.



There is a boundary condition in the derivation process from equation (2.8) to equation (2.9): when t equals to zero, q_t equals to zero.

$$dq_t / dt = k_2(q_{e2} - q_t)^2 \quad (2.8)$$

$$t / q_t = 1 / (k_2 \times q_{e2}^2) + t / q_{e2} \quad (2.9)$$

Table 2-4 Pseudo-second-order model

	Unit	Definition
t	min	Agitation time
q_{e2}	mg-Hg ²⁺ /g-AC	Amount of mercury (II) adsorbed per unit mass of added activated carbon at equilibrium (from regression)
q_t	mg-Hg ²⁺ /g-AC	Amount of mercury (II) adsorbed per unit mass of added activated carbon at time t
k_2	g/mg-min	Model constant

The Elovich kinetic model was first established for the gas adsorption. Recently, it was also used in adsorption in aqueous solution (Attari *et al.*, 2016; Allen and Scaife, 1966).

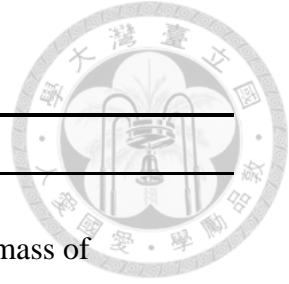
The Elovich kinetic model equation is given as equation (2.10). The linear form of Elovich kinetic model is given as equation (2.11) (Allen and Scaife 1966). Terms in the Elovich kinetic model equation are described in Table 2-5. In the derivation process from equation (2.10) to equation (2.11), there is a step: when the value of $\alpha \times \beta \times t$ is far larger than 1, then the equation (2.11) is built. Thus, after α and β were calculated, the value of $\alpha \times \beta \times t$ must be checked.

$$dq_t / dt = \alpha e^{-\beta q_t} \quad (2.10)$$

$$q_t = \ln(\alpha \beta) / \beta + \ln(t) / \beta \quad (2.11)$$

Table 2-5 Elovich kinetic model

	Unit	Definition
t	min	Agitation time
q _t	mg-Hg ²⁺ /g-AC	Amount of mercury (II) adsorbed per unit mass of added activated carbon at time t
α	mg/g-min	Model constant
β	g/mg	Model constant





2.3.4 Adsorption isotherm model

Adsorption isotherm models are used to describe adsorption capacity for specific pollutant such as heavy metal at equilibrium and given temperature (Attari *et al.*, 2016).

There were three models commonly used in adsorption isotherm experiment: Langmuir model, Freundlich model, and Temkin model.

Langmuir model is a rational formula, which has several assumptions: (1) all the active sites are equivalent, distinguishable and independent on the sorbents, (2) a molecule can only be bound on one active site, (3) molecules on the active site don't interact with each other. The Langmuir equation is given as equation (2.12). The linear form of Langmuir equation is given as equation (2.13). Terms in the Langmuir equation are described in Table 2-6.

$$q_e = q_m \times (K_L C_e) / (1 + K_L \times C_e) \tag{2.12}$$

$$C_e / q_e = 1 / (q_m \times K_L) + C_e / q_m \tag{2.13}$$

Table 2-6 Langmuir adsorption isotherm model

Unit	Definition
C_e mg-Hg ²⁺ /L	Mercury (II) concentration of solution at equilibrium
q_e mg-Hg ²⁺ /g-AC	Amount of mercury (II) adsorbed per unit mass of added activated carbon at equilibrium
q_m mg-Hg ²⁺ /g-AC	Monolayer adsorption capacity
K_L L/mg	Model constant

Freundlich model is an empirical model. The Freundlich equation it is given as equation (2.14). The linear form of Freundlich equation is given as equation (2.15). Terms the in Freundlich equation are described in Table 2-7.



$$q_e = K_F C_e^{1/n_f} \quad (2.14)$$

$$\ln(q_e) = \ln(K_F) + (1/n_f) \times \ln(C_e) \quad (2.15)$$

Table 2-7 Freundlich adsorption isotherm model

	Unit	Definition
C_e	mg-Hg ²⁺ /L	Mercury (II) concentration of solution at equilibrium
q_e	mg-Hg ²⁺ /g-AC	Amount of mercury (II) adsorbed per unit mass of added activated carbon at equilibrium
K_f	(mg-g)×(mg/L) ^{-1/n_f}	Model constant
n_f	dimensionless	Model constant

The assumptions of Temkin model: (1) heat of adsorption of all molecules in the layer decreases linearly as the surface coverage increases. (2) The binding energy distribution is uniform. The Temkin equation it is given as equation (2.16). Terms in the Temkin equation are described in Table 2-8.

$$q_e = K_1 \ln(K_2) + K_1 \ln(C_e) \quad (2.16)$$

Table 2-8 Temkin adsorption isotherm model

	Unit	Definition
C_e	mg-Hg ²⁺ /L	Mercury (II) concentration of solution at equilibrium
q_e	mg-Hg ²⁺ /g-AC	Amount of mercury (II) adsorbed per unit mass of added activated carbon at equilibrium
K_1	mg/g	Model constant
K_2	L/g	Model constant

2.4 Waste Oil sands coke

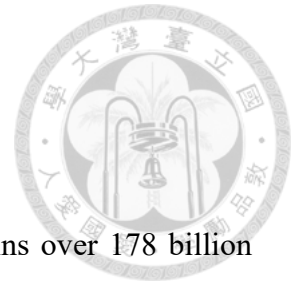
2.4.1 Oil sands

Alberta, which is one of the largest proven oil reserves contains over 178 billion barrels. Oil sands are a mixture of 10-18% bitumen, quartz sand, clay, 3-5% water and trace minerals. Bitumen is capable of being extracted from the oil sands and upgrading synthetic crude oil. There are three steps for upgrading synthetic crude oil from oil sands: coking, desulphurization and hydrogen addition. It is the step, coking, that will produce the coke rich in carbon (Chen and Hashisho 2012a; Engelhardt and Todirescu 2005).

2.4.2 Oil sands coke

Oil sands coke also named petroleum coke is a byproduct of upgrading crude oil from oil sand. Oil sands cokes have different types, and it can be mainly categorized as delayed coke and fluid coke, because of two major coking technologies: delayed coking and fluid coking. These two processes are different. Delayed coking is a semi-batch process and fluid coking is a continuous process. Delayed coke is produced at 688-723K (415-450°C) and fluid coke is produced at 753-838K (480-565°C). Compared with delayed coke, fluid coke is produced at the higher temperature causing that fluid coke has much graphite-like structure and lower content of volatiles (Hill *et al.*, 2014; Rambabu *et al.*, 2013; Burrowes *et al.*, 2011; Cai, 2010).

The morphologies (Figure 2-4) of fluid coke and delayed coke shows that fluid coke particles are more spherical and delayed coke particles are irregular form and chunky. Figure 2-4 shows the delayed coke which has been ground. The several elemental analysis of fluid coke and delayed coke are shown in Table 2-9. Cokes contains 78.5-86.1% carbon, which means that coke is a good precursor of activated carbon because it doesn't have to be carbonized before activation. In other words, it can reduce the consumption of energy.



Simultaneously, it contains 3.8-10.6% sulfur, which is helpful for removal of mercury (II) from aqueous solution.

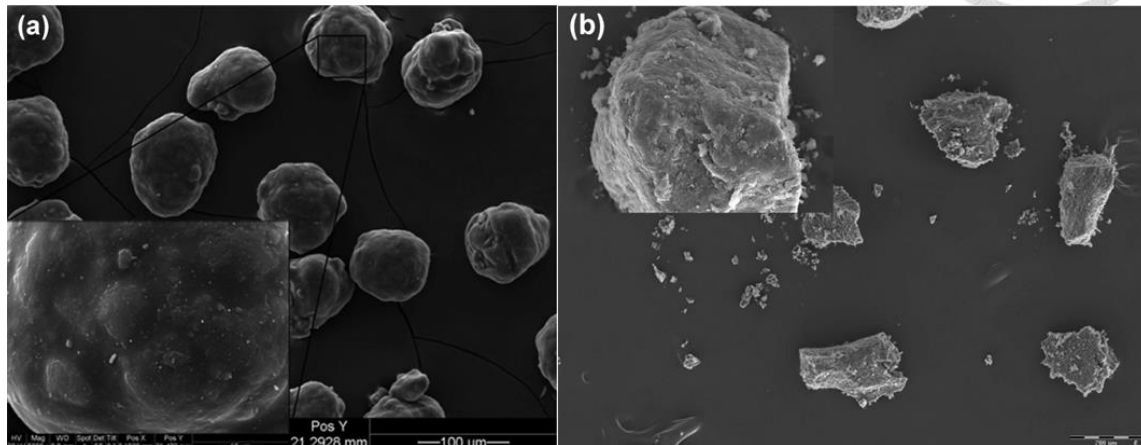


Figure 2-4 SEM images of (a) Fluid coke and (b) Delayed coke (Hill *et al.*, 2014)

Table 2-9 Elemental analysis of cokes

Type of coke	Elemental analysis (wt%)					Reference
	C	N	S	H	O	
Fluid coke	84	1.9	2.2	7.5	4.8	(Hill <i>et al.</i> , 2014)
Delayed coke	84	3.8	1.8	6.5	3.8	
Fluid coke	78.5	1.8	7.2	1.9	10.6	(Chen and Hashisho, 2012a)
Delayed coke	82.3	1.6	6.8	3.7	5.7	
Fluid coke	82.7		7.4		6.4	(Cai, 2010)
Fluid coke	86.1		1.8		9.8	

Some oil sands coke is used as fuel for boilers, but most of it is stockpiled. By the end of 2012, 77 million tons of oil sands coke has been stockpiled, which has occupied a great amounts of lands (Hill *et al.*, 2014; Burrowes *et al.*, 2011). Moreover, oil sands coke as fuel is misdoubted for its high sulfur content, which may lead to the emission of sulfur oxides. Table 2-10 shows activated carbon derived from oil sands coke in recent years.

Zhang *et al.*, (2015) shown that when IR is 1 and activation condition is 800°C for 1 hour by tube furnace, the S_{BET} is 986 m²/g.

Kawano *et al.*, (2008) shown that when IR is 2 and activation condition is 500°C for 1 hour by tube furnace the S_{BET} is 142 m²/g.

Chen and Hashisho (2012a) shown that when IR is 1 and activation condition is 616 W for 10 min by microwave the S_{BET} is 1131 m²/g.

Chen and Hashisho (2012b) shown that when IR is 1 and activation condition is 616 W for 40 min by microwave the S_{BET} is 1163 m²/g. Thus, the S_{BET} would increase little between 10 min and 40 min.

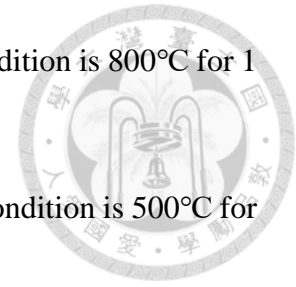
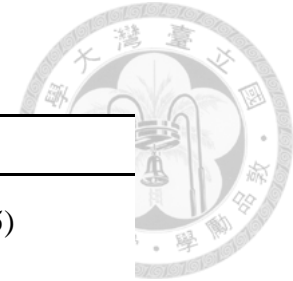


Table 2-10 Review of activated carbon from oil sands coke



Precursor	Activation method	Condition	Time	S _{BET} (m ² /g)	Reference
Petroleum coke	KOH : Coke 1 : 1-7 : 1	800°C (tube furnace)	1 hr	986-2859	(Zhang <i>et al.</i> , 2015)
Delayed coke	CO ₂	900°C (tube furnace)	2-15 hr	50-646	(Karimi <i>et al.</i> , 2013)
Delayed coke	KOH : Coke 1 : 1	616W (microwave)	10 min	1131	(Chen and Hashisho 2012a)
Fluid coke	KOH : Coke 1 : 1	616W (microwave)	10 min	440	
Delayed coke	KOH : Coke 1 : 1	616W (microwave)	40 min	1163	(Chen and Hashisho 2012b)
Fluid coke	KOH : Coke 1 : 1	616W (microwave)	40 min	658	
Petroleum coke (Three sources)	KOH : Coke 5 : 1	500°C (tube furnace)	1 hr	275-791	(Kubota <i>et al.</i> , 2011)
Petroleum coke	KOH : Coke 2 : 1	500-800°C (tube furnace)	1 hr	142-990	(Kawano <i>et al.</i> , 2008)



2.5 Response Surface Methodology

Response surface methodology (RSM) is one of the design of experiment. It is consisted by a group of mathematical and statistical techniques and usually applied on optimizing the operating parameters to the desired result. RSM is able to establish the relationship between the y (response) and $x_1, x_2, x_3, \dots, x_k$ (factors). Where k means the number of the factors. Thus, the graph can be drawn like Figure 2-5.

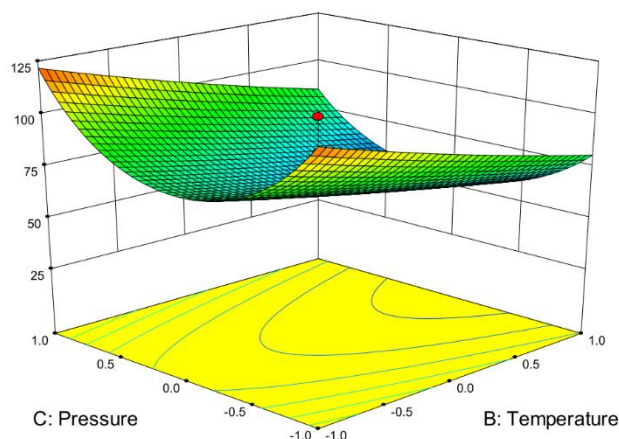


Figure 2-5 Figure of RSM (Anderson and Whitcomb, 2007)

There are two common models, which are used in RSM: first-degree model (2.17) and second-degree model (2.18).

$$y = a_0 + \sum_{i=1}^k a_i x_i + \epsilon \quad (2.17)$$

$$y = a_0 + \sum_{i=1}^k a_i x_i + \sum_{i < j} a_{ij} x_i x_j + \sum_{i=1}^k a_{ii} x_i^2 + \epsilon \quad (2.18)$$

Where k is the number of variables, a_0 is the constant term, a_i is the coefficients of the linear parameters, x_i represents the factors, and ϵ is the residual associated with the experiments.

Utilizing RSM combination with central composite design (CCD-RSM) is one of the most frequent designs (Khuri and Mukhopadhyay, 2010).

CCD is composed of the following three portions. Factorial portion (F): number of factorial portions is 2^k . Where k is the number of variables. In Figure 2-6, it shows as black points (●). Axial portion: number of axial portions is $2k$. In Figure 2-6, it shows as white circle points (○) without center points. Center points: number of center points (□) is n_0 . Thus, total experiment number (N) is required as $N=2^k+2k+n_0$.

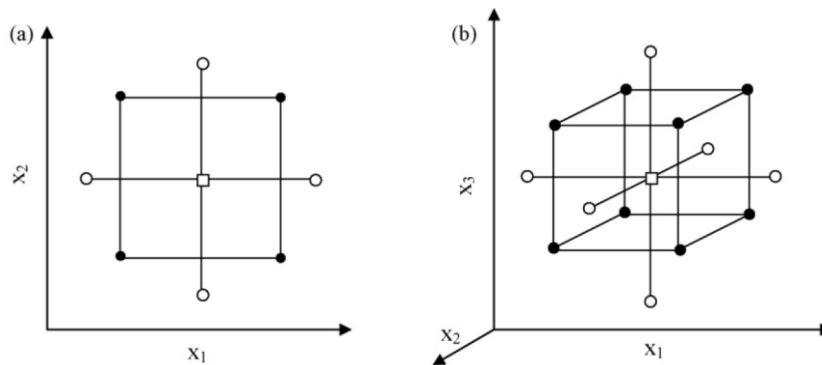


Figure 2-6 CCD for (a) two variables and (b) three variables (Bezerra *et al.*, 2008).

It can be observed that there are five points at any factor axis. The value of these five points are $(-\alpha, -1, 0, +1, +\alpha)$. α is calculated by $\alpha=F^{1/4}$. Where F= number of factorial portions so that $\alpha=2^{2k/4}$. For two factors, three factors and four factors, α is 1.414, 1.682 and 2.000. Among these five value, $+\alpha$ means the maximum of the factor value and $-\alpha$ means the minimum of the design value.

Table 2-11 shows the recent studies of preparation of activated carbon using CCD-RSM.

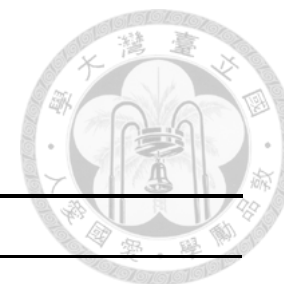


Table 2-11 Review of CCD-RSM used in preparation of activated carbon

Precursor	Factors			Reference
Moso bamboo	Temperature	Activation time	-	(Huang <i>et al.</i> , 2015)
Albizia lebbeck seed pods	Power (W)	Activation time	Impregnation ratio	(Ahmed and Theydan, 2014)
Olive stone	Power (W)	Activation time	Impregnation ratio	(Alslaibi <i>et al.</i> , 2013)
Peanut hull	Power (W)	Activation time	Impregnation concentration	(Zhong <i>et al.</i> , 2012)
Palm shell	Temperature	Activation time	Impregnation ratio	(Arami-Niya <i>et al.</i> , 2012)
Bamboo waste	Temperature	Activation time	Impregnation ratio	(Ahmad and Hameed, 2010)
Oil palm fronds	Temperature	Activation time	Impregnation ratio	(Salman and Hameed, 2010)

Chapter 3 Materials and Methods



3.1 Research Framework

Figure 3-1 illustrates the procedures of this research. Through literature review, the basic properties of oil sands coke were known, the activation conditions of both microwave chemical activation and conventional chemical activation were set, the adsorption conditions were set. In order to compare microwave chemical activation with conventional chemical activation, they must have the property in common. The S_{BET} was chosen for their comparison.

CCD-RSM was used in observed the process of change. Yield, S_{BET} and sulfur content are set as the response. Factors in microwave chemical activation are power level and activation time. Factors in conventional chemical activation are temperature and activation time.

Through the characterization of activated carbon, some of the prepared activated carbon would be chosen for fitting mercury (II) adsorption kinetic model and adsorption isotherm model. All activated carbon samples were used to do the mercury (II) adsorption capacity experiments.

The causes of adsorption capacity would be analyzed from all the characterizations of prepared activated carbon.

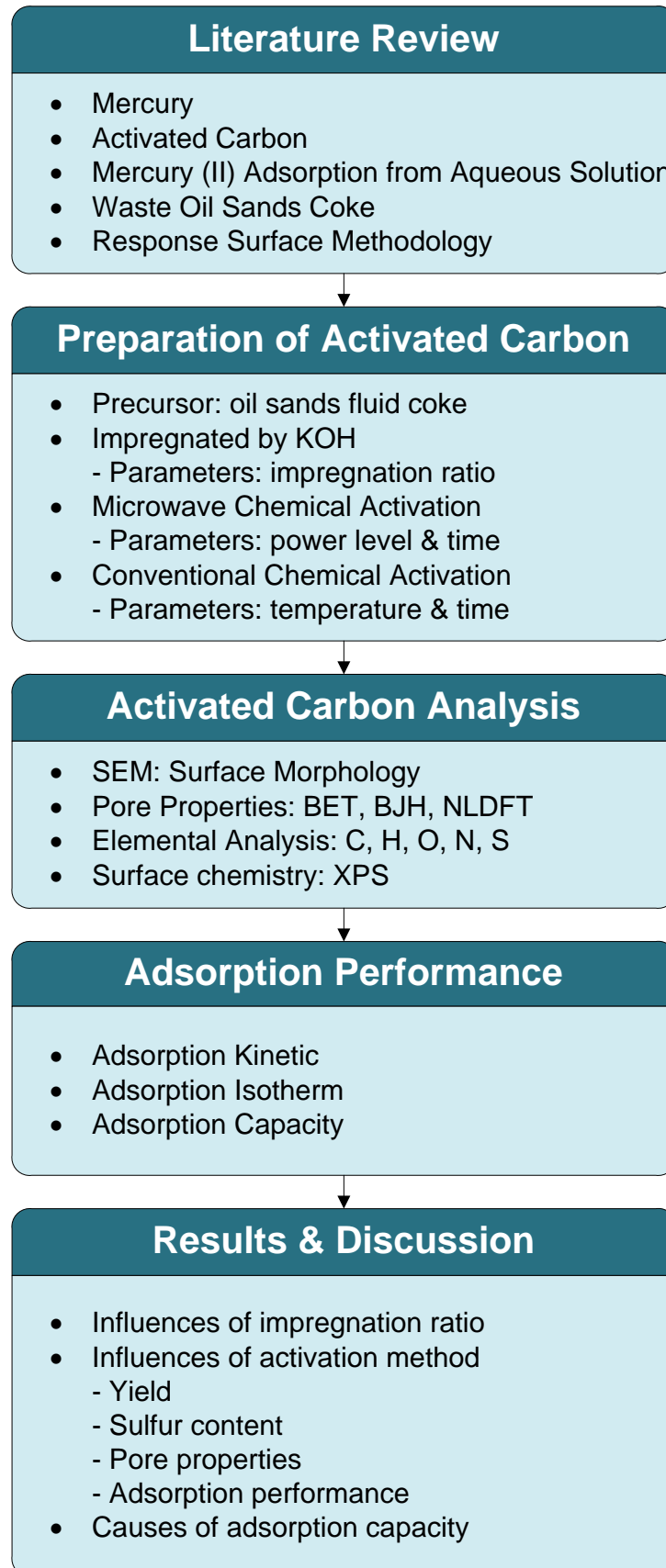


Figure 3-1 Research framework



3.2 Design of Experiment

3.2.1 Preparation of activated carbon

In order to prepare the activated carbon with similar S_{BET} by two different activation methods, the power level of microwave muffle furnace was set from 600 W to 1000 W and the activation time was set from 4 min to 16 min for microwave chemical activation. The activation temperature was set from 400°C to 800°C and the activation time was set from 30 min to 150 min for conventional chemical activation.

The experiment was designed by CCD-RSM from MINITAB 14 (Table 3-1 and Table 3-2). The result of the design of experiment was also analyzed by MINITAB 14.

The difference between the value from the experiment (V_e) and from the CCD-RSM ($V_{CCD-RSM}$) was expressed by error (%):

$$\text{Error (\%)} = (V_{CCD-RSM} - V_e) / V_{CCD-RSM} \times 100\% \quad (3.1)$$

Table 3-1 CCD-RSM used in microwave chemical activation

Run	Coded value		Actual value	
	Factor1	Factor2	Microwave chemical activation	
			Activation time (min)	Power level (W)
1	-1.4142	0	4.00	800.00
2	-1	-1	5.76	658.58
3	-1	1	5.76	941.42
4	0	-1.4142	10.00	600.00
5	0	0	10.00	800.00
6	0	0	10.00	800.00
7	0	0	10.00	800.00
8	0	1.4142	10.00	1000.00
9	1	-1	14.24	658.58
10	1	1	14.24	941.42
11	-1.4142	0	16.00	800.00

Table 3-2 CCD-RSM used in conventional chemical activation

Run	Coded value		Actual value	
	Factor1	Factor2	Conventional chemical activation	
			Activation time (min)	Temperature (°C)
1	-1.4142	0	30.00	600.00
2	-1	-1	47.57	458.58
3	-1	1	47.57	741.42
4	0	-1.4142	90.00	400.00
5	0	0	90.00	600.00
6	0	0	90.00	600.00
7	0	0	90.00	600.00
8	0	1.4142	90.00	800.00
9	1	-1	132.43	458.58
10	1	1	132.43	741.42
11	-1.4142	0	150.00	600.00

3.3 Preparation of Activated Carbon

The experimental equipment, instruments, and chemicals used in the preparation of activation are shown as Tables 3-3 to 3-5.



3.3.1 Materials and instruments

Table 3-3 Experiment equipment

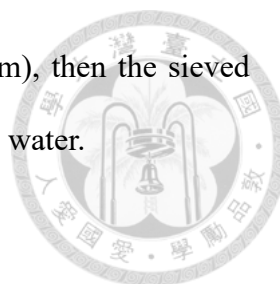
Equipment	Dimensions
Ceramic crucible	50 mL
Polypropylene (PP) bottle	250 mL
Cylindrical quartz reactor	Diameter: 105 mm; Height: 45 mm; Volume: 389.7 mL
Cylindrical quartz tube	Diameter: 35 mm; Length: 950 mm; Volume: 914 mL
Combustion boat	Length: 80 mm; Height: 13 mm ; Width: 17 mm
Glass sample vial	20 mL

Table 3-4 Instruments

Instrument	Manufacturer	Model
Digital stirring hot plate	CCTCL	Inno-Pro
pH meter	SUNTEX	SP-2300
Water purification system	Millipore	Milli-Q
Microwave muffle furnace	Milestone	Pyro 260
Tubular furnace	DENGYNG	MC-2438P

Table 3-5 Chemicals

Chemicals	Properties	Manufacturer
Fluid coke	0.037-0.149 mm	
De-ionized water	Resistivity <18.2 Mohm	Milli-Q
Potassium hydroxide (KOH)	99.2%, A.C.S. Reagent	Macron
Hydrochloric acid (HCl)	36.5-38%, analyzed reagent	J.T. Baker
Nitrogen (N ₂)	99.995%	Chiaotai



Fluid coke was sieved into selected sizes (0.037 mm-0.149 mm), then the sieved coke was placed in a laboratory oven at 110°C for one day to remove water.

3.3.2 Impregnation

KOH pellets were dissolved in de-ionized water, and then this solution was mixed with 3 g fluid coke on digital stirring hot plate at 300 rpm and room temperature for 10 min with different impregnation ratio (IR) until the KOH was totally dissolved. Impregnation ratio (IR) was defined as:

$$IR = W_{\text{KOH}} / W_{\text{Fluid coke}} \quad (3.2)$$

In this research, IR were 1, 2 and 4 by mass for microwave chemical activation and 1 for conventional chemical activation. Then the mixture was placed in the laboratory oven at 110°C for several days (listed in Table 3-6) until the mixture was dried.

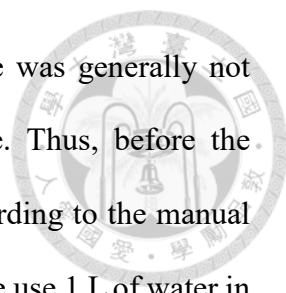
Table 3-6 Impregnation ratio corresponding drying days

Impregnation ratio (IR)	Drying days
1	1-2
2	2-3
4	3-4

3.3.3 Microwave chemical activation

The dried mixture was put into the 50 mL ceramic crucible (Figure 3-2) then ceramic crucible was put into the cylindrical quartz reactor, which allows gas flowing in and out. Nitrogen flowed through the gas flow meter and entered into the cylindrical quartz reactor at 50 mL/min for 20 min (retention time multiplied by 2.57) in the microwave muffle furnace (Figure 3-3) to make an oxygen-free environment. Then the heating process was started. The range of power level was 600 W to 1000 W. The range of heating time was 4 min to 12 min. The operating parameters are set by CCD-RSM.

It is important to note that the real power level of microwave was generally not completely equal to the setting power level shown in the device. Thus, before the activation the microwave muffle furnace should be calibrated. According to the manual of the microwave muffle furnace of Milestone PYRO 260 manual, we use 1 L of water in a beaker, operated the furnace, and recorded the temperatures before and after heating. The real power level can then be calculated by the built-in program. The calibration curve is shown in Figure 3-4. Table 3-7 listed the setting power level, which indicates the power level which was entered in the microwave muffle furnace. The value of real power level was calculated by equation (3.3).



$$\text{Real power level} = 1.0733 \times (\text{Setting power level}) - 132.2 \quad (3.3)$$

Table 3-7 Comparison of setting and real power level

Setting power level	real power level
682	599.8
737	658.8
869	800.5
1000	941.1
1055	1000.1



Figure 3-2 Dried mixture in the 50 mL Ceramic Crucible



Figure 3-3 Microwave muffle furnace

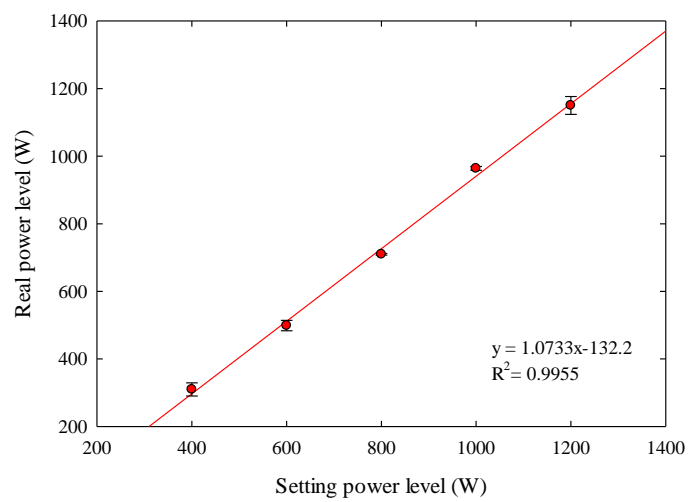


Figure 3-4 Calibration curve of microwave muffle furnace

3.3.4 Conventional chemical activation

The dried mixture was put into the combustion boat (Figure 3-5) and placed into the cylindrical quartz tube in the tubular furnace (Figure 3-6). Both ends of cylindrical quartz tube were sealed up and only allowed nitrogen to flow through. Nitrogen flowed through the gas flow meter and then entered the cylindrical quartz tube at 50 mL/min for 40 min (retention time multiplied by 2.19) to make an oxygen-free environment. The temperature was raised to 400°C at the speed of 10°C/min from room temperature and then raised to the set temperature at the speed of 4°C/min.



Figure 3-5 Combustion boat

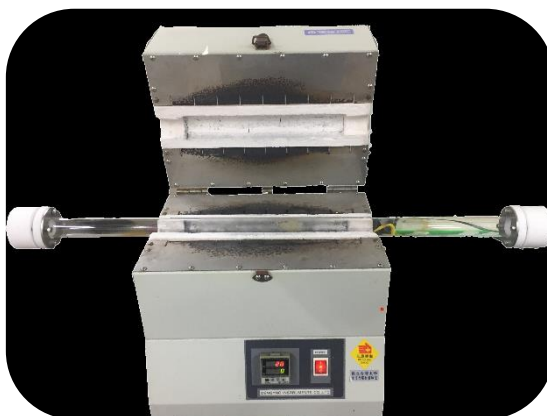


Figure 3-6 Cylindrical quartz tube in the tubular furnace

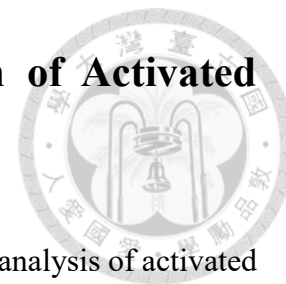
3.3.5 After activation

After activation, the mixture in the ceramic crucible was washed by 10-20 mL of 1M HCl_(aq) and poured into 250 mL PP bottle. Then, the mixture in PP bottle was washed by 500-750 mL de-ionized water. After washing, the mixture was neutralized (pH=6-8) by 0.2 M HCl_(aq) and 0.2M KOH_(aq). The mixture was further washed by 1250-1500 mL de-ionized water. Then, the mixture was dried in the laboratory oven at 110°C for one day. After being dried, activated carbon was produced and further weighed. Yield is defined as:

$$\text{Yield} = W_{AC} / W_{\text{Fluid coke}} \times 100\% \quad (3.4)$$

where W_{AC} and $W_{\text{Fluid coke}}$ are the dry weight of activated carbon (g) and fluid coke (g) respectively. The activated carbon was put in the glass sample vial and stored in damp-proofing case of the electron.

3.4 Physical and Chemical Characterization of Activated Carbon



The instruments used in physical and chemical characterization analysis of activated carbon are listed in Table 3-8.

Table 3-8 Instruments of physical and chemical characterization

Analysis Project	Model
Surface Area and Pore Volume	ASAP 2020
Scanning Electron Microscope	Hitachi TM-3000
Elemental Analysis (C, H, N, S)	vario EL cube
Elemental Analysis (O)	FLASH 2000 OEA

3.4.1 Surface area, pore volume and pore size distribution

The specific surface area (S_{BET}), total pore volume (V_{total}), micropore surface area (S_{micro}), and micropore volume (V_{micro}) of samples were determined by N_2 adsorption at 77 K. There were two steps for physical property measurement: the degas step and analysis step. In degas step, each sample was degassed at 150°C for 12-24 h before analysis. The degas condition must be checked that the pressure in the sample tube was maintained below 5 $\mu\text{m-Hg}$ in 300 s. In analysis step, the N_2 isotherm adsorption curve was measured at 77 K.

The method of Barrett, Joyner, and Halenda (BJH) is commonly used to calculate the PSD of mesopore and small macropore size range from N_2 adsorption isotherm (Barrett *et al.*, 1951). The BJH method is based on the Kelvin equation, which utilizes the phenomenon of capillary condensation in mesoporous systems. It is effective at P/P_0 larger than 0.35 (Hornyak *et al.*, 2008).

Nonlocal density functional theory (NLDFT) has been widely used for the characterization of PSD of activated carbons and other porous materials (Jagiello and Thommes, 2004). It can provide the micropores and mesopores PSD.

BET method was applied to evaluate S_{BET} , and the t-plot method was applied to evaluate the S_{micro} and V_{micro} . NLDFT method was applied to evaluate PSD of micropore. BJH method was applied to evaluate PSD of mesopore and macropore. V_{total} was calculated by total N_2 volume adsorbed by activated carbon at the relative pressure near one.

3.4.2 Scanning electron microscope (SEM)

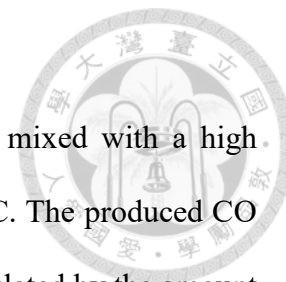
The principle of scanning electron microscopy (SEM) is utilizing two electron beams (one strikes the sample, the other one strikes a cathode ray tube) to produce a variety of electron and photon missions so that these two signals will produce a bright spot on the cathode ray tube. If the display area of the cathode ray tube is $A \times A$ in size and the area scanned is $B \times B$ in size, the brightness is with a magnification of A/B . An image of the sample is produced without imaging lenses. In short, SEM is capable of taking images from the surface of the sample (Joy, 2006). In this research the images from SEM can be used for observing the changing from fluid coke to activated carbon.

3.4.3 Elemental analysis (EA)

Carbon (C), hydrogen (H), nitrogen (N) and sulfur (S) contents were measure using an elemental analyzer. The tested material was combusted at 1200°C (temporarily 1800°C) with oxygen injection directly on the sample. Nitrogen oxides are reduced to N_2 . The gas mixture was separating by specific adsorber columns for CO_2 , SO_2 and H_2O by thermally controlling the release of the individual gases. The individual gases detected by a thermal conductivity detector (TCD). The ratio of C, H, N and S in the material was calculated by

the amount of these gases.

For the oxygen (O) content determination, the material was mixed with a high carbon-content compound and combusted without oxygen at 1100°C. The produced CO and CO₂ were detected by a TCD. The oxygen content was calculated by the amount of CO and CO₂.



3.4.4 X-ray photoelectron spectroscope (XPS)

XPS was employed to understand the surface chemical compositions of the prepared activated carbon. Through XPS, the binding energies of peaks can be used to determine the types of functional groups existing on the surface of activated carbon. In this study, all binding energies were referenced to the C 1s peak at 285 eV. The corresponding binding energies of various C and S functional groups are listed in Table 3-9.

Table 3-9 The assignment of the XPS peaks (Terzyk, 2001)

	Binding energy	Functional group	Assignment
C 1s			
1	284.6	C	Graphitic carbon
2	268.0	C-O-	Phenolic, alcoholic, etheric
3	287.3	C=O	Carbonyl or quinone
4	288.9	COO	Carboxyl or ester
5	290.5	C=O/C=C	Carbonate, occluded CO, π -electrons in aromatic ring
6	291.5	π - π transition	The transition due to conjugation
S 2p			
7	163.1, 163.7	PhSH, CS ₂	Thiol or carbon bisulfide
8	164.3	C-S-C, R-S-S-OR	Sulfides, Thioethers
9	167.5, 167.2,	R ₂ S=O, SO ₃ ²⁻	Thioethers
10	168.0	R-SO ₂ -R	Sulfoxides, Sulphite
11	168.6, 168.4	SO ₄ ²⁻ , SO ₃ ²⁻	Sulphate, Sulphite, Sulphonic acids
12	169.7, 169.0	RO ₂ -S-S-R R-SO ₃ H	

3.5 Mercury (II) Adsorption Experiment



The equipment, instruments, and chemicals used in the mercury adsorption tests are listed in Tables 3-10 to 3-12.

3.5.1 Materials and instruments

Table 3-10 Experiment equipment

Equipment	Dimensions
Volumetric flask	200 mL; 50 mL; 1 L
High-density polyethylene (HDPE) Bottle	100 mL
Beaker	1 L
Syringe filter and Syringe	0.45 μm ; mixed cellulose ester
Glass sample vial	20 mL

Table 3-11 Instruments

Instrument	Manufacturer	Model
Digital stirring hot plate	CCTCL	Inno-Pro
pH meter	SUNTEX	SP-2300
Water purification system	Millipore	Milli-Q
Reciprocal shaking bath	Chemist	DKW-40
Cold Vapor-Atomic Absorption Spectroscopy (CVAAS)	HIRANUMA	HG-310

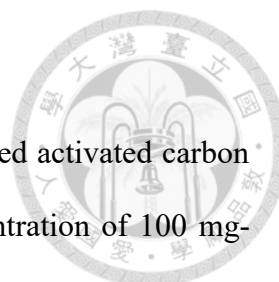
Table 3-12 Chemicals

Chemicals	Properties	Manufacturer
Mercuric chloride (HgCl_2)	99.9%, A.C.S. Reagent	J.T. Baker
De-ionized water	Resistivity <18.2 Mohm	Milli-Q
Buffer solution	pH=4.00, 7.00, 10.00	SUNTEX
Potassium hydroxide (KOH)	99.2%, A.C.S. Reagent	Macron
Hydrochloric acid (HCl)	36.5-38%, analyzed reagent	J.T. Baker
Nitric acid (HNO_3)	69-70%, analyzed reagent	J.T. Baker
Stannous Chloride (SnCl_2)	Powder, A.C.S. Reagent	Marcon
Sulfuric acid (H_2SO_4)	95.0-98.0%, analyzed reagent	J.T. Baker
$\text{Hg}(\text{NO}_3)_2$ standard solution	1000 mg- Hg^{2+} /L, analyzed reagent	J.T. Baker

The mercury stock solution was prepared by dissolving 5.0055 g of HgCl₂ powder in 200 mL deionized water in the volumetric flask. The solution was stirred at 300 rpm on the digital stirring hot plate for 24 h. The concentration of stock solution was 18485 mg-Hg²⁺/L and preserved in the refrigerator at 4°C.

$$\text{Concentration} = \frac{5005.5 \text{ mg}}{0.2 \text{ L}} \times \frac{200.6 \text{ g-Hg}^{2+}}{271.6 \text{ g-HgCl}_2} = 18485 \text{ (mg-Hg}^{2+}\text{/L)} \quad (3.5)$$

Batch adsorption experiment: stock solution with specific volume was diluted into 1 L in the volumetric flask. The diluted solution was poured into the 1 L beaker and stirred at 300 rpm on the digital stirring hot plate. Simultaneously, pH of the solution was adjusted by 1M KOH solution and 1M HCl to 6.9-7.1. Then, the solution was separated by 50 mL volumetric flask to 100 mL high-density polyethylene (HDPE) wide mouth bottle.



3.5.2 Adsorption kinetic experiment

In mercury (II) adsorption kinetic experiment, 0.05 g of prepared activated carbon was added to 50 mL HgCl₂ solution with an initial mercury concentration of 100 mg-Hg²⁺/L in a 100 mL HDPE wide mouth bottle. The solution with activated carbon was shaken in a reciprocal shaking bath at 150 rpm and 30°C for 24 h or more to achieve equilibrium. Then the solution with activated carbon was filtered with a syringe filter (0.45). The filtered solution of 19.6 mL was mixed with 0.4 mL concentrated nitric acid (69-70%) and stored in the 20 mL glass sample vial, so that the stored concentration is the filtered concentration multiplied by 0.98. Before analysis, the stocked solution was diluted with 2% nitric acid to 0-25 µg-Hg²⁺/L. Then, the 1 mL diluted solution was analyzed by CVAAS. The chosen activated carbon sample was duplicated tested. The highest coefficient of determinations (R²) of model would be chosen to determine the equilibrium time (t_e).

Table 3-13 Adsorption condition of mercury (II) adsorption kinetic

Mercury (II) adsorption kinetic	
Initial conc. (mg-Hg ²⁺ /L)	100
AC dosage (g/L)	1
Solution volume (mL)	50
Agitation time (h)	0.5-21.5
pH	6.9-7.1
Temperature (°C)	30

3.5.3 Adsorption isotherm experiment

In mercury (II) adsorption isotherm experiment, 0.05 g of prepared activated carbon was added to 50 mL HgCl₂ solution with an initial mercury concentration of 100 mg-

Hg²⁺/L in a 100 mL HDPE wide mouth bottle. The solution with activated carbon was shaken in a reciprocal shaking bath at 150 rpm and 30°C for 24 h or more to achieve equilibrium. Then the solution with activated carbon was filtered with a syringe filter (0.45 μm). The filtered solution of 19.6 mL was mixed with 0.4 mL concentrated nitric acid (69-70%) and stored in the 20 mL glass sample vial, so that the stored concentration is the filtered concentration multiplied by 0.98. Before analysis, the stocked solution was diluted with 2% nitric acid to 0-25 μg-Hg²⁺/L. Then, the 1 mL diluted solution was analyzed by CVAAS. The chosen activated carbon sample was triplicated tested.

Table 3-14 Adsorption condition of mercury (II) adsorption isotherm

Mercury (II) adsorption isotherm	
Initial conc. (mg-Hg ²⁺ /L)	1, 25, 100
AC dosage (g/L)	1
Solution volume (mL)	50
Agitation time (h)	24
pH	6.9-7.1
Temperature (°C)	30

3.5.4 Adsorption capacity experiment

In mercury (II) adsorption capacity experiment, 0.05 g of prepared activated carbon was added to 50 mL HgCl₂ solution with an initial mercury concentration of 100 mg-Hg²⁺/L in a 100 mL HDPE wide mouth bottle. The solution with activated carbon was shaken in the reciprocal shaking bath at 150 rpm and 30°C for 24 h or more to achieve equilibrium. Then the solution with activated carbon was filtered with a syringe filter. The filtered solution of 19.6 mL with was mixed with 0.4 mL concentrated nitric acid (69-70%) and stored in the 20 mL glass sample vial so that the stored concentration is the filtered concentration multiplied by 0.98. Before analysis, the stocked solution was

diluted with 2% nitric acid to 0-25 $\mu\text{g-Hg}^{2+}/\text{L}$. Then, the 1 mL diluted solution was analyzed by CVAAS. Each activated carbon sample was triplicated tested.

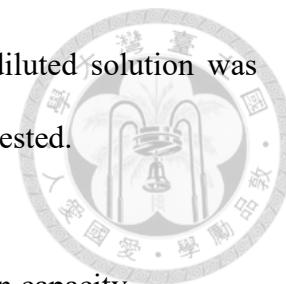


Table 3-15 Adsorption condition of mercury (II) adsorption capacity

Mercury (II) adsorption capacity	
Initial conc. ($\text{mg-Hg}^{2+}/\text{L}$)	100
AC dosage (g/L)	1
Solution volume (mL)	50
Agitation time (h)	24
pH	6.9-7.1
Temperature ($^{\circ}\text{C}$)	30

3.5.5 Cold vapor atomic absorption spectroscopy (CVAAS)

CVAAS is a technology able to detect the total mercury concentration in aqueous system. The detection limit CVAAS is $0.0005 \text{ mg-Hg}^{2+}/\text{L}$.

In this research, different forms of mercury in aqueous solution was first oxidized to Hg^{2+} by nitric acid. After that Hg^{2+} in solution was reduced to Hg^0 by SnCl_2 and then carried to the CVAAS by gas. The absorbance of Hg^0 was measured by CVAAS. Through the calibration curve, the amount of Hg^0 per unit volume can be obtained.

To obtain the calibration curve, 28.6 mL of 70% HNO_3 solution was diluted by de-ionized water to 1 L in a volumetric flask to prepare the 2% HNO_3 solution. 1 mL of 1000 $\text{mg-Hg}^{2+}/\text{L}$ $\text{Hg}(\text{NO}_3)_2$ solution was diluted by 2% HNO_3 solution to 100 mL in volumetric flask to prepare the solution 10 $\text{mg-Hg}^{2+}/\text{L}$ $\text{Hg}(\text{NO}_3)_2$ solution. 1 mL of 10 $\text{mg-Hg}^{2+}/\text{L}$ $\text{Hg}(\text{NO}_3)_2$ solution was diluted by 2% HNO_3 solution to 100 mL in a volumetric flask to prepare the solution 100 $\mu\text{g-Hg}^{2+}/\text{L}$ $\text{Hg}(\text{NO}_3)_2$ solution. The $\text{Hg}(\text{NO}_3)_2$ solution with various concentration was prepared based on mixing ratios, shown in Table 3-16. 1 mL

of the mixed solution was measured triplicated by CVAAS. A typical calibration curve of CVAAS is shown in Figure 3-7. Each sample solution was measured duplicated. The concentration of the solution was calculated by the equation (3.6):

$$C_{(aq)} = (C_{CVAAS} \times DR) / (0.98 \times 1000) \quad (3.6)$$

Where $C_{(aq)}$ is the mercury (II) concentration in aqueous solution, and the unit of $C_{(aq)}$ is mg-Hg²⁺/L. C_{CVAAS} is the concentration detected by CVAAS, and the unit of C_{CVAAS} is μg-Hg²⁺/L. DR is the dilution rate from the stored solution to the solution. The number 0.98 is the filtered solution diluted by concentrated HNO₃.

The amount of mercury (II) adsorbed per unit mass of added activated carbon at equilibrium was calculated by the equation (3.7):

$$q_e = (C_e - C_0) \times V / W_{AC} \quad (3.7)$$

Where q_e is the amount of mercury (II) adsorbed per unit mass of added activated carbon at equilibrium and the unit of q_e is mg-Hg²⁺/g-AC. C_e is the mercury (II) concentration in aqueous solution at equilibrium and the unit of C_e is mg-Hg²⁺/L. C_0 is the initial concentration of the solution, and the unit of C_0 is mg-Hg²⁺/L. W_{AC} is the weight of activated carbon added in solution.

The amount of mercury (II) adsorbed per unit mass of added activated carbon at specific agitation time was calculated by the equation (3.8).

$$q_t = (C_t - C_0) \times V / W_{AC} \quad (3.8)$$

Where q_t is the amount of mercury (II) adsorbed per unit mass of added activated carbon at specific agitation time and the unit of q_t is mg-Hg²⁺/g-AC. C_t is the mercury (II) concentration in aqueous solution at specific agitation time with the unit of C_t at mg-Hg²⁺/L.

When the recovery rate of prepared mercury (II) concentration was between 85% and 115%, the results of adsorption experiment were acceptable based on equation (3.9).

$$\text{Recovery rate} = \text{real } C_0 / \text{setting } C_0 \times 100\% \quad (3.9)$$

Where real C_0 is the mercury (II) concentration of the prepared solution and setting C_0 is the mercury (II) concentration that the experiment step should produce.

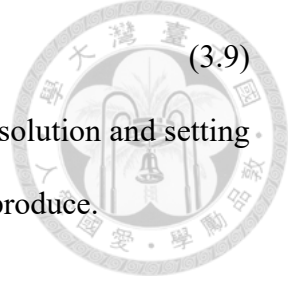


Table 3-16 Calibration curve concentration

Volume of 2% HNO ₃ solution (mL)	Volume of 100 μg-Hg ²⁺ /L Hg(NO ₃) ₂ solution (mL)	Concentration (μg-Hg ²⁺ /L)
10	0	0
9.5	0.5	5
9	1	10
8.5	1.5	15
8	2	20
7.5	2.5	25

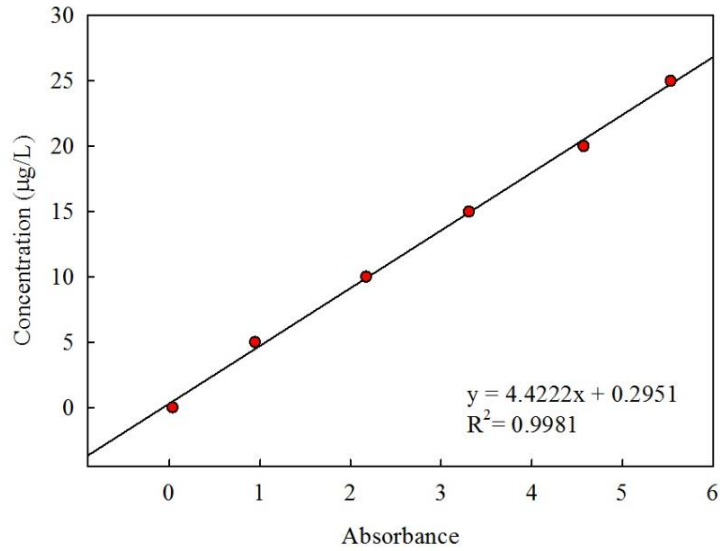
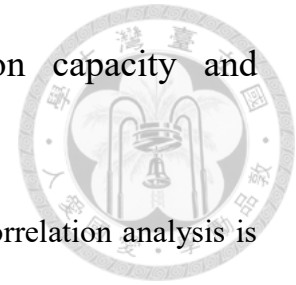


Figure 3-7 Calibration curve of CVAAS

3.5.6 Correlation analysis of mercury (II) adsorption capacity and characteristics of activated carbon



In order to analyze the dependences of adsorption capacity, correlation analysis is applied to understand the relationship between the mercury (II) adsorption capacity or removal efficiency and the physical and chemical characterization of activated carbon. The physical and chemical characterization of activated carbon includes S_{BET} , S_{micro} , V_{total} , V_{micro} , carbon content, nitrogen content, sulfur content, hydrogen content, and oxygen content. The Pearson correlation coefficient is used to describe the correlation. The data were analyzed by software SPSS version 12.0. After correlation analysis, the regression analysis is utilized to establish the equation between the chosen characterization of activated carbon and adsorption capacity or removal efficiency.

Chapter 4 Results and Discussion

4.1 Physical and Chemical Characterization of Activated Carbon



In this chapter, code name was used to describe the parameters in the activation process. For example, R1-M-P800-t4 represents that IR equals to 1 (R), the material is activated by microwave heating (M), the power level (P) equals to 800 W and activation time is 4 min (t). R1-C-T600-t30 represents that IR equals to 1, the material is activated by conventional the heating (C), heating temperature is maintained at 600°C (T) for 30 min. RAW represents that the fluid coke which was only heated at 110°C to remove water.

4.1.1 Morphology of activated carbon

The SEM images of RAW were observed that it contained irregular particles with small sizes (Figure 4-1 (a)). RAW was also shown to have layer structure (Figure 4-1 (b)) and there are seldom cracks on the surface (Figure 4-1 (c)).

Compared with RAW, the SEM images showed that R1-M-P941-t14.25 contained dense strip-shaped cracks (Figure 4-2 (b) and (c)), which suggested that the pore structures was developed due to microwave chemical activation.

Moreover, the SEM image of R4-M-P941-t14.25 showed that when the IR was increased to 4, the surface of the layer structure would be eroded and bared the ball-shaped pore inter-structure. It can also be noted that high S_{BET} was achieved for R4-M-P941-T14.25 ($1853.07 \text{ m}^2/\text{g}$) and its S_{micro} is $1584.73 \text{ m}^2/\text{g}$.

Compared with the SEM images of R1-M-P941-t14.25 (Figure 4-2), R1-C-T741-t132 (Figure 4-4) also contained strip-shaped cracks but they are smaller and thinner, which means that the activation level of R1-C-T741-t132 is lower than R1-M-P941-t14.25. S_{BET} also supported the observation that microwave chemical activation could be more effective than the conventional chemical activation. The S_{BET} of R1-M-P941-t14.25 (i.e., S_{BET} : $903.02 \text{ m}^2/\text{g}$) is larger than that of R1-C-T741-t132 (i.e., S_{BET} : $615.36 \text{ m}^2/\text{g}$).

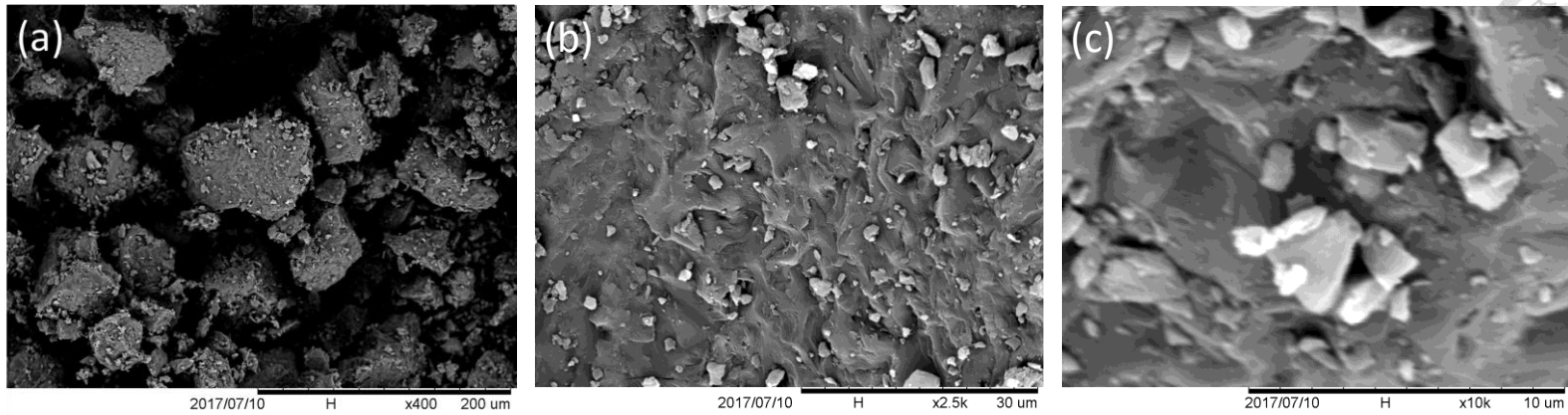


Figure 4-1 SEM images of RAW: (a) 400x, (b) 2500x and (c) 10000x

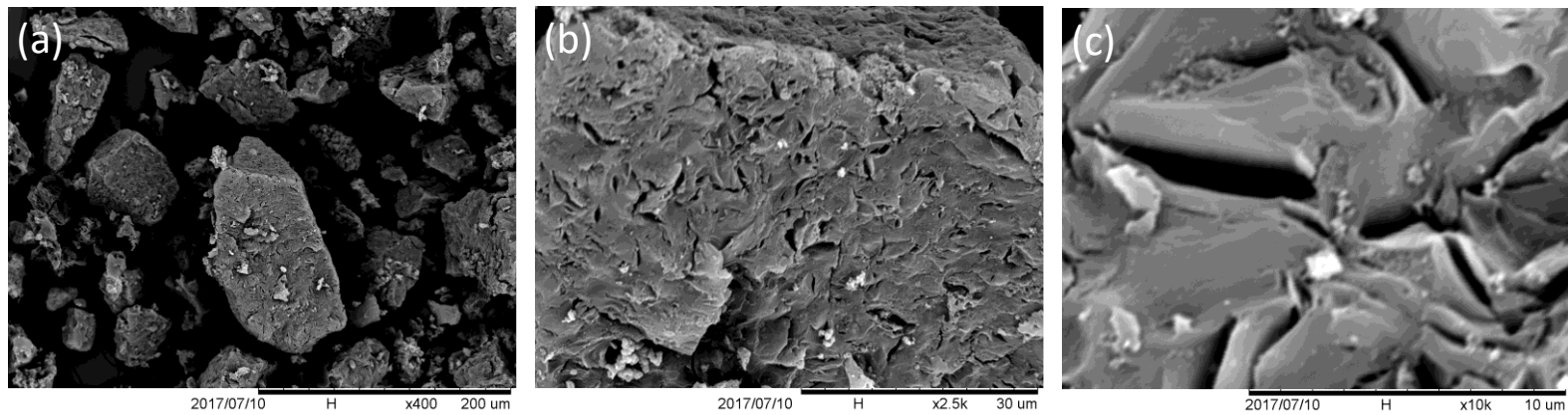


Figure 4-2 SEM images of R1-M-P941-t14.25: (a) 400x, (b) 2500x and (c) 10000x

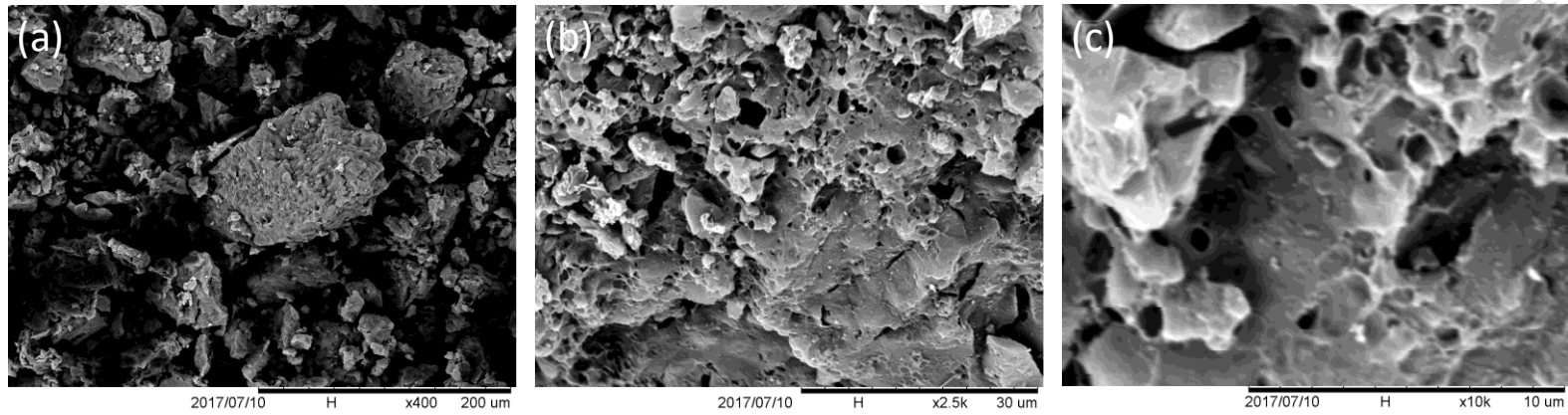


Figure 4-3 SEM images of R4-M-P941-t14.25: (a) 400x, (b) 2500x and (c) 10000x

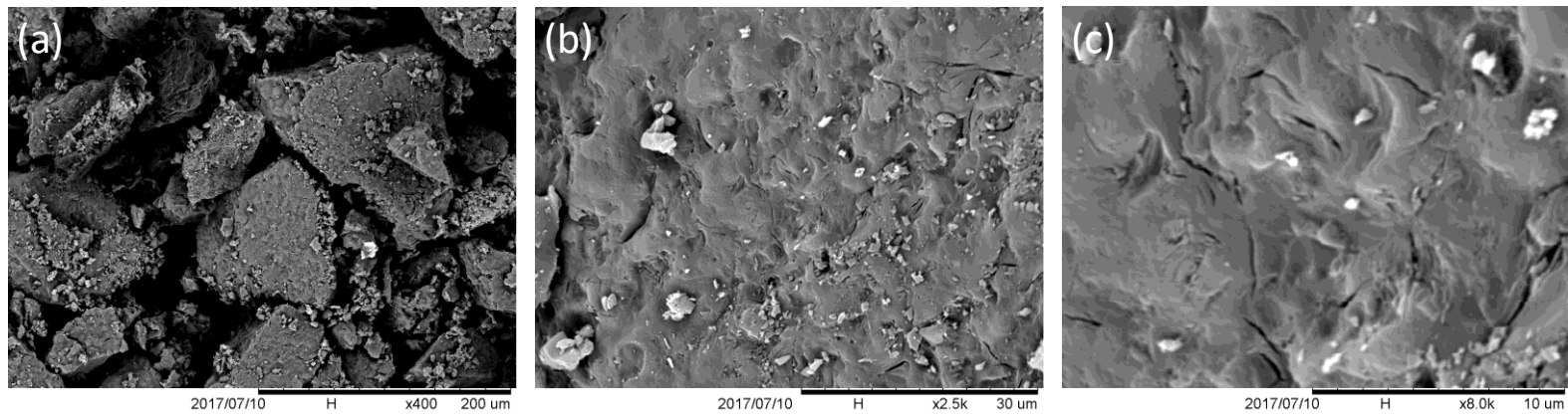


Figure 4-4 SEM images of R1-C-T741-t132: (a) 400x, (b) 2500x and (c) 10000x

4.1.2 Production yield

The activated carbon prepared by microwave chemical activation:

The yields ranged from 39.48% to 74.81%, which are listed in



Table 4-1. Through CCD-RSM analysis, the relationship between the response (yield: y) and factors (power level: x_1 and time: x_2) is shown as equation (4.1). Based on equation (4.1) the three-dimension figure and contour figure of CCD-RSM can be drawn as Figure 4-5, which reveals that the yield would decrease as the time increases and the power level increases. The R^2 of the equation (4.1) from CCD-RSM is 0.796 and the adjusted R^2 is 0.591. $V_{\text{CCD-RSM}}$ is the value predicted by CCD-RSM.

Owing to the thermal-runaway effect, the microwave heating technology has problems. One of them is the local temperature would not uniformly increase, which would create the undesired hot spot (Jerby *et al.*, 2002). Thus, the properties of activated carbons from microwave activation would be more unstable and unpredictable.

$$y = 9.75679 + (0.206527) x_1 + (0.832248) x_2 + (-0.000143041) x_1^2 + (-0.00388092) x_2^2 + (-0.00339974) x_1 x_2 \quad (4.1)$$

Table 4-1 Yield of activated carbon from microwave chemical activation

Sample	Yield (%)	V _{CCD-RSM}	Error (%)
R1-M-P800-t4	74.81	75.82	1.33
R1-M-P659-t5.75	73.28	75.51	2.96
R1-M-P941-t5.75	68.81	63.7	-8.02
R1-M-P600-t10	72.38	69.71	-3.82
R1-M-P800-t10	64.62	64.17	-0.70
R1-M-P800-t10	71.72	64.17	-11.77
R1-M-P800-t10	56.13	64.17	12.53
R1-M-P1000-t10	39.48	47.18	16.32
R1-M-P659-t14.25	62.83	62.88	0.08
R1-M-P941-t14.25	50.23	42.92	-17.03
R1-M-P800-t16	48.19	52.24	7.75

The activated carbon prepared by conventional chemical activation also showed a wide variety of production yields.

The yields ranged from 63.13% to 89.25%, which were listed in Table 4-2. Through CCD-RSM analysis, the relationship between the response (yield: y) and factors (temperature: x_1 and time: x_2 and) is shown as equation (4.2). Based on the equation (4.2) the three-dimension figure and contour figure of CCD-RSM can be drawn (Figure 4-6), which reveals that the yield would decrease as the time increases at specific power level or as the power level increases at specific time. The R^2 of the equation (4.2) from CCD-RSM is 0.960 and the adjusted R^2 is 0.921.

$$y = 15.4174 + (0.258161) x_1 + (0.320546) x_2 + (-0.000239882) x_1^2 + (-0.000775409) x_2^2 + (-0.000401579) x_1 x_2 \quad (4.2)$$

Table 4-2 Yield of activated carbon from conventional chemical activation

Sample	Yield (%)	V _{CCD-RSM}	Error (%)
R1-C-T600-t30	86.40	85.65	-0.88
R1-C-T459-t48	87.39	88.13	0.84
R1-C-T741-t48	73.39	74.32	1.25
R1-C-T400-t90	89.25	88.41	-0.95
R1-C-T600-t90	87.09	84.84	-2.65
R1-C-T600-t90	86.94	84.84	-2.48
R1-C-T600-t90	80.50	84.84	5.11
R1-C-T800-t90	63.25	62.08	-1.89
R1-C-T459-t132	86.74	87.85	1.26
R1-C-T741-t132	63.13	64.52	2.16
R1-C-T600-t150	79.72	78.45	-1.62

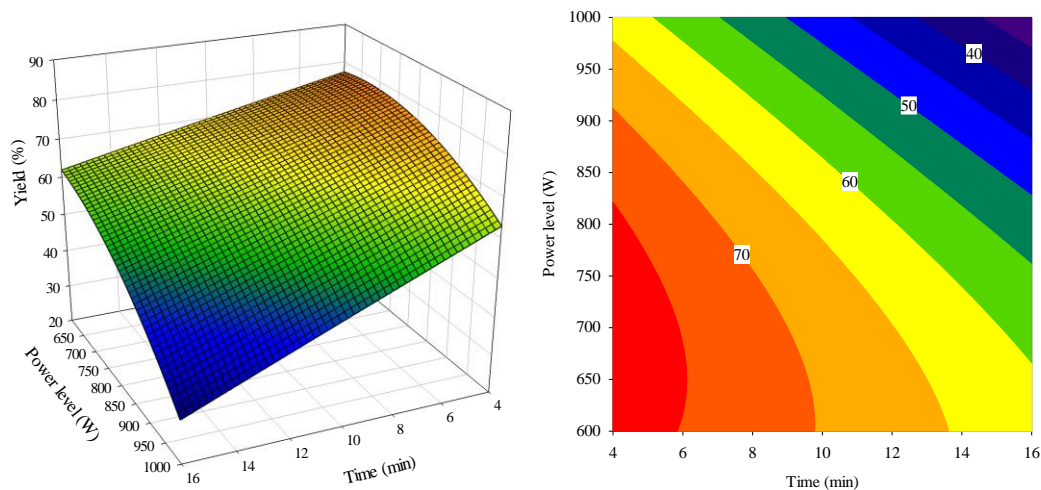


Figure 4-5 CCD-RSM analysis for the production yield versus power level and time of microwave chemical activation

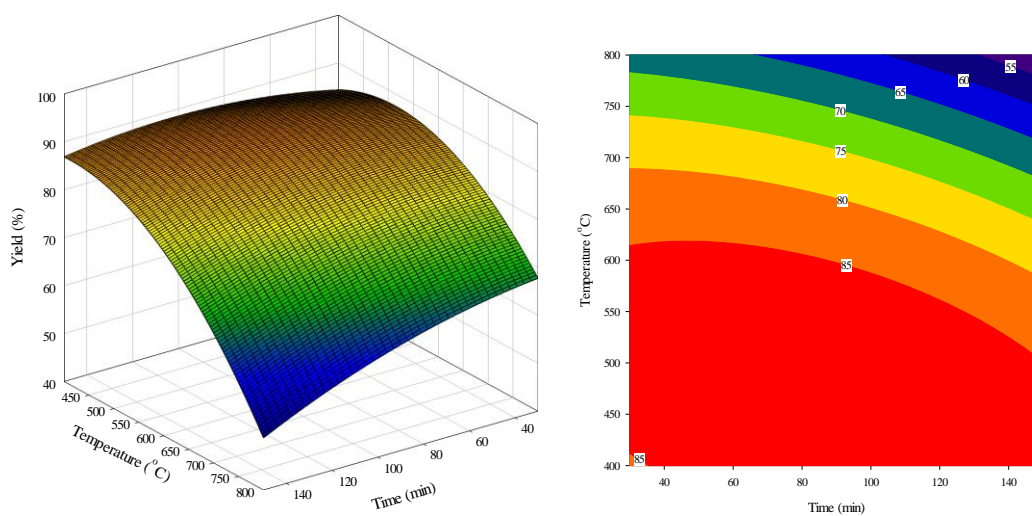
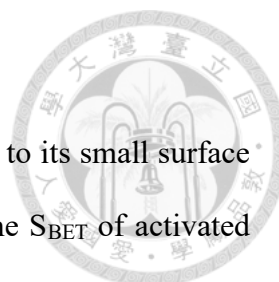


Figure 4-6 CCD-RSM analysis for the production yield versus temperature and time of conventional chemical activation



4.1.3 Surface area and pore volume

Table 4-3 reveals that there was few pore in raw fluid coke due to its small surface area ($0.81 \text{ m}^2/\text{g}$). Moreover, after microwave chemical activation, the S_{BET} of activated carbons increased from 453.99 to $1029.75 \text{ m}^2/\text{g}$. V_{total} of activated carbons are also enhanced from 0.228 to $0.513 \text{ cm}^3/\text{g}$. Most of the pores are shown to be micropores. S_{micro} accounts for 91.40-98.54% of S_{BET} and V_{micro} accounts for 81.05-91.47% of V_{total} .

Among the prepared activated carbons from microwave activation, the conditions of the three samples with the highest S_{BET} are chosen to prepare the activated carbons with different IR for observing the effects of different IR on physical and chemical characteristics. The physical properties of them are listed in Table 4-4.

After conventional chemical activation, the S_{BET} of activated carbons increased from 62.39 to $697.26 \text{ m}^2/\text{g}$. V_{total} of activated carbons are also enhanced from 0.045 to $0.365 \text{ cm}^3/\text{g}$. Most of the pores are shown to be micropores. S_{micro} accounts for 91.17-99.34% of S_{BET} and V_{micro} accounts for 65.63-97.70% of V_{total} .

Based on S_{BET} , R1-M-P800-t4 (i.e., S_{BET} : $676.94 \text{ m}^2/\text{g}$), R1-M-P600-t10 (i.e., S_{BET} : $721.96 \text{ m}^2/\text{g}$), and R1-M-P800-t10 (i.e., S_{BET} : $721.02 \text{ m}^2/\text{g}$) were chosen to represent the microwave chemical activation and R1-C-T800-t90 (i.e., S_{BET} : $697.26 \text{ m}^2/\text{g}$) were chosen to represent the conventional chemical activation for the comparison of the two different activation methods.

The results of CCD-RSM analysis used in the physical properties are listed in Table 4-5. It also can be observed that the physical properties of activated carbon from conventional chemical activation had higher R^2 which means that, they are more predictable than those from microwave chemical activation.

Table 4-3 The physical properties of activated carbon from microwave chemical activation

Sample	S_{BET} (m ² /g)	S_{micro} (m ² /g)	$S_{\text{micro}} / S_{\text{BET}}$ (%)	V_{total} (cm ³ /g)	V_{micro} (cm ³ /g)	$V_{\text{micro}} / V_{\text{total}}$ (%)
R1-M-P800-t4	676.94	646.04	95.44	0.385	0.336	87.39
R1-M-P659-t5.75	759.73	723.45	95.22	0.438	0.378	86.34
R1-M-P941-t5.75	836.33	824.13	98.54	0.475	0.429	90.50
R1-M-P600-t10	721.96	696.11	96.42	0.397	0.362	91.04
R1-M-P800-t10	453.99	435.90	96.01	0.262	0.228	86.98
R1-M-P800-t10	721.02	709.35	98.38	0.405	0.370	91.47
R1-M-P800-t10	642.70	587.43	91.40	0.380	0.308	81.05
R1-M-P1000-t10	766.63	738.84	96.38	0.430	0.387	90.05
R1-M-P659-t14.25	1029.75	982.73	95.43	0.586	0.513	87.58
R1-M-P941-t14.25	903.02	850.96	94.23	0.529	0.444	83.91
R1-M-P800-t16	991.99	949.47	95.71	0.588	0.495	84.13
RAW	0.81	-	-	-	-	-

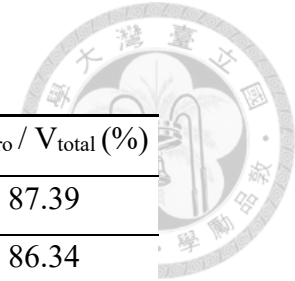
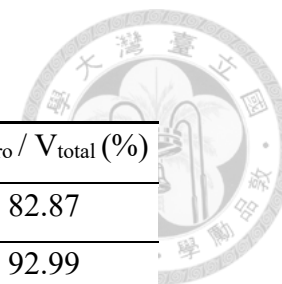


Table 4-4 The physical properties of activated carbon from microwave chemical activation

Sample	S_{BET} (m ² /g)	S_{micro} (m ² /g)	$S_{\text{micro}} / S_{\text{BET}}$ (%)	V_{total} (cm ³ /g)	V_{micro} (cm ³ /g)	$V_{\text{micro}} / V_{\text{total}}$ (%)
R2-M-P659-T14.25	1259.69	1174.12	93.21	0.740	0.613	82.87
R2-M-P941-T14.25	1386.89	1361.12	98.14	0.763	0.709	92.99
R2-M-P800-T16	1301.82	1207.81	92.78	0.772	0.633	81.95
R4-M-P659-T14.25	1677.90	1613.26	96.15	0.946	0.838	88.64
R4-M-P941-T14.25	1853.07	1584.73	85.52	1.140	0.831	72.89
R4-M-P800-T16	1873.41	1827.03	97.52	1.022	0.947	92.67



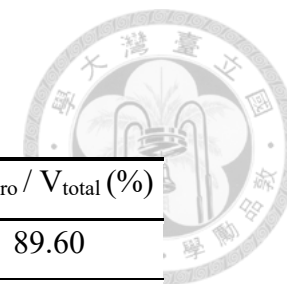


Table 4-5 The physical properties of activated carbon from conventional chemical activation

Sample	S_{BET} (m ² /g)	S_{micro} (m ² /g)	$S_{\text{micro}} / S_{\text{BET}}$ (%)	V_{total} (cm ³ /g)	V_{micro} (cm ³ /g)	$V_{\text{micro}} / V_{\text{total}}$ (%)
R1-C-T600-t30	283.96	280.58	98.81	0.164	0.147	89.60
R1-C-T459-t48	120.01	113.11	94.25	0.079	0.060	75.95
R1-C-T741-t48	663.10	657.22	99.11	0.365	0.343	94.12
R1-C-T400-t90	62.39	56.88	91.17	0.045	0.030	65.63
R1-C-T600-t90	220.88	217.96	98.68	0.128	0.114	88.65
R1-C-T600-t90	301.83	299.84	99.34	0.169	0.155	92.16
R1-C-T600-t90	262.15	260.11	99.22	0.152	0.135	88.57
R1-C-T800-t90	697.26	683.42	98.02	0.362	0.354	97.70
R1-C-T459-t132	108.56	104.41	96.18	0.068	0.054	79.67
R1-C-T741-t132	615.36	608.93	98.96	0.339	0.317	93.50
R1-C-T600-t150	287.44	267.53	93.07	0.178	0.140	78.86
RAW	0.81	-	-	-	-	-

Table 4-6 CCD-RSM for physical properties

Method	y	x ₁	x ₂	CCD-RSM equation	R ²	Adjusted R ²
Microwave	S _{BET}	Power level	Time	$y = 3406.21 + (-6.52790) x_1 + (-61.7767) x_2 + (0.00461866) x_1^2 + (7.64270) x_2^2 + (-0.0850269) x_1 x_2$	0.783	0.566
	S _{micro}	Power level	Time	$y = 3242.00 + (-6.35089) x_1 + (-47.9418) x_2 + (0.00459314) x_1^2 + (7.33927) x_2^2 + (-0.0972041) x_1 x_2$	0.773	0.546
	V _{total}	Power level	Time	$y = 1.81979 + (-0.00330053) x_1 + (-0.0463984) x_2 + (0.00000232332) x_1^2 + (0.00461300) x_2^2 + (-0.0000393082) x_1 x_2$	0.790	0.580
	V _{micro}	Power level	Time	$y = 1.68487 + (-0.00330183) x_1 + (-0.0246880) x_2 + (-0.000239882) x_1^2 + (0.00379406) x_2^2 + (-0.0000501807) x_1 x_2$	0.771	0.542
Conventional	S _{BET}	Temperature	Time	$y = 526.918 + (-2.34843) x_1 + (-1.55653) x_2 + (0.00350506) x_1^2 + (0.0127993) x_2^2 + (-0.00151205) x_1 x_2$	0.979	0.959
	S _{micro}	Temperature	Time	$y = 469.608 + (-2.19913) x_1 + (-1.19051) x_2 + (0.00338135) x_1^2 + (0.0108776) x_2^2 + (-0.00164955) x_1 x_2$	0.977	0.954
	V _{total}	Temperature	Time	$y = 0.263274 + (-0.00105268) x_1 + (-0.00137985) x_2 + (0.00000166458) x_1^2 + (0.00000946758) x_2^2 + (-0.000000624988) x_1 x_2$	0.971	0.941
	V _{micro}	Temperature	Time	$y = 0.248938 + (-0.00114366) x_1 + (-0.000708874) x_2 + (0.00000175521) x_1^2 + (0.0000060301) x_2^2 + (-0.000000833317) x_1 x_2$	0.977	0.953

4.1.4 Pore size distribution (PSD)

a. BJH model

BJH model is suitable for PSD of mesopore (2-50 nm) and macropore (>50 nm) analysis. As far as the Figure 4-7 Figure 4-8 are concerned, The activated carbons from microwave chemical activation contained the similar shapes of PSD. When the peak area of activated carbon increases, the pore volume of specific pore diameter also increases, which may be attributed that the amount of mesopore and macropore increases. Simultaneously, there were no obvious peak shift, which means that there were few disintegrated pores.

Figure 4-9 reveals that the pore development process activated carbons from conventional chemical activation. It can be observed that the pore develop primarily happened below the pore diameter of 10 nm.



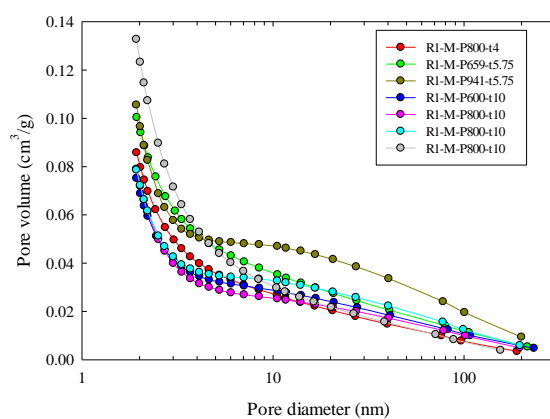


Figure 4-7 PSD of activated carbons with IR=1 from microwave chemical activation fitted by BJH (a)

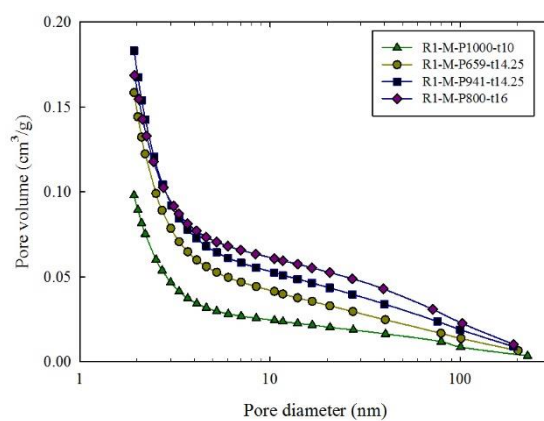


Figure 4-8 PSD of activated carbons with IR=1 from microwave chemical activation fitted by BJH (b)

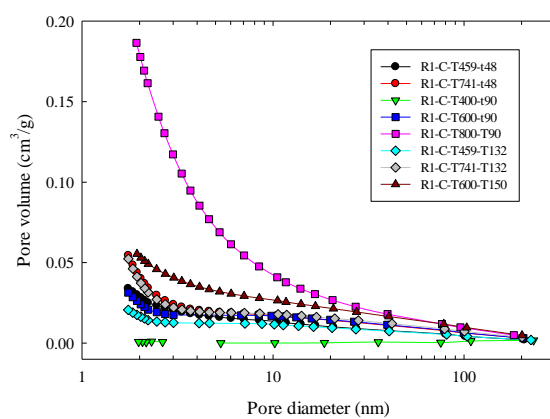
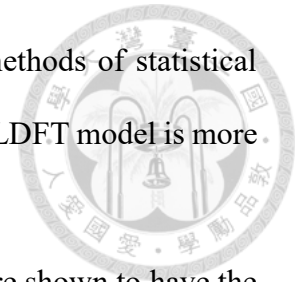


Figure 4-9 PSD of activated carbons with IR=1 from conventional chemical activation fitted by BJH

NLDFT model based on BJH model using the microscopic methods of statistical mechanics and molecular simulation. Compared with BJH model, NLDFT model is more suitable applied to the PSD at micropore (Binns, 2010).



The activated carbons from microwave chemical activation were shown to have the similar peak locations of PSD. The micropores are developed obviously at pore width of 0.7-0.9, 1.1-1.5, 1.6-1.8, and 1.9-2.0 nm.

The NLDFT results revealed in the conventional activation samples are shown in Figure 4-12. It also clearly demonstrated the difference in pore development between the R1-C-T800-t90 and R1-C-T600-t150. The peaks increased sharply at pore width of 0.7-0.8, 1.1-1.2, 1.3-1.5, 1.6-1.8, and 1.9-2.0 nm. Moreover, there is a peak shift at pore width between 1.0-1.1 nm, which means that the pore width of 1.0-1.1 nm was formed and then be increased.

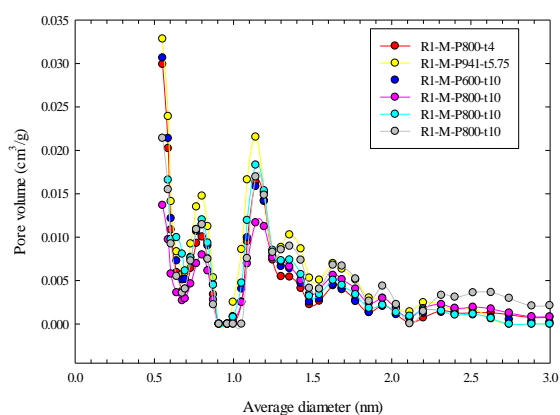


Figure 4-10 PSD of activated carbons with IR=1 from microwave chemical activation fitted by NLDFIT (a)

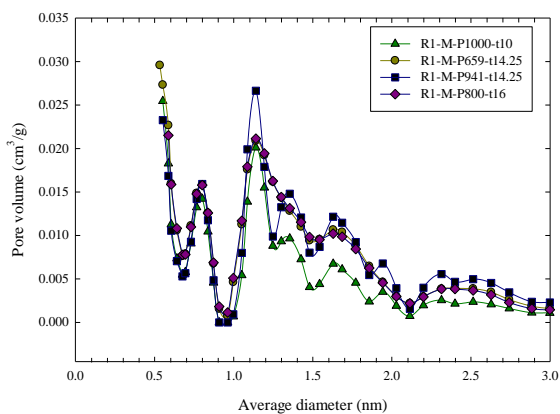


Figure 4-11 PSD of activated carbons with IR=1 from microwave chemical activation fitted by NLDFIT (b)

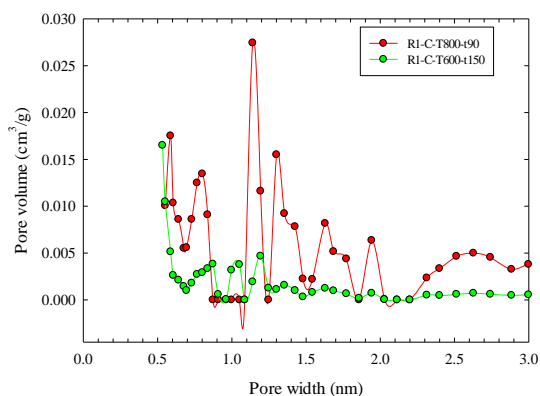
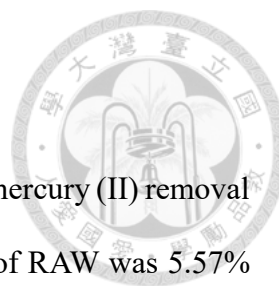


Figure 4-12 PSD of activated carbons with IR=1 from conventional chemical activation fitted by NLDFIT



4.1.5 Elemental analysis (EA)

It has been known that sulfur content plays an important rule on mercury (II) removal from aqueous solution. The results of EA shows that sulfur content of RAW was 5.57% (Table 4-7). After microwave chemical activation, all the sulfur contents of activated carbons were reduced to below 1%. Through CCD-RSM analysis, the relationship between the response (sulfur content: y) and the factors (power level: x_1 and time: x_2) is shown as equation (4.3). The R^2 of equation (4.3) is 0.645, and the adjusted R^2 is 0.290. The equation (4.3) can be drawn as Figure 4-13. Sulfur contents does not show the obvious trend from the two factors.

$$y = 2.92583 + (-0.00149801) x_1 + (-0.348014) x_2 + (-0.000000787284) x_1^2 + (0.00565679) x_2^2 + (0.000267630) x_1 x_2 \quad (4.3)$$

Table 4-7 Elemental analysis: microwave chemical activation

Sample	Elemental analysis (wt%)					
	N	C	S	H	O	Total
R1-M-P800-t4	0.82	74.57	0.86	2.49	7.49	86.22
R1-M-P659-t5.75	0.60	73.19	0.68	2.42	7.12	84.01
R1-M-P941-t5.75	0.33	70.37	0.47	2.30	5.89	79.36
R1-M-P600-t10	0.64	74.67	0.50	2.13	4.39	82.32
R1-M-P800-t10	0.46	78.92	0.32	1.68	4.65	86.01
R1-M-P800-t10	0.71	75.51	0.60	2.00	5.95	84.77
R1-M-P800-t10	0.54	77.41	0.43	1.89	10.90	91.17
R1-M-P1000-t10	0.86	85.45	0.28	1.31	7.64	95.54
R1-M-P659-t14.25	0.50	77.19	0.34	1.86	3.43	83.31
R1-M-P941-t14.25	0.46	75.77	0.77	1.59	2.18	80.77
R1-M-P800-t16	0.69	82.35	0.39	1.56	3.29	88.28
RAW	1.45	76.19	5.57	3.37	4.11	90.69

After conventional chemical activation, all the sulfur contents of activated carbons were also reduced. Through CCD-RSM analysis, the relationship between the response (Sulfur content: y) and the factors (temperature: x_1 and time: x_2) is shown as equation (4.4). The R^2 of equation (4.4) is 0.874, and the adjusted R^2 is 0.749. The equation (4.4) can be drawn as Figure 4-14. Figure 4-14 illustrates that the sulfur content highly depends on the activation temperature.

$$y = -2.26998 + (0.0232167) x_1 + (0.00664367) x_2 + (-0.0000257918) x_1^2 + (0.00000231315) x_2^2 + (-0.00000749986) x_1 x_2 \quad (4.4)$$

Table 4-8 Elemental analysis: conventional chemical activation

Sample	Elemental analysis (wt%)					
	N	C	S	H	O	Total
R1-C-T600-t30	1.11	66.78	2.52	2.49	18.92	91.82
R1-C-T459-t48	1.37	69.62	3.28	3.10	12.12	89.49
R1-C-T741-t48	0.83	74.16	0.36	2.15	14.93	92.43
R1-C-T400-t90	1.30	69.51	3.10	3.32	10.89	88.11
R1-C-T600-t90	1.07	66.33	2.60	2.23	15.42	87.65
R1-C-T600-t90	1.07	64.73	2.36	2.39	18.47	89.02
R1-C-T600-t90	1.14	68.72	2.80	2.38	17.27	92.30
R1-C-T800-t90	0.57	77.79	0.63	1.75	8.91	89.65
R1-C-T459-t132	1.25	68.49	3.26	3.07	12.17	88.24
R1-C-T741-t132	0.85	77.13	0.16	1.97	12.21	92.32
R1-C-T600-t150	1.27	70.24	3.29	2.29	18.15	95.24
RAW	1.45	76.19	5.57	3.37	4.11	90.69

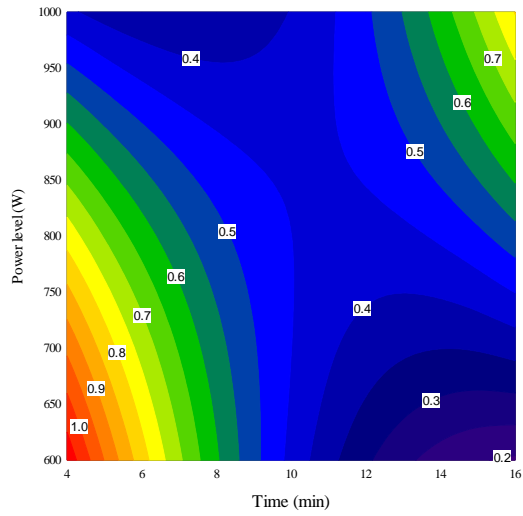
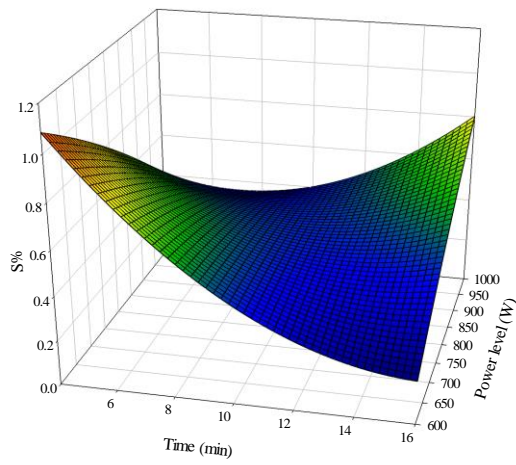


Figure 4-13 CCD-RSM analysis for the sulfur content versus power level and time of microwave chemical activation

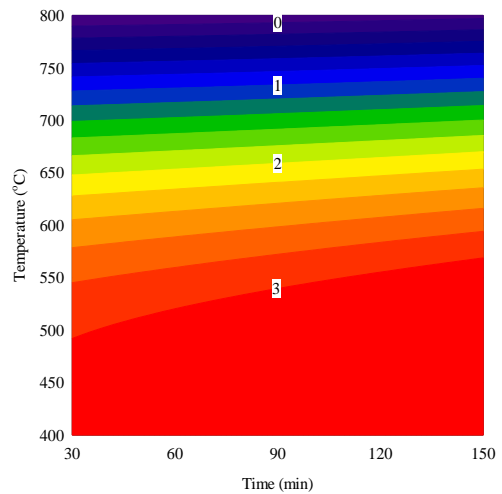
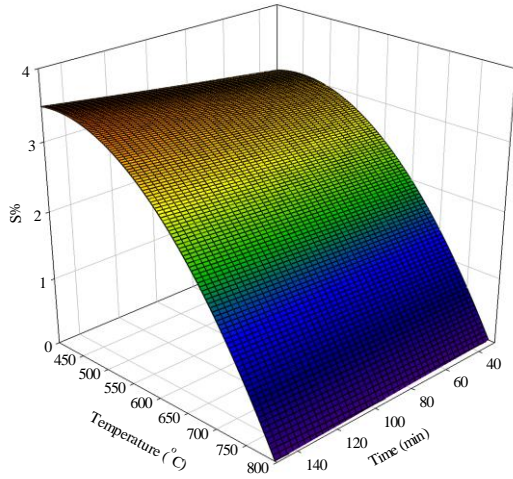


Figure 4-14 CCD-RSM analysis for the sulfur content versus temperature and time of conventional chemical activation

4.1.6 X-ray photoelectron spectroscopy (XPS)

XPS analysis results are shown in Figure 4-15 and Figure 4-16. Two major peaks of C_{1s} and O_{1s} in the survey scan were shown for all the activated carbons and RAW, indicating that the surface of activated carbons and RAW are majorly composed by carbon and oxygen. It should be also noted that there was no obvious peak at binding energy of 160-168 eV, which means that there was seldom S_{2p} on the surface of the resulting activated carbons. Thus, through both microwave and conventional chemical activation, the sulfur content would significantly decrease, which is consistent with the results of EA. Additionally, the residual sulfur in activated carbon would not exist on the surface of activated carbon.

Table 4-9 and Table 4-10 indicates that after activation, the relative content of graphitic carbon decreased, which can be attributed to the formation of the other oxygen functional groups. More phenolic and carboxyl functional groups formed on the carbon surface may result in an increase in hydrophilicity of activated carbon.

Table 4-9 also indicates that the phenolic, alcoholic, etheric functional groups (C-O-) and carboxyl or ester (COO) would increase after activation. These functional groups may offer the binding site of mercury (II) adsorption. Hydrophilic functional groups like carboxyl and hydroxyl can improve adsorption of inorganic ions in solution by ion-exchange reaction. Activated carbon impregnated with KOH would increase the surface density of hydrophilic groups (Zou *et al.*, 2008).

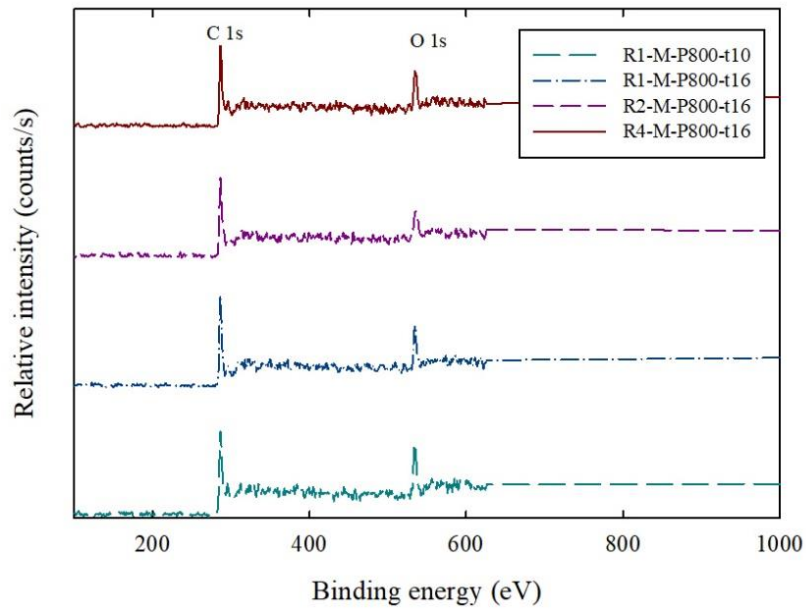
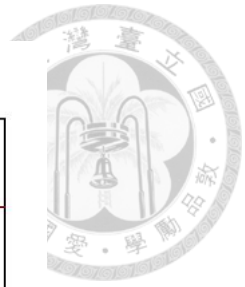


Figure 4-15 Survey scan for activated carbons from microwave activation

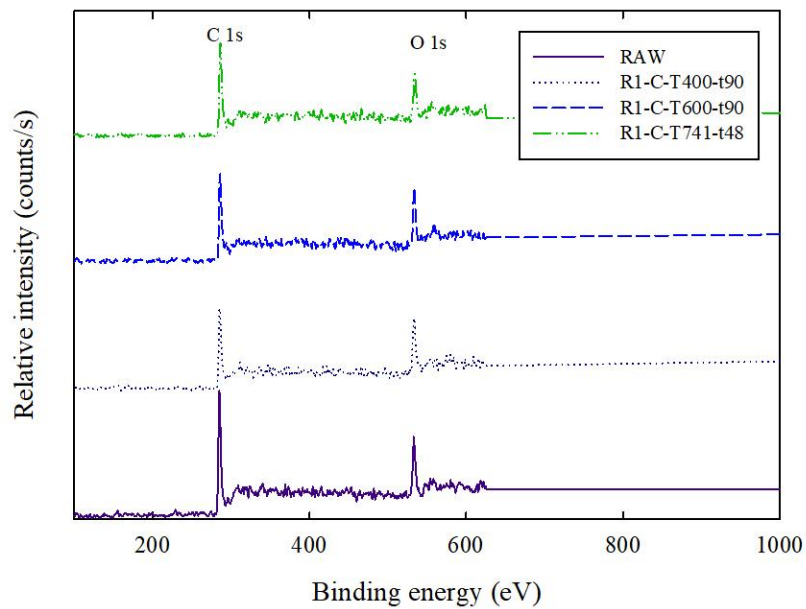


Figure 4-16 Survey scan for activated carbons from conventional activation

Table 4-9 The relative content of carbon functional group on the surface of activated carbons from microwave activation

Functional group	Assignment	RAW	R1-M-P800-t10	R1-M-P800-t16	R2-M-P800-t16	R4-M-P800-t16
C	Graphitic carbon	71.1%	62.7%	58.7%	57.6%	57.3%
C-O-	Phenolic, alcoholic, etheric	18.5%	21.2%	26.2%	24.7%	25.5%
C=O	Carbonyl or quinone	-	-	-	-	-
COO	Carboxyl or ester	5.9%	7.1%	8.8%	11.4%	9.4%
C=O/C=C	Carbonate, occluded CO, π electrons in aromatic ring	4.6%	3.2%	6.4%	6.2%	7.8%

Table 4-10 The relative content of carbon functional group on the surface of activated carbons from conventional activation

Functional group	Assignment	RAW	R1-C-T400-t90	R1-C-T600-t90	R1-C-T741-t48
C	Graphitic carbon	71.1%	65.0%	63.7%	51.5%
C-O-	Phenolic, alcoholic, etheric	18.5%	20.3%	22.1%	29.1%
C=O	Carbonyl or quinone	-	-	-	-
COO	Carboxyl or ester	5.9%	10.3%	9.2%	11.2%
C=O/C=C	Carbonate, occluded CO, π electrons in aromatic ring	4.6%	4.5%	5.0%	8.3%

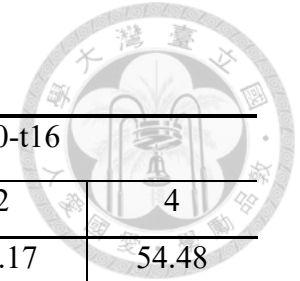
4.1.7 Comparison of different impregnation ratios (IR)

When IR is equal to 1, the three activation conditions (R1-M-P659-T14.25, R1-M-P941-T14.25 and R1-M-P800-T16) of activated carbons containing high S_{BET} were chosen for preparing the activated carbons with different IR. Table 4-11 reveals that all the physical properties of resulting activated carbon including S_{BET} , S_{micro} , V_{total} , and V_{micro} increase as IR increases.

The yield and the sulfur content of activated carbons do not show any obvious trend as IR increases. Nevertheless, the hydrogen and oxygen contents increased as IR increased.

Figure 4-147 to Figure 4-189 show the similar trends that the volume of pore width at 1-2 nm would increase as IR increases. There was also no peak shift in these figures, which means that even if the IR increases to 4, few pores were widened.

Table 4-11 Comparison of different impregnation ratios (IR)



IR	P659-t14.25			P941-t14.25			P800-t16		
	1	2	4	1	2	4	1	2	4
Yield (%)	62.83	57.01	68.43	50.23	54.91	50.43	48.19	52.17	54.48
S _{BET} (m ² /g)	1029.75	1259.69	1677.9	903.02	1386.89	1853.07	991.99	1301.82	1873.41
S _{micro} (m ² /g)	982.73	1174.12	1613.26	850.96	1361.12	1584.73	949.47	1207.81	1827.03
S _{micro} / S _{BET} (%)	95.43	93.21	96.15	94.23	98.14	85.52	95.71	92.78	97.52
V _{total} (m ³ /g)	0.586	0.74	0.946	0.529	0.763	1.14	0.588	0.772	1.022
V _{micro} (m ³ /g)	0.513	0.613	0.838	0.444	0.709	0.831	0.495	0.633	0.947
V _{micro} / V _{total} (%)	87.58	82.87	88.64	83.91	92.99	72.89	84.13	81.95	92.67
N (%)	0.5	0.89	0.21	0.46	0.85	0.46	0.69	0.82	0.68
C (%)	77.19	73.71	58.16	75.77	75.75	77.64	82.35	73.94	72.84
S (%)	0.34	0.63	0.11	0.77	0.21	0.38	0.39	0.18	0.17
H (%)	1.86	1.86	3.24	0.50	1.64	2.19	1.56	1.75	1.86
O (%)	3.43	16.2	16.28	2.18	12.93	6.18	3.29	13.47	17.09

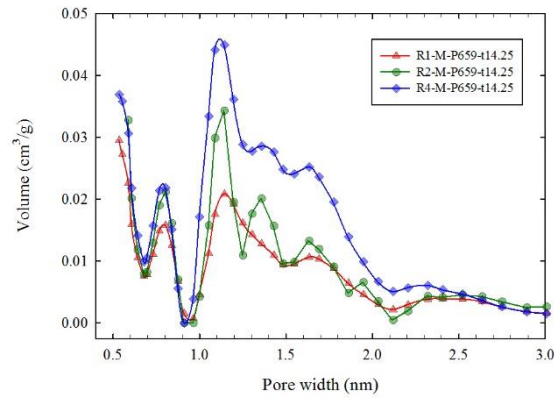


Figure 4-17 PSD of R1-M-P659-t14.25, R2-M-P659-t14.25 and R4-M-P659-t14.25 from microwave chemical activation fitted by NLDFT

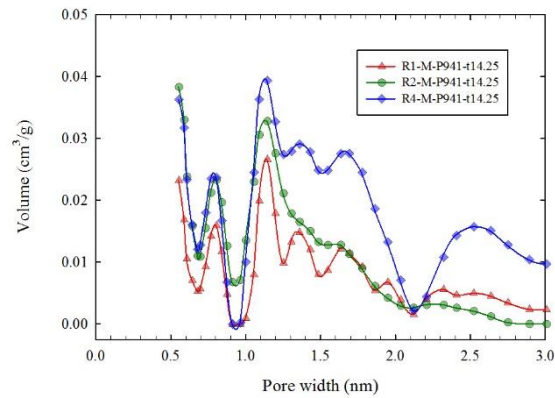


Figure 4-18 PSD of R1-M-P941-t14.25, R2-M-P941-t14.25 and R4-M-P941-t14.25 from microwave chemical activation fitted by NLDFT

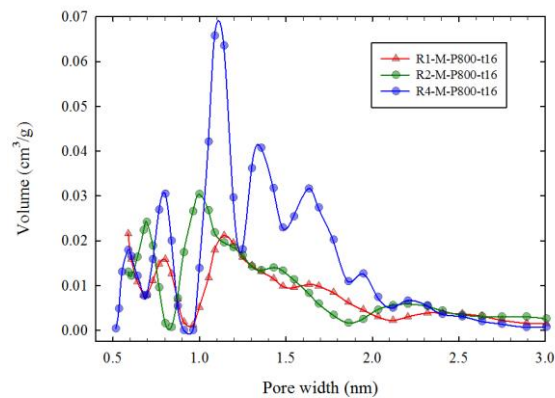


Figure 4-19 PSD of R1-M-P800-t16, R2-M-P800-t16 and R4-M-P800-t16 from microwave chemical activation fitted by NLDFT

4.1.8 Comparison of activation methods

According to the physical properties analysis, activated carbons with similar S_{BET} , which is one of the most important properties of activated carbon, were chosen for the comparison of different activation methods.

Table 4-12 reveals that activated carbons from microwave chemical activation had the higher yield, which can be attributed to that conventional heating is heating slowly and cooling slowly so that activated carbon may be maintained at high temperature for relatively long time. The S_{micro}/S_{BET} were all higher than 95%. The V_{micro}/V_{total} of R1-C-T800-t90 was larger than those of R1-M-P800-t4, R1-M-P600-t10, and R1-M-P800-t10, which can also be verified by the results from the PSD results of BJH and NLDFT model analysis (Figure 4-20 and Figure 4-21).

Moreover, the PSD peaks of R1-C-T800-t90 fitted by NLDFT is the sharper than those of R1-M-P800-t4, R1-M-P600-t10, and R1-M-P800-t10, Which means that the conventional chemical activation can develop pores at the narrow range of pore width.

The sulfur contents were all lower than 1%. Compared with the samples prepared from microwave chemical activation, R1-C-T800-t90 had lower hydrogen content and higher oxygen content.



Table 4-12 Comparison of different activation methods

	R1-M-P800-t4	R1-M-P600-t10	R1-M-P800-t10	R1-C-T800-t90
Yield (%)	74.81	72.38	71.72	63.62
S_{BET} (m^2/g)	676.94	721.96	721.02	697.26
S_{micro} (m^2/g)	646.04	696.11	709.35	683.42
$S_{\text{micro}}/S_{\text{BET}}$ (%)	95.44	96.42	98.38	98.02
V_{total} (m^3/g)	0.385	0.397	0.405	0.362
V_{micro} (m^3/g)	0.336	0.362	0.370	0.354
$V_{\text{micro}}/V_{\text{total}}$ (%)	87.39	91.04	91.47	97.70
N (%)	0.82	0.64	0.71	0.57
C (%)	74.57	74.67	75.51	77.79
S (%)	0.86	0.50	0.60	0.63
H (%)	2.49	2.13	2.00	1.75
O (%)	7.49	4.39	5.95	8.91

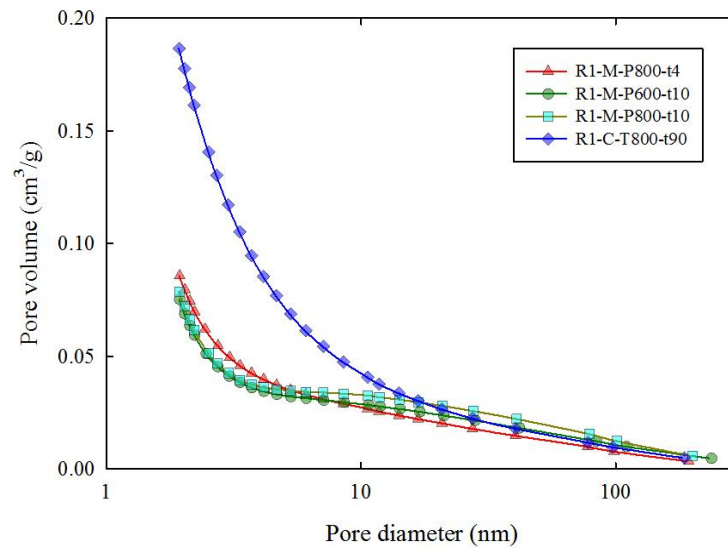


Figure 4-20 Comparison of different activation methods: PSD of BJH model

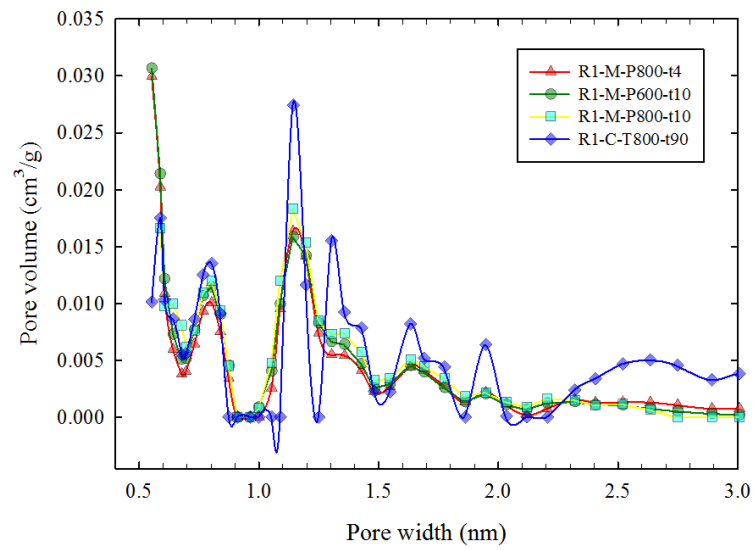


Figure 4-21 Comparison of different activation methods: PSD of NLDFT model



4.2 Mercury (II) Adsorption Experiment

4.2.1 Adsorption kinetic experiment

Through the adsorption kinetic model, the agitation time at equilibrium can be observed. Thus, it can decide the agitation time when the adsorption capacity is determined. In this study, R1-M-P800-t4 and R1-M-P659-t14.25 were chosen to represent the activated carbons from microwave chemical activation. R1-C-T400-t90 and R1-C-T800-t90 were chosen to represent the activated carbons from conventional chemical activation. Figure 4-22 shown that the change of the amount of mercury (II) adsorbed by activated carbon (q_t) along with the agitation time.

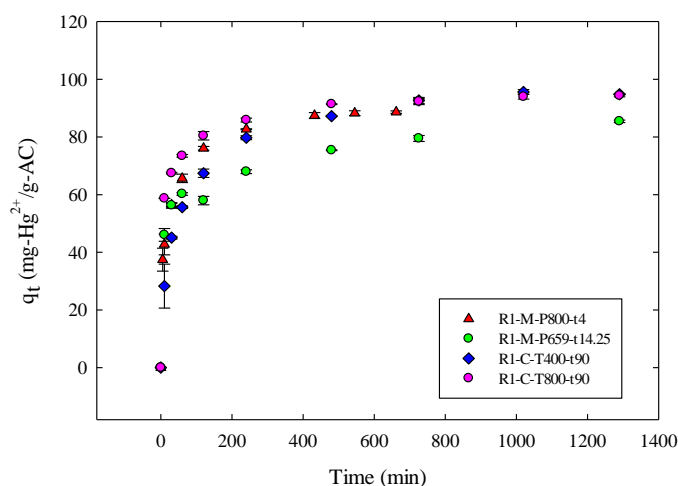


Figure 4-22 Effect of agitation time on adsorption of mercury

The linear fitting based on the pseudo-first kinetic model, pseudo-second kinetic model, and Elovich kinetic model were performed, and the results are shown in Table 4-13 to Table 4-15, Figure 4-22 to Figure 4-24. The details findings based on fitting of these three model were described below.

Based on the boundary condition of pseudo-first kinetic model, the regression line

must go through the origin.



Table 4-13 Pseudo-first kinetic model parameters for samples from microwave and conventional chemical activation

Sample	R ²	q _e	k ₁
R1-M-P800-t4	0.903	88.64	1.04×10 ⁻²
R1-M-P659-t14.25	0.210	85.44	4.31×10 ⁻³
R1-C-T400-t90	0.855	94.80	5.57×10 ⁻³
R1-C-T800-t90	0.603	94.35	5.86×10 ⁻³

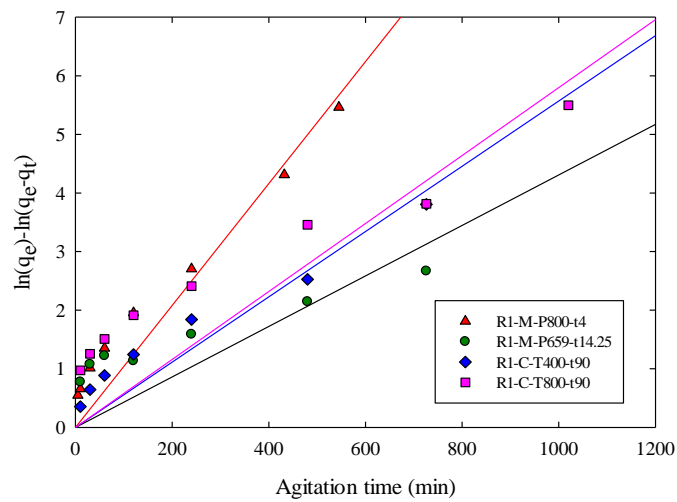


Figure 4-22 Pseudo-first kinetic model

Table 4-14 Pseudo-second kinetic model for samples from microwave and conventional chemical activation

Sample	R ²	q _e	k ₂
R1-M-P800-t4	1.000	90.09	8.09×10 ⁻⁴
R1-M-P659-t14.25	0.997	85.47	3.68×10 ⁻⁴
R1-C-T400-t90	0.999	97.47	2.86×10 ⁻⁴
R1-C-T800-t90	1.000	94.97	7.39×10 ⁻⁴

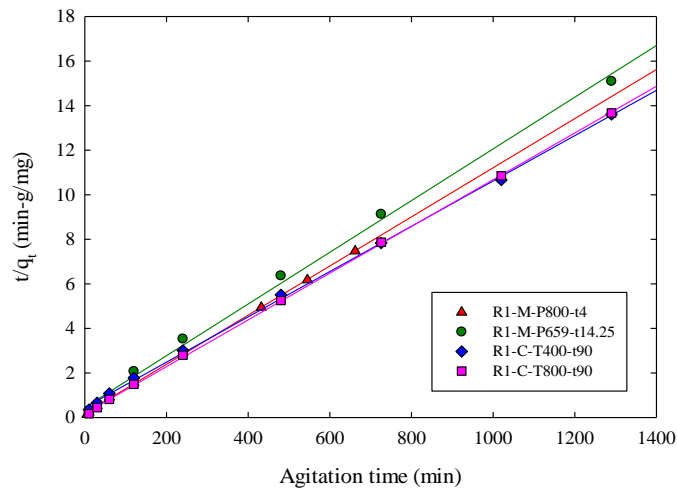
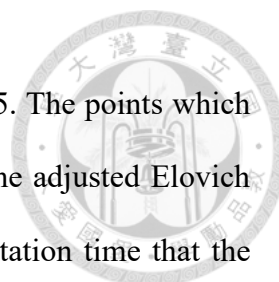


Figure 4-23 Pseudo-second kinetic model fitting for samples from microwave and conventional chemical activation



The constants in Elovich kinetic model are shown in Table 4-15. The points which the value of $\alpha \times \beta \times t$ is lower than 100 were used to regress so that the adjusted Elovich kinetic model results was shown in Table 4-16. Where t_0 is the agitation time that the regression starts at. R1-M-P800-t4 was regressed at 30 min after adjusted. R1-C-T400-t90 was regressed at 120 min after adjusted.

Table 4-15 Elovich kinetic model for samples from microwave and conventional chemical activation

Sample	R ²	α	β	$\alpha \times \beta \times t_0$
R1-M-P800-t4	0.989	62.23	8.95×10^{-2}	33.42
R1-M-P659-t14.25	0.950	257.7	1.29×10^{-1}	332.4
R1-C-T400-t90	0.989	11.82	6.99×10^{-2}	7.886
R1-C-T800-t90	0.985	2041	1.32×10^{-1}	2694

Table 4-16 Adjusted Elovich kinetic model parameters for samples from microwave and conventional chemical activation

Sample	R ²	α	β	$\alpha \times \beta \times t_0$
R1-M-P800-t4	0.972	91.98	9.50×10^{-2}	262.1
R1-C-T400-t90	0.963	35.54	8.45×10^{-2}	360.2

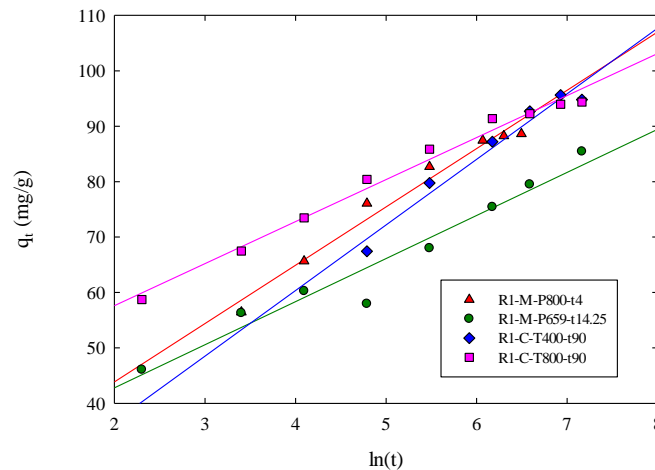


Figure 4-24 Elovich kinetic model

In summary, the pseudo-second kinetic model showed the higher R^2 . Therefore, we consider that the pseudo-second kinetic mechanism can best describe the adsorption of mercury by activated carbon in aqueous system; the pseudo-second kinetic model was further used to determine the equilibrium time. If the adsorption performance were assumed that it fulfills the pseudo-second kinetic model, q_e would be constant as t approaches infinity, but it takes too much time to reach the equilibrium. This study used the following method to acquire the equilibrium time (t_e).

There are three steps in determining t_e . First of all, if the last point of adsorption kinetic model is lower than the second-last point, the agitation time of the last point can be regarded as t_e . Second, there is a q_{e2} calculated from the pseudo-second kinetic model, and when the q_t from model reach 99% of q_{e2} , t can be regard as the t_e . Third, if not, the t_e was calculated from the pseudo-second kinetic model. When q_t arrives 99% of q_{e2} , the value of t_e is calculated.

Table 4-17 Calculated equilibrium time for samples from microwave and conventional chemical activation

Sample	q_{e1}	q_{e2}	99% q_{e2}	k_2	t_e (min)
R1-M-P800-t4	88.64	90.09	89.18	8.04×10^{-4}	1367
R1-M-P659-t14.25	85.44	85.47	84.61	3.59×10^{-4}	1290
R1-C-T400-t90	94.80	97.47	96.49	2.70×10^{-4}	1290
R1-C-T800-t90	94.35	94.97	94.02	7.43×10^{-4}	1290

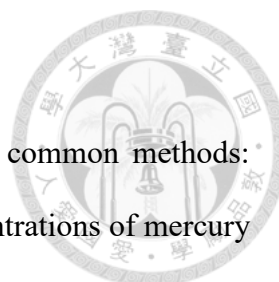
From the first step, t_e of R1-C-T400-t90 can be determined. From the second step, R1-M-P659-t14.25 and R1-C-T800-t90 can be determined.

From the third steps, R1-C-T400-t90 can be determined. The q_{e1} of R1-C-T400-t90 is less than 99% q_{e2} so that t_e should be calculated. Equation (4.1) was the linear form of the pseudo-second kinetic model. Then, the q_t was substituted into 99% q_{e2} to achieve equation (4.2). Hence, the equilibrium can be calculated.

$$t / q_t = 1 / (k_2 \times q_{e2}^2) + t / q_{e2} \quad (4.1)$$

$$t_e = 99 / (k_2 \times q_{e2}) \quad (4.2)$$

To sum up, the t_e of all the samples do not exceed 1290 min so that the agitation time was selected as 1440 min (24 h) in the adsorption capacity experiment and adsorption isotherm experiment to make sure all the samples achieve equilibrium.



4.2.2 Adsorption isotherm experiment

The adsorption isotherm experiment can be achieved by two common methods: dosing constant amount of activated carbon to different initial concentrations of mercury (II) or dosing a variety weights of activated carbon to a constant concentration of mercury (II). This study chose the second one. Through common adsorption model, the most fitted model can be used to predict the relationship between C_e and q_e . The above Figure 4-25 Figure 4-27 and Table 4-18 Table 4-20 reveal the linear regressions of models.

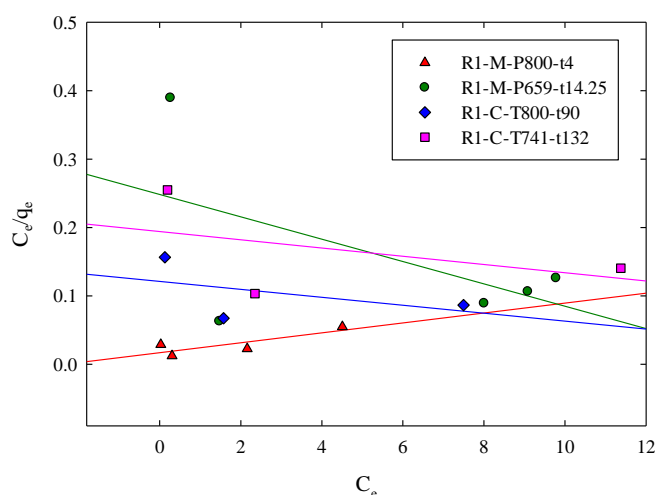


Figure 4-25 Langmuir adsorption isotherm model for samples from microwave and conventional chemical activation

Table 4-18 Langmuir adsorption isotherm model parameters for samples from microwave and conventional chemical activation

Sample	R^2	q_m	K_L
R1-M-P800-t4	0.686	59.00	2.338
R1-M-P659-t14.25	0.304	4.028	-15.195
R1-C-T800-t90	0.234	8.254	-20.85
R1-C-T741-t132	0.205	5.1496	-32.20

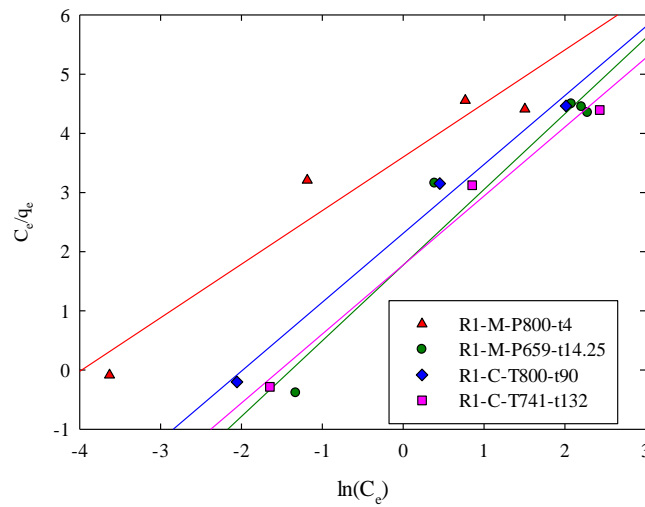


Figure 4-26 Freundlich adsorption isotherm model for samples from microwave and conventional chemical activation

Table 4-19 Freundlich adsorption isotherm model parameters for samples from microwave and conventional chemical activation

Sample	R ²	n _f	K _F
R1-M-P800-t4	0.929	1.105	36.55
R1-M-P659-t14.25	0.935	0.783	5.903
R1-C-T800-t90	0.987	0.859	10.09
R1-C-T741-t132	0.984	0.848	5.091

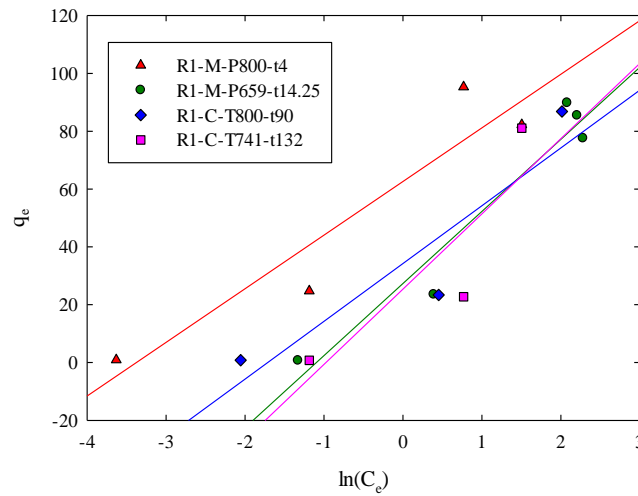


Figure 4-27 Temkin adsorption isotherm model for samples from microwave and conventional chemical activation

Table 4-20 Temkin adsorption isotherm model parameters for samples from microwave and conventional chemical activation

Sample	R^2	K_1	K_2
R1-M-P800-t4	0.887	18.54	29.26
R1-M-P659-t14.25	0.941	24.92	2.999
R1-C-T800-t90	0.847	19.98	5.557
R1-C-T741-t132	0.761	26.02	2.657

From these three models, All of the samples cannot be well predicted by Langmuir adsorption isotherm model. It can be observed that samples fitted Freundlich adsorption isotherm model had relatively high R^2 . For R1-M-P659-t14.25, it also had relatively high R^2 . For R1-M-P659-t14.25, it also had relatively high R^2 when fitted Temkin adsorption isotherm model.



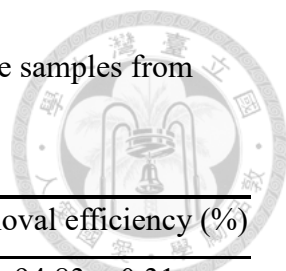
4.2.3 Adsorption capacity experiment

The adsorption capacities of mercury (II) and removal efficiency of microwave chemical activation and conventional chemical activation are respectively listed in Table 4-21 and Table 4-22. The value after the symbol \pm is the standard deviation of triplication of adsorption capacity experiments. The adsorption capacity of RAW was 12.58 ± 4.49 mg-Hg²⁺/g-AC and the removal efficiency is $14.44 \pm 5.17\%$, which represents that the original oil sand coke is not effective to removal mercury (II) from aqueous solution.

After microwave chemical activation, the mercury (II) adsorption capacity of activated carbons were significantly increased to 70.73-82.26 mg-Hg²⁺/g-AC and the removal efficiency was 81.11-94.83%. After conventional chemical activation, the mercury (II) adsorption on activated carbon was also increased to 75.29-92.89 mg-Hg²⁺/g-AC and the removal efficiency were 79.83-97.81%. Thus, it can be concluded that both microwave and conventional chemical activation are able to increase the adsorption capacity.

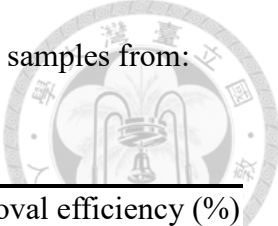
Moreover, it was also noted that even though the activated carbon with a low S_{BET} ($62.39 \text{ m}^2/\text{g}$), the mercury (II) adsorption capacity of the samples was still significant, and was not lower than those with a high S_{BET} . This results indicate that high S_{BET} is not necessary for activated carbon to achieve a high removal mercury (II) from aqueous solution.

Table 4-21 Mercury adsorption performance for raw coke and the samples from
microwave chemical activation



Sample	S _{BET} (m ² /g)	mg-Hg ²⁺ /g-AC	Removal efficiency (%)
R1-M-P800-t4	676.94	82.26 ± 0.32	94.83 ± 0.31
R1-M-P659-t5.75	759.73	80.47 ± 0.44	92.58 ± 0.31
R1-M-P941-t5.75	836.33	80.47 ± 1.38	91.92 ± 1.40
R1-M-P600-t10	721.96	80.25 ± 0.44	91.66 ± 0.30
R1-M-P800-t10	453.99	79.34 ± 0.50	91.58 ± 0.50
R1-M-P800-t10	721.02	81.84 ± 0.26	94.47 ± 0.10
R1-M-P800-t10	642.70	74.34 ± 4.13	85.26 ± 4.75
R1-M-P1000-t10	766.63	79.77 ± 1.09	91.55 ± 1.07
R1-M-P659-t14.25	1029.75	77.58 ± 2.74	88.86 ± 3.05
R1-M-P941-t14.25	903.02	70.73 ± 0.47	81.11 ± 0.63
R1-M-P800-t16	991.99	79.22 ± 0.29	91.09 ± 0.20
R2-M-P659-t14.25	1259.69	83.12 ± 0.13	96.84 ± 0.04
R2-M-P941-t14.25	1386.89	78.35 ± 0.29	91.40 ± 0.11
R2-M-P800-t16	1301.82	75.94 ± 0.36	88.65 ± 0.52
R4-M-P659-t14.25	1677.90	91.36 ± 0.66	96.67 ± 0.11
R4-M-P941-t14.25	1853.07	84.79 ± 0.61	93.58 ± 0.39
R4-M-P800-t16	1873.41	86.30 ± 0.22	94.87 ± 0.02
RAW	0.8	12.58 ± 4.49	14.44 ± 5.17

Table 4-22 Mercury adsorption performance for raw coke and the samples from:
conventional chemical activation



Sample	S _{BET} (m ² /g)	mg-Hg ²⁺ /g-AC	Removal efficiency (%)
R1-C-T600-t30	283.96	81.51 ± 0.96	88.15 ± 0.61
R1-C-T459-t48	120.01	75.73 ± 5.24	82.18 ± 5.61
R1-C-T741-t48	663.10	85.24 ± 0.50	92.75 ± 0.65
R1-C-T400-t90	62.39	92.89 ± 0.96	95.50 ± 0.12
R1-C-T600-t90	220.88	90.68 ± 0.49	97.81 ± 0.31
R1-C-T600-t90	301.83	87.35 ± 1.80	94.47 ± 1.70
R1-C-T600-t90	262.15	84.88 ± 0.93	87.38 ± 0.63
R1-C-T800-t90	697.26	86.81 ± 1.20	92.05 ± 1.12
R1-C-T459-t132	108.56	86.84 ± 1.58	89.11 ± 1.45
R1-C-T741-t132	615.36	81.06 ± 1.03	87.66 ± 0.79
R1-C-T600-t150	287.44	75.29 ± 1.05	79.83 ± 0.73
RAW	0.8	12.58 ± 4.49	14.44 ± 5.17

In order to know whether the activated carbons in this study is effective on mercury (II) adsorption, data in a doctoral dissertation (Cai and Jia, 2010) were cited to compare with data in this study. The differences between the doctoral dissertation and this study are listed in Table 4-23.

Table 4-23 The differences between a previous work and this study

Mercury (II) adsorption capacity	This study	(Cai and Jia, 2010)
Raw material	Fluid coke	Fluid coke
Activation method	Conventional and microwave activation	Conventional activation
Activation agent	KOH	KOH and SO ₂
Chemicals	HgCl ₂	HgCl ₂
AC particle size	0.037-0.149 mm	0.212-0.300 mm
Initial conc. (mg-Hg ²⁺ /L)	100	100
AC dosage (g/L)	1	1
Solution volume (mL)	50	100
Agitation time (h)	24	15.5
pH	6.9-7.1	4.8
Temperature (°C)	30	25

Figure 4-28 and Figure 4-29 show that almost all the activated carbons from this study had the higher adsorption capacities and efficiency than those shown in Cai and Jia (2010). All of the activated carbons from this study have the higher removal efficiency. The results might be attributed to the particle sizes of activated carbons in this study is smaller, and an adequate surface functionality is developed via chemical activation, which has to be further examined. It is also important to note that the effect of pH is diverse from different references.

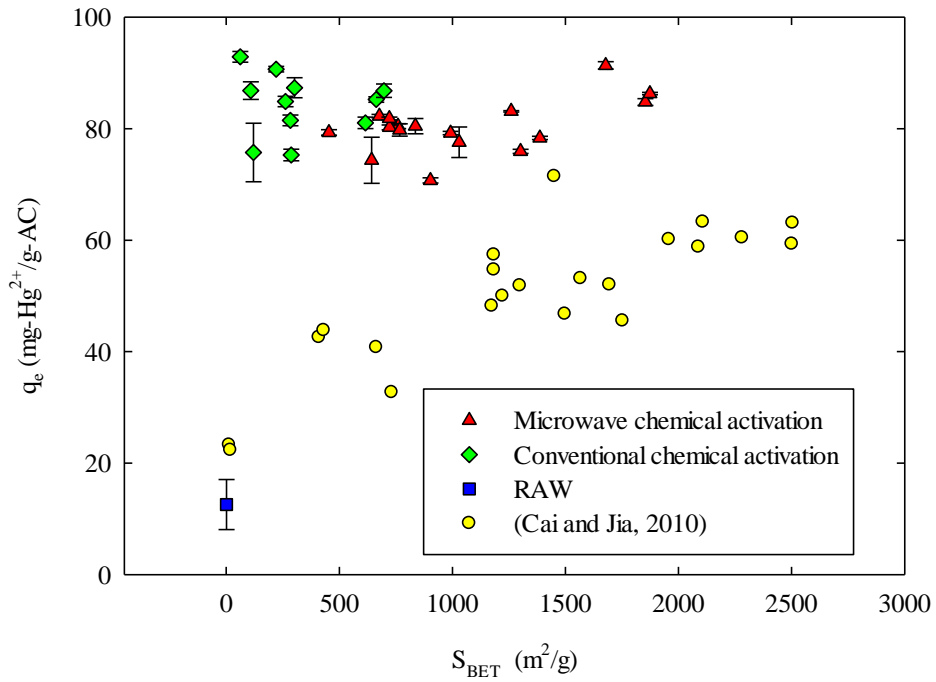
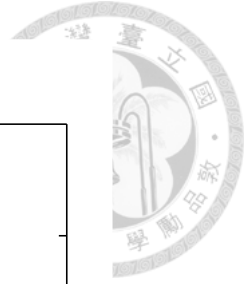


Figure 4-28 Effect of S_{BET} on Hg^{2+} adsorption capacity

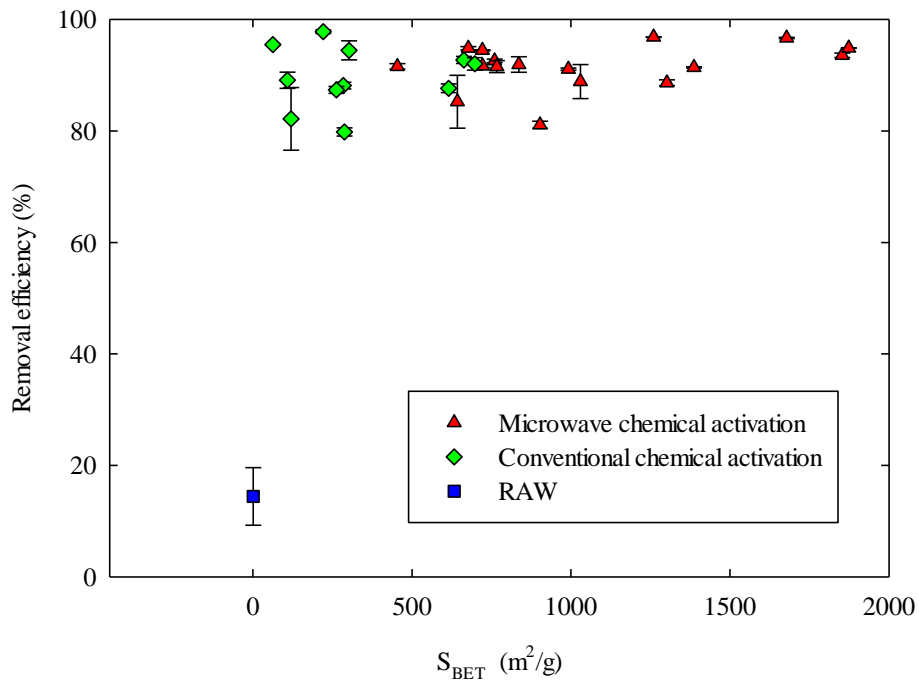


Figure 4-29 Effect of S_{BET} on Hg^{2+} removal efficiency

Through CCD-RSM analysis, the results of removal efficiency versus operating factors are shown in Figure 4-30, Figure 4-31 and Table 4-24. The optimized operating condition of microwave chemical activation can be observed at the power level of 750-1000 W and time of 4-5 min and the removal efficiency would achieve 94%. The optimized operating condition of conventional chemical activation can be observed at the temperature of 700-800°C and time of 45-85 min and the removal efficiency would achieve 94%.

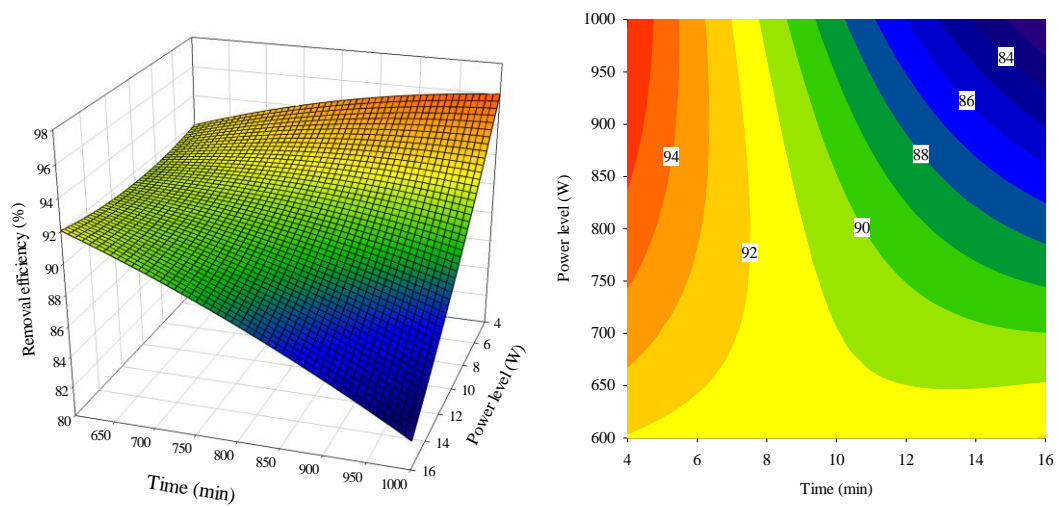


Figure 4-30 CCD-RSM analysis for the removal efficiency versus power level and time of microwave chemical activation

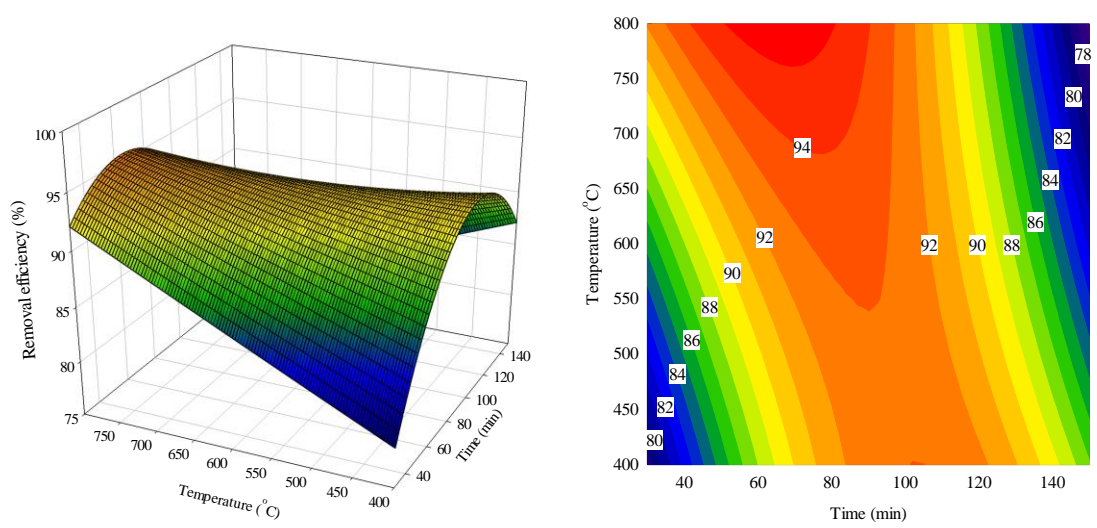
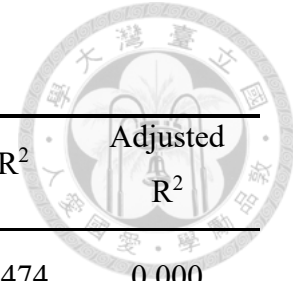


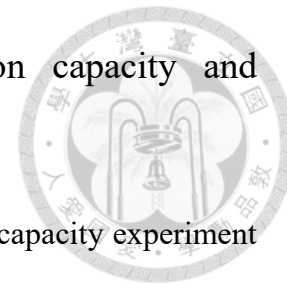
Figure 4-31 CCD-RSM analysis for the removal efficiency versus temperature and time of conventional chemical activation

Table 4-24 CCD-RSM for mercury (II) adsorption capacity and removal efficiency



Method	y	x ₁	x ₂	CCD-RSM equation	R ²	Adjusted R ²
Microwave	Adsorption capacity	Power level	Time	$y = 67.642 + (0.0225481) x_1 + (1.39895) x_2 + (-0.000000349823) x_1^2 + (0.0196886) x_2^2 + (-0.00286448) x_1x_2$	0.474	0.000
	Removal efficiency	Power level	Time	$y = 70.1693 + (0.0480163) x_1 + (1.40014) x_2 + (-0.0000162120) x_1^2 + (0.0193855) x_2^2 + (-0.00296484) x_1x_2$	0.445	0.000
Conventional	Adsorption capacity	Temperature	Time	$y = 44.7195 + (0.0152456) x_1 + (0.886264) x_2 + (0.0000314898) x_1^2 + (-0.00283067) x_2^2 + (-0.000637071) x_1x_2$	0.761	0.523
	Removal efficiency	Temperature	Time	$y = 45.4004 + (0.0465343) x_1 + (0.756685) x_2 + (0.00000190698) x_1^2 + (-0.00269687) x_2^2 + (-0.000500824) x_1x_2$	0.650	0.300

4.2.4 Correlation analysis of mercury (II) adsorption capacity and characteristics of activated carbon



Owing to the initial concentration of each batch of adsorption capacity experiment was variable, the Pearson correlation coefficient was used to decide whether the property is reliable to predict the removal efficiency of mercury (II). The value of Pearson correlation coefficient is between +1 and -1, where 1 represents total positive linear correlation, 0 represents no linear correlation, and -1 represents total negative linear correlation. Simultaneously, the signal “*” shown near the Pearson correlation analysis in Table 4-25 represents that the p-value of the Pearson correlation analysis, where “***” means that p-value is lower than 0.01, where “**” means that the p-value is larger than 0.01 and lower than 0.05, and no “*” means that the p-value is larger than 0.05.

According to the Pearson correlation analysis, it can be found that the q_e , is independent of the physical properties and there are linear correlation between q_e and carbon content, hydrogen content and oxygen content.

Monser and Adhoum (2002) indicated that metal ion removal by activated carbons occurred, when ion exchange happened between the metal ions and acidic functional groups. Moreover, the sites of functional groups comprised little fraction of the carbon surface area.

This phenomenon may be attributed to that the formation of the acidic functional groups during activation process, which plays an important rule on ion exchange process on the surface of activated carbon. On the other hand, Cai and Jia (2010) also recorded the change of pH during the mercury (II) adsorption. The pH value would decrease as the agitation time increased, which indicated that the adsorption of mercury (II) would release the H^+ .

Table 4-25 Pearson's correlation coefficient applied in microwave chemical activation

Property	Pearson's correlation coefficient	
	q_e	Removal efficiency (%)
S_{BET}	-0.038	0.306
S_{micro}	-0.033	0.315
S_{micro}/S_{BET}	0.189	0.147
V_{total}	-0.052	0.290
V_{micro}	-0.036	0.313
V_{micro}/V_{total}	0.039	0.217
N (%)	0.152	-0.220
C (%)	-0.496**	-0.142
S (%)	0.224	-0.283
H (%)	0.579**	0.219
O (%)	0.388*	0.055

The linear regression of hydrogen content and removal efficiency is shown in Figure 4-32. However, this is a hypothesis, the relationship between acidic functional groups and hydrogen content as well as oxygen content needs to be further verified.

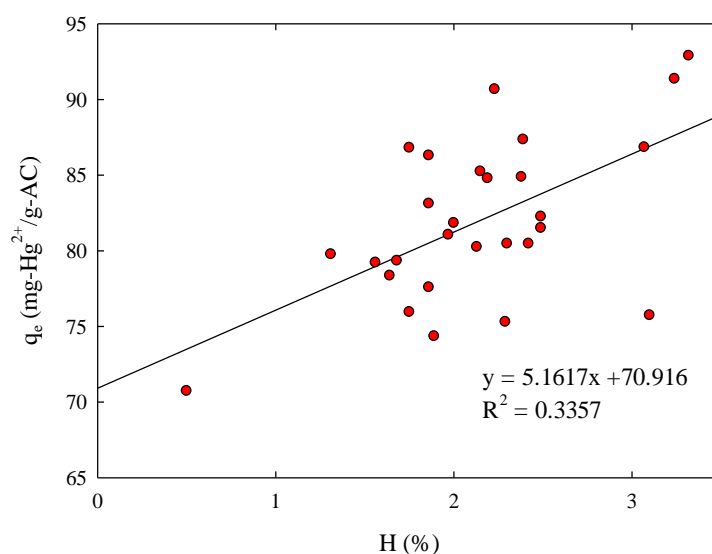


Figure 4-32 Effect of hydrogen content on removal efficiency

Chapter 5 Conclusions and Recommendations



5.1 Conclusions

In this study, four goals were previously set to achieve, including:

- preparing activated carbons by microwave and conventional chemical activation and observe the change from different activation conditions;
- discovering the differences between activated carbons from microwave chemical activation at similar S_{BET} .
- the mercury (II) adsorption performances of the prepared activated carbons, including understanding the adsorption kinetic, isotherm and adsorption capacity;
- analyzing the influencing factors determining the mercury adsorption capacity;

Based on the achievement of these goals, the corresponding conclusions of this study were listed below.

1. Activated carbons with high S_{BET} can be prepared in relatively short times by microwave chemical activation. Most of the pores were formed as micropores. Thus, microwave chemical activation is a time-effective methodology to prepare activated carbon.

The production yield of activated carbon decrease as the power level or activation time increased. The inherent sulfur contents of activated carbons were clearly shown to mostly escape during the microwave chemical activation process. The activated carbons from microwave chemical activation have the similar peak locations of PSD but various contents.

2. The extent of sulfur contents of activated carbons produced by conventional chemical activation primarily depended on the activation temperatures. Most of the pores of

activated carbons from conventional chemical activation are also micropores, similar to those from microwave chemical activation.

3. Compared with activated carbon from conventional chemical activation, activated carbon from microwave chemical activation has the higher yield, lower $V_{\text{micro}}/V_{\text{total}}$, lower hydrogen content, higher oxygen content and similar sulfur content. Moreover, based on the PSD fitted by NLDFT, conventional chemical activation can develop pores at the narrow range of pore width. The types of energy provided would determine the PSD of activated carbons. Moreover, the properties of activated carbons from microwave activation would be more unstable and unpredictable owing to formation of hot spot during microwave heating process.

4. Pseudo-second order kinetic model best fitted the adsorption kinetic of both the activated carbons from microwave and conventional chemical activation. The equilibrium times was close to 24 h. Freundlich model best fitted the adsorption isotherm experiments of both the activated carbons from microwave and conventional chemical activation, indicating the adsorption equilibrium can only be described empirically.

5. Before activation, the mercury (II) adsorption capacity of fluid coke was 12.58 ± 4.49 mg-Hg²⁺/g-AC and the removal efficiency was $14.44 \pm 5.17\%$. After microwave chemical activation, the mercury (II) adsorption capacity of activated carbons was 70.73-82.26 mg-Hg²⁺/g-AC and the removal efficiency were 81.11-94.83%. After conventional chemical activation, the mercury (II) adsorption on activated carbon was 75.29-92.89 mg-Hg²⁺/g-AC to and the removal efficiency was 79.83-97.81%. Based on the Pearson correlation analysis, the adsorption capacity of activated carbons from microwave and conventional chemical activation depends on the hydrogen content and oxygen content. It can be attributed to that the content of the phenolic, alcoholic, etheric functional groups (C-O-) and carboxyl or ester functional groups (COO) was increased during activation process.

It might also suggest that the content of the acidic functional groups on the surface of the activated carbon determining the mercury adsorption of the resulting activated carbon.

6. Through CCD-RSM analysis, the optimized operating condition of microwave chemical activation can be observed at the power level of 750-1000 W and time of 4-5 min and the removal efficiency would achieve 94%. The optimized operating condition of conventional chemical activation can be observed at the temperature of 700-800°C and time of 45-85 min and the removal efficiency would achieve 94%.

5.2 Recommendations

The study shows that even though the activated carbon with a low S_{BET} ($62.39 \text{ m}^2/\text{g}$), the mercury (II) adsorption capacity of the samples still significant, and is not lower than those with a high S_{BET} . Hence, owing to the time-consuming and energy-consuming reasons for both microwave and conventional chemical activation, the modest level of activation conditions, namely a shorter but considering adequate activation time, temperature, and power usage can be applied to produce activated carbons with proper properties for removal of mercury from aqueous solution.

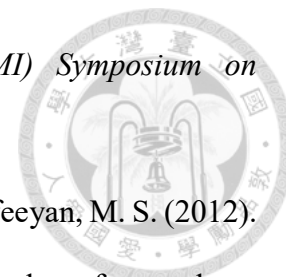
The larger scale of preparation of activated carbon from microwave oven can be established for testing whether the technology is able to applied in industrial scale. Moreover, the consumption of energy between conventional activation and microwave activation can be further achieved.

Reference



- Abdelouahab-Reddam, Z., Wahby, A., Mail, R. E., Silvestre-Albero, J., Rodríguez-Reinoso, F., and Sepúlveda-Escribano, A. (2014). Activated carbons impregnated with Na_2S and H_2SO_4 : Texture, surface chemistry and application to mercury removal from aqueous solutions. *Adsorption Science and Technology*, 32(2-3), 101-115.
- Ahmad, A. A., and Hameed, B. H. (2010). Effect of preparation conditions of activated carbon from bamboo waste for real textile wastewater. *Journal of Hazardous Materials*, 173(1), 487-493.
- Ahmed, M. J., and Theydan, S. K. (2014). Optimization of microwave preparation conditions for activated carbon from Albizia lebbek seed pods for methylene blue dye adsorption. *Journal of Analytical and Applied Pyrolysis*, 105, 199-208.
- Allen, J. A., and Scaife, P. H. (1966). The Elovich equation and chemisorption kinetics. *Australian Journal of Chemistry*, 19(11), 2015-2023.
- Almeida, P., and Stearns, L. B. (1998). Political opportunities and local grassroots environmental movements: The case of Minamata. *Social Problems*, 45(1), 37-60.
- Alslaibi, T. M., Abustan, I., Ahmad, M. A., and Foul, A. A. (2013). Application of response surface methodology (RSM) for optimization of Cu^{2+} , Cd^{2+} , Ni^{2+} , Pb^{2+} , Fe^{2+} , and Zn^{2+} removal from aqueous solution using microwaved olive stone activated carbon. *Journal of Chemical Technology and Biotechnology*, 88(12), 2141-2151.
- Anderson, M. J., and Whitcomb, P. J. (2007). Response surface methods (RSM) for peak process performance at the most robust operating conditions. In *Proceeding from*

*International SEMATECH Manufacturing Initiative (ISMI) Symposium on
Manufacturing Effectiveness.*



Arami-Niya, A., Daud, W. M. A. W., Mjalli, F. S., Abnisa, F., and Shafeeyan, M. S. (2012).

Production of microporous palm shell based activated carbon for methane adsorption: modeling and optimization using response surface methodology. *Chemical Engineering Research and Design*, 90(6), 776-784.

Attari, M., Bukhari, S. S., Kazemian, H., and Rohani, S. (2017). A low-cost adsorbent from coal fly ash for mercury removal from industrial wastewater. *Journal of Environmental Chemical Engineering*, 5(1), 391-399.

Atwood, D. A., and Zaman, M. K. (2006). Mercury removal from water. In *Recent Developments in Mercury Science* (pp. 163-182). Springer Berlin Heidelberg.

Azizian, S. (2004). Kinetic models of sorption: a theoretical analysis. *Journal of Colloid and Interface Science*, 276(1), 47-52.

Bansal, R. C., and Goyal, M. (2005). *Activated carbon adsorption*. CRC press.

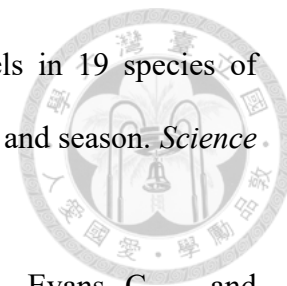
Barrett, E. P., Joyner, L. G., and Halenda, P. P. (1951). The determination of pore volume and area distributions in porous substances. I. Computations from nitrogen isotherms. *Journal of the American Chemical Society*, 73(1), 373-380.

Bezerra, M. A., Santelli, R. E., Oliveira, E. P., Villar, L. S., and Escaleira, L. A. (2008). Response surface methodology (RSM) as a tool for optimization in analytical chemistry. *Talanta*, 76(5), 965-977.

Binns, C. (2010). *Introduction to nanoscience and nanotechnology* (Vol. 14). John Wiley & Sons.

Budinova, T., Petrov, N., Parra, J., and Baloutzov, V. (2008). Use of an activated carbon from antibiotic waste for the removal of Hg (II) from aqueous solution. *Journal of Environmental Management*, 88(1), 165-172.

Burger, J., and Gochfeld, M. (2011). Mercury and selenium levels in 19 species of saltwater fish from New Jersey as a function of species, size, and season. *Science of the Total Environment*, 409(8), 1418-1429.



Burrowes, A., Teare, M., Marsh, R., Gigantelli, P., Macgillivray, J., Evans, C., ... and Hurst, T. (2011). Alberta's energy reserves 2010 and supply/demand outlook 2011–2020. *Annual Report ST98-2011, Energy Resources Conservation Board, Calgary, Alberta (June 2011)*.

Cai, H. (2010). *Sulphur Chemistry in KOH-SO₂ Activation of Fluid Coke and Mercury Adsorption from Aqueous Solutions* (Doctoral dissertation). University of Toronto, Canada.

Cai, J. H., and Jia, C. Q. (2010). Mercury removal from aqueous solution using coke-derived sulfur-impregnated activated carbons. *Industrial and Engineering Chemistry Research*, 49(6), 2716-2721.

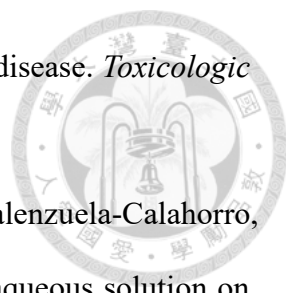
Cecen, F. (2014). Activated carbon. Retrieved from https://www.researchgate.net/publication/263062486_Activated_Carbon

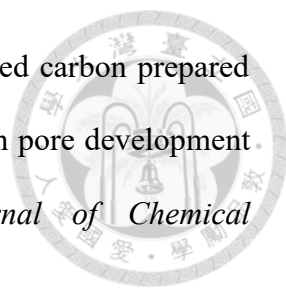
Chen, H., and Hashisho, Z. (2012a). Fast preparation of activated carbon from oil sands coke using microwave-assisted activation. *Fuel*, 95, 178-182.

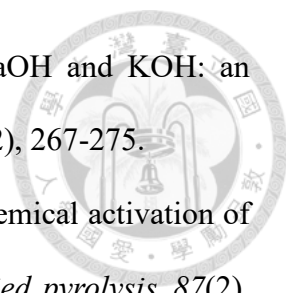
Chen, H., and Hashisho, Z. (2012b). Effects of microwave activation conditions on the properties of activated oil sands coke. *Fuel processing technology*, 102, 102-109.

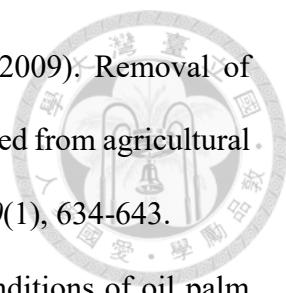
Clarkson, T. W., and Magos, L. (2006). The toxicology of mercury and its chemical compounds. *Critical Reviews in Toxicology*, 36(8), 609-662.

Engelhardt, R. and M. Todirescu, School of Business at University of Alberta. (2012). *An Introduction to Development in Alberta's Oil Sands*. Retrieved from <http://www.beg.utexas.edu/energyecon/thinkcorner/Alberta%20Oil%20Sands.pdf>

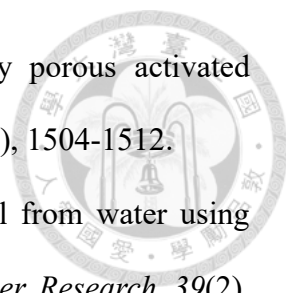
- 
- Eto, K. (1997). Review article: pathology of minamata disease. *Toxicologic Pathology*, 25(6), 614-623.
- Gomez-Serrano, V., Macias-Garcia, A., Espinosa-Mansilla, A., and Valenzuela-Calahorro, C. (1998). Adsorption of mercury, cadmium and lead from aqueous solution on heat-treated and sulphurized activated carbon. *Water Research*, 32(1), 1-4.
- Hill, J. M., Karimi, A., and Malekshahian, M. (2014). Characterization, gasification, activation, and potential uses for the millions of tonnes of petroleum coke produced in Canada each year. *The Canadian Journal of Chemical Engineering*, 92(9), 1618-1626.
- Hornyak, G. L., Dutta, J., Tibbals, H. F., and Rao, A. (2008). *Introduction to nanoscience*. CRC press.
- Huang, Y. P., Hou, C. H., Hsi, H. C., and Wu, J. W. (2015). Optimization of highly microporous activated carbon preparation from Moso bamboo using central composite design approach. *Journal of the Taiwan Institute of Chemical Engineers*, 50, 266-275.
- Ioannidou, O., and Zabaniotou, A. (2007). Agricultural residues as precursors for activated carbon production—a review. *Renewable and Sustainable Energy Reviews*, 11(9), 1966-2005.
- Jagiello, J., and Thommes, M. (2004). Comparison of DFT characterization methods based on N₂, Ar, CO₂, and H₂ adsorption applied to carbons with various pore size distributions. *Carbon*, 42(7), 1227-1232.
- Jerby, E., Dikhtyar, V., Aktushev, O., and Groszlick, U. (2002). The microwave drill. *Science*, 298(5593), 587-589.
- Joy, D. C. (2006). Scanning electron microscopy. In *Materials Science and Technology* (pp. 221-249). Wiley-VCH Verlag GmbH and Co. KGaA.

- 
- Karimi, A., Thinon, O., Fournier, J., and Hill, J. M. (2013). Activated carbon prepared from Canadian oil sands coke by CO₂ activation: I. Trends in pore development and the effect of pre-oxidation. *The Canadian Journal of Chemical Engineering*, 91(9), 1491-1499.
- Kawano, T., Kubota, M., Onyango, M. S., Watanabe, F., and Matsuda, H. (2008). Preparation of activated carbon from petroleum coke by KOH chemical activation for adsorption heat pump. *Applied Thermal Engineering*, 28(8), 865-871.
- Khuri, A. I., and Mukhopadhyay, S. (2010). Response surface methodology. *Wiley Interdisciplinary Reviews: Computational Statistics*, 2(2), 128-149.
- Kim, K. H., Kabir, E., and Jahan, S. A. (2016). A review on the distribution of Hg in the environment and its human health impacts. *Journal of Hazardous Materials*, 306, 376-385.
- Krishnan, K. A., and Anirudhan, T. S. (2002). Removal of mercury (II) from aqueous solutions and chlor-alkali industry effluent by steam activated and sulphurised activated carbons prepared from bagasse pith: kinetics and equilibrium studies. *Journal of Hazardous Materials*, 92(2), 161-183.
- Kubota, M., Ito, T., Watanabe, F., and Matsuda, H. (2011). Pore structure and water adsorptivity of petroleum coke-derived activated carbon for adsorption heat pump—Influence of hydrogen content of coke. *Applied Thermal Engineering*, 31(8), 1495-1498.
- Landis, M. S., Ryan, J. V., ter Schure, A. F., and Laudal, D. (2014). Behavior of mercury emissions from a commercial coal-fired power plant: The relationship between stack speciation and near-field plume measurements. *Environmental Science and Technology*, 48(22), 13540-13548.
- Lillo-Ródenas, M. A., Cazorla-Amorós, D., and Linares-Solano, A. (2003).

- 
- Understanding chemical reactions between carbons and NaOH and KOH: an insight into the chemical activation mechanism. *Carbon*, 41(2), 267-275.
- Lu, C., Xu, S., and Liu, C. (2010). The role of K_2CO_3 during the chemical activation of petroleum coke with KOH. *Journal of Analytical and Applied pyrolysis*, 87(2), 282-287.
- Lu, X., Jiang, J., Sun, K., Wang, J., and Zhang, Y. (2014). Influence of the pore structure and surface chemical properties of activated carbon on the adsorption of mercury from aqueous solutions. *Marine pollution bulletin*, 78(1), 69-76.
- Marsh, H., and Reinoso, F. R. (2006). *Activated carbon*. Elsevier.
- Menéndez, J. A., Arenillas, A., Fidalgo, B., Fernández, Y., Zubizarreta, L., Calvo, E. G., and Bermúdez, J. M. (2010). Microwave heating processes involving carbon materials. *Fuel Processing Technology*, 91(1), 1-8.
- Mohan, D., Gupta, V. K., Srivastava, S. K., and Chander, S. (2001). Kinetics of mercury adsorption from wastewater using activated carbon derived from fertilizer waste. *Colloids and Surfaces A: Physicochemical and Engineering Aspects*, 177(2), 169-181.
- Monser, L., and Adhoum, N. (2002). Modified activated carbon for the removal of copper, zinc, chromium and cyanide from wastewater. *Separation and purification technology*, 26(2), 137-146.
- Nabi, S. (2014). Methylmercury and Minamata Disease. In *Toxic Effects of Mercury* (pp. 187-199). Springer India.
- Rambabu, N., Azargohar, R., Dalai, A. K., and Adjaye, J. (2013). Evaluation and comparison of enrichment efficiency of physical/chemical activations and functionalized activated carbons derived from fluid petroleum coke for environmental applications. *Fuel Processing Technology*, 106, 501-510.

- 
- Rao, M. M., Reddy, D. K., Venkateswarlu, P., and Seshaiyah, K. (2009). Removal of mercury from aqueous solutions using activated carbon prepared from agricultural by-product/waste. *Journal of Environmental Management*, 90(1), 634-643.
- Salman, J. M., and Hameed, B. H. (2010). Effect of preparation conditions of oil palm fronds activated carbon on adsorption of bentazon from aqueous solutions. *Journal of Hazardous Materials*, 175(1), 133-137.
- Saucier, C., Adebayo, M. A., Lima, E. C., Cataluña, R., Thue, P. S., Prola, L. D., ... and Dotto, G. L. (2015). Microwave-assisted activated carbon from cocoa shell as adsorbent for removal of sodium diclofenac and nimesulide from aqueous effluents. *Journal of Hazardous Materials*, 289, 18-27.
- Sekar, M., Sakthi, V., and Rengaraj, S. (2004). Kinetics and equilibrium adsorption study of lead (II) onto activated carbon prepared from coconut shell. *Journal of Colloid and Interface Science*, 279(2), 307-313.
- Sowlat, M. H., Abdollahi, M., Gharibi, H., Yunesian, M., and Rastkari, N. (2014). Removal of vapor-phase elemental mercury from stack emissions with sulfur-impregnated activated carbon *Reviews of Environmental Contamination and Toxicology volume* (pp. 1-34): Springer.
- Terzyk, A. P. (2001). The influence of activated carbon surface chemical composition on the adsorption of acetaminophen (paracetamol) in vitro: Part II. TG, FTIR, and XPS analysis of carbons and the temperature dependence of adsorption kinetics at the neutral pH. *Colloids and Surfaces A: Physicochemical and Engineering Aspects*, 177(1), 23-45.
- Torres-Pérez, J., Soria-Serna, L. A., Solache-Ríos, M., and McKay, G. (2015). One Step Carbonization/Activation Process for Carbonaceous Material Preparation from Pecan Shells for Tartrazine Removal and Regeneration after

- Saturation. *Adsorption Science and Technology*, 33(10), 895-913.
- UNEP. (2013). Global Mercury Assessment 2013. Retrieved from <https://www.zaragoza.es/contenidos/medioambiente/onu/942-eng.pdf>
- USEPA. (2016). *Artisanal and Small-Scale Gold Mining Without Mercury*. Retrieved from <https://www.epa.gov/international-cooperation/artisanal-and-small-scale-gold-mining-without-mercury>.
- USEPA. (2016). *Basic Information about Mercury*. Retrieved from <https://www.epa.gov/mercury/basic-information-about-mercury>.
- Wajima, T., and Sugawara, K. (2011). Adsorption behaviors of mercury from aqueous solution using sulfur-impregnated adsorbent developed from coal. *Fuel Processing Technology*, 92(7), 1322-1327.
- Warkany, J., and Hubbard, D. M. (1953). Acrodynia and mercury. *The Journal of Pediatrics*, 42(3), 365-386.
- WHO. (1991). Inorganic mercury. *Environmental Health Criteria 118*. International Program on Chemical Safety, World Health Organization.
- Yang, K., Peng, J., Srinivasakannan, C., Zhang, L., Xia, H., and Duan, X. (2010). Preparation of high surface area activated carbon from coconut shells using microwave heating. *Bioresource Technology*, 101(15), 6163-6169.
- Yardim, M. F., Budinova, T., Ekinici, E., Petrov, N., Razvigorova, M., and Minkova, V. (2003). Removal of mercury (II) from aqueous solution by activated carbon obtained from furfural. *Chemosphere*, 52(5), 835-841.
- Zabihi, M., Ahmadpour, A., and Asl, A. H. (2009). Removal of mercury from water by carbonaceous sorbents derived from walnut shell. *Journal of Hazardous Materials*, 167(1), 230-236.
- Zhang, D., Yin, J., Zhao, J., Zhu, H., and Wang, C. (2015). Adsorption and removal of

- 
- tetracycline from water by petroleum coke-derived highly porous activated carbon. *Journal of Environmental Chemical Engineering*, 3(3), 1504-1512.
- Zhang, F. S., Nriagu, J. O., and Itoh, H. (2005). Mercury removal from water using activated carbons derived from organic sewage sludge. *Water Research*, 39(2), 389-395.
- Zhong, Z. Y., Yang, Q., Li, X. M., Luo, K., Liu, Y., and Zeng, G. M. (2012). Preparation of peanut hull-based activated carbon by microwave-induced phosphoric acid activation and its application in Remazol Brilliant Blue R adsorption. *Industrial Crops and Products*, 37(1), 178-185.
- Zou, L., Morris, G., and Qi, D. (2008). Using activated carbon electrode in electrosorptive deionisation of brackish water. *Desalination*, 225(1-3), 329-340.